Molecular and phenotypic characterization of *Ire1α* gene deletion in mouse embryo fibroblasts and pancreatic β cells.

By

Justin Ray Hassler

A dissertation submitted in partial fulfillment
of the requirements for the degree of
Doctor of Philosophy
(Biological Chemistry)
in The University of Michigan
2012

Doctoral Committee:

Professor Randal J. Kaufman, Chair
Professor Peter Arvan
Professor Robert S. Fuller
Associate Professor Aaron Goldstrohm
Associate Professor Maureen Sartor

ACKNOWLEDGEMENTS

Dr. Randal J. Kaufman made everything I have learned in the past 6 years possible and scientifically enjoyable. I am forever in his debt for the time he afforded me to study the fascinating molecules of the Unfolded Protein Response. He is a stellar example of a critical thinker, molecular scientist and author to learn from and I deeply admire the discoveries he has made and will continue to make as well as the stories he has shared with me.

Thank you to my committee members for their graciousness in offering me their valuable time and advice throughout the course of my studies at the University of Michigan. A special thank you to my apprentice students Jenny George, Cory Davis and Julie Nguyen. My co-workers, Shiyu Wang, Jaeseok Han, Sung Hoon Back, Benbo Song, Donalyn Scheuner, Robert Clark, Andrew Fribley, Sean Ferris, Li Li, Stewart Cao, Vamsi Kodali and Gregory Baudouin. I also thank Dr. James Cavalcoli and Dr. Yongsheng Bai for their bioinformatics expertise. Thank you sincerely to those that sacrificed the most in my studies, *Mus musculus*. I would also thank Dr. John S. Graham, Karen and Marvin Brautigam for being my most steadfast personal supporters, without them I would be much worse off.

Thank you

PREFACE

Chapter one is an introduction to the Unfolded Protein Response (UPR) with an emphasis on PERK and IRE1α in the murine β adapted from (*Diabetes Obes Metab, 2010*). Chapter two is a publication being submitted by Justin Hassler *et al*. (*Cell, 2012*) Chapter three presents data on the function *Ire1α* in mouse embryo fibroblasts and is being prepared for submission by Justin Hassler, *et al* and Dr. Randal Kaufman (*2013*). Chapter four summarizes the future experiments and questions to be addressed for both the fibroblast and β cell projects if possible.

TABLE OF CONTENTS

LIST OF FIGURES

CHAPTER I

THE PERK AND IRE1α UNFOLDED PROTEIN RESPONSE PATHWAYS ARE REQUIRED TO MAINTAIN THE INTEGRITY OF THE ER, PREVENT OXIDATIVE STRESS, AND PRESERVE DIFFERENTIATION IN β CELLS

INTRODUCTION

Diabetes affects approximately 285 million people worldwide and is expected to grow to 438 million by the year 2030 [1]. Over 90% are cases of type 2 diabetes (T2D) making it an epidemic of worldwide proportions caused by three factors: inactivity, dietary excess of saturated fats and sugars and an individual's genetic susceptibilities all of which contribute to the destruction of β–cell function over time. T2D manifests systemically as a metabolic syndrome where tissues, such as muscle, fat, and liver, become resistant to insulin which causes pancreatic β cell failure as they are unable to compensate adequately [2, 3]. Once insulin deficiency occurs characteristics of the diabetic state such as hyperglycemia and hyperlipidemia begin to wreak havoc on the patient's vasculature especially in the retina and over time in the limb extremities [4-7]. Unfortunately, little is known about how the β–cell responds to elevated blood glucose to increase insulin transcription, translation, and secretion or why they eventually fail. However, one unavoidable consequence of the β–cell increasing production of insulin during compensation to insulin resistance is that the endoplasmic reticulum (ER) must increase the structure and function of its secretory apparatus to support higher-levels of insulin production (Figure 1-1). Therefore, the ability of β–cells to compensate for hyperglycemia-driven increases in insulin production inherently requires the ER and the unfolded protein response (UPR) (Figure 1-2) [8-11].

The UPR is an adaptive signaling pathway that promotes cell survival upon accumulation of unfolded protein in the endoplasmic reticulum (ER) (Figure 1-2) [12-23]. The β–cell is unique even among secretory cells because it engages its secretory pathway with great frequency assuming ease of access to food. Since insulin is an ER-Golgi secreted protein, its synthesis, folding and secretion are central for the post-prandial production of insulin to the bloodstream. Our current understanding for the roles of each unfolded protein

response (UPR) sensors is discussed further. Genetic disruption in mice of *Perk*, *Eif2α*, *Ire1α* and *Xbp1* are linked to embryonic lethality and β cell-specific deletion studies have shown acute β cell dysfunction occurs in all these models for overlapping and unique reasons [24-28]. Contrary to the detrimental effects reported for the deletion of the previous four pathways, ATF6α and CHOP whole body deletions are not embryonic lethal and of little consequence and in CHOP's case even protective when deleted in the β cell respectively. The protective role of the UPR in human diabetes has been reported through the presence of patients carrying mutations for *Perk* and the XBP1 target, *Wfs1* associated with Wolcott-Rallison and Wolfram syndrome patients respectively [29, 30].

PERK phosphorylation of eukaryotic initiation factor 2 on the alpha subunit (eIF2α) is critical for β–cell function because it attenuates protein synthesis, thereby reducing the biosynthetic burden [31, 32]. Unabated protein synthesis in β–cells is sufficient to initiate a cascade of events, including oxidative stress, characteristic of β–cell failure observed in type 2 diabetes [20, 27]. As opposed to the beneficially adaptive UPR activation that occurs in the short-term, chronic activation increases expression of the pro-apoptotic transcription factor CAAT-enhancer binding protein homologous protein (CHOP). It has been reported prolonged PERK activation causes increased ATF4 translation which increases CHOP mRNA expression [33,-43]. CHOP is detrimental to the β–cell by increasing mRNA expression of pro-apoptotic factors [44-48]. In contrast, *Chop* deletion in insulin-resistant mice profoundly increases β–cell mass and prevents β–cell failure to forestall the progression of diabetes [49]. Recently it was shown that cell death and protein synthesis were increased by co-expression of ATF4 and CHOP to a greater extent than being expressed alone compared to controls.[50] Because increased *Chop* mRNA levels were detected in *Ire1α*-deficient β cells, tunicamycin-treated ATF6α null murine kidney and XBP1 was found to occupy *Chop's* promoter by chromatin immunoprecipitation massive parallel sequence analysis (CHIP-Seq) the regulation of CHOP is likely affected by the non-PERK/EIF2α/ATF4 pathways as well [51-53].

In contrast to PERK/EIF2α, the diabetic phenotype caused by deletion of the *Ire1α* and/or *Xbp1* pathways is not due to unabated protein synthesis (Chapter II). Yet the deletion of either IRE1α or XBP1 causes diabetes at least in part due to reduced proinsulin synthesis due to decreased expression of critical ribosome recruitment factors, translocon and signal peptidase and many other pro-secretory mRNAs (Chapter II) [54]. Despite ATF6α and XBP1 having very similar DNA-binding motifs, results indicate by comparing murine hyperglycemic phenotypic studies presented in Chapter II suggest the IRE1α-XBP1s pathway is more important for β cell function than reports on the ATF6α pathway [18, 19, 55-58]. Ongoing

experiments are aimed at determining whether spliced *Xbp1* mRNA occurs at a higher rate in *Atf6α* -/- β cells and if the double knock-out *Atf6 α* x *Ire1α* β cells are less functional than the single gene ablations. These experiments will address whether there is compensation occurring between the ATF6α and XBP1s pathways at a common set of promoters to increase the β cell's ER capacity for protein synthesis, quality control and secretion when the other fails. The reported findings as of now suggest unprecedented links by which uncontrolled protein synthesis and misfolding in the ER cause oxidative stress and should be taken into consideration for the development of novel ER-based strategies to treat diabetes through a better understanding of the UPR pathways in β cells.

I. The Endoplasmic Reticulum: The main cellular calcium reservoir coordinates protein synthesis, translocation, folding, signal cleavage, N-linked glycosylation, recycling, and export

The ER is the site where proteins destined for the cell surface and endomembrane system enter the secretory pathway. Approximately one-third of all proteins translocate across the ER membrane where they fold into their proper three-dimensional structures and are subject to glycosylation, hydroxylation, lipidation, and disulfide bond formation (Figure 1-1) [59, 60, 61] The ER contains an extremely high Ca^{2+} concentration and is occupied by chaperone proteins, catalysts of protein folding and enzymatic machinery for post-translational modifications [62]. Only properly folded proteins exit the ER to the Golgi compartment for further processing prior to trafficking to their final destination. The mechanisms for this exquisitely sensitive and specific quality controls are under active investigation, but are not yet well defined. Retention of unfolded proteins in the ER lumen occurs through interaction with ER resident peptide-binding proteins, such as BIP and GRP94. ER-associated protein degradation (ERAD) is the process whereby misfolded proteins are recognized in the ER, targeted to a channel within the ER membrane, extracted from the ER membrane, and delivered to the proteasome [63]. At a minimum, quality control is mediated through the processing of *N*-linked glycans that are primarily recognized by lectin-binding proteins in the ER lumen (Figure 1-1) [64]. These lectins direct refolding (CNX, CRT), anterograde transport (LMAN1), and ER-Associated Degradation "ERAD" (EDEMs, OS-9, XPT3-B) [65, 66].

Protein misfolding occurs in the ER as a consequence of a number of insults, including pharmacological perturbation, alterations in Ca^{2+}, redox status, or nutrient

availability, mutations in ER chaperones or their client proteins, pathogen infection, as well as differentiation of cells that secrete large amounts of proteins. The accumulation of unfolded proteins in the ER lumen activates the UPR (Figure 1-2) [62, 67]. The UPR is an adaptive response designed to resolve the protein folding defect by: 1) reducing protein influx into the ER; 2) increasing the capacity to promote productive protein folding; and 3) increasing clearance of misfolded proteins in the ER lumen through ERAD and autophagy. These strategies may exhibit temporally separate phases of the UPR [68]. Reduced influx occurs rapidly and transiently, and prevents further generation of misfolded proteins, while upregulation of protein maturation and degradation machinery occurs after UPR-dependent gene induction. Over time, homeostasis may be re-established in the ER to resolve the protein-folding defect [69]. If homeostasis is not restored, the UPR is chronically activated and leads to apoptosis (Figure 1-3). Hence, the mechanisms that decipher the protein folding status and orchestrate a coordinated downstream response, either adaptive or apoptotic, are fundamentally significant, unknown, and require further investigation.

II. UPR initiation, translational and transcriptional control

a. UPR initiation begins with BiP

The UPR field would not be possible if it weren't for the early studies on immunoglobulin binding protein (BiP/GRP78) that described it as being induced by glucose starvation and later by viral infection [70, 71]. In the unstressed state, the three UPR sensors PERK, IRE1α and ATF6α are maintained in an inactive state through ER luminal interaction with the protein chaperone BiP until it is competed away by unfolded proteins [72]

b. PERK: A negative feed-back loop that inhibits global protein synthesis with notable exceptions

Activated PERK phosphorylates the alpha subunit of the translation initiation factor 2 (eIF2α) leading to rapid and transient inhibition of protein synthesis [73]. eIF2 is a heterotrimeric GTPase required to bring initiator methionyl tRNA to the ribosome for AUG initiation codon selection [74]. Phosphorylation of eIF2α inhibits the GDP/GTP exchange reaction on eIF2, thereby preventing eIF2 recycling and the initial step of polypeptide synthesis [73, 75, 76]. Paradoxically, eIF2α phosphorylation is required for the translation of several mRNAs (*Gadd34, Atf5, Cat1*), including the bZiP transcription factor ATF4 [77]. This mechanism apparently involves ribosomes scanning through upstream open reading frames in the 5' end of the mRNA due to limiting amounts of GTP-bound eIF2-tRNAmet. During periods of ER stress, the selective translation of *Atf4* mRNA produces a factor that binds to the amino acid response element (AARE) in target genes such as *Atf3, Chop/Gadd153, Atf3*

and *Gadd34/MyD116/Ppp1r15a* [78-81]. Recent studies, as well as our own, indicate chronic UPR activation causes induction of CHOP that is essential for the apoptotic response to chronic protein misfolding in the ER [82-84]. CHOP was originally isolated as a gene induced in response to DNA damage and it consists of a transcriptional activation/repression domain followed by a basic leucine zipper domain at its C terminus [85]. Although it was thought that CHOP functions as a negative regulator to sequester binding partners [85], subsequent studies demonstrated that a CHOP-C/EBP heterodimer could bind DNA and function as a transcriptional activator [86, 87]. It is proposed that CHOP mediates induction of the apoptotic genes *Gadd34*, *Dr5*, *Bim*, and *Trb3*, and repression of anti-apoptotic *Bcl2* expression [83, 88].

Surprisingly, cells in which the UPR is chronically activated at a low level can propagate indefinitely because they have adapted/compensated to the stress from the initial insult and accomplished a new, survivable baseline activity [89]. In that study, the adapted cells demonstrated compensatory up-regulation of ER chaperones and ERAD machinery [89]. Survival under these conditions is associated with attenuated expression of CHOP, and its target *Gadd34* [90, 91]. In the presence of perpetual CHOP expression, cells succumb to apoptotic death. It was demonstrated that the half-lives for mRNAs and proteins encoding adaptive functions of the UPR (i.e. BiP, GRP94, p58IPK, etc) are long-lived, whereas those encoding apoptotic functions, ATF4, CHOP, and GADD34 are short-lived [89]. Under adaptive conditions, the steady-state levels of proteins that promote protein folding and ERAD are increased, which feeds back to shut off UPR signaling. In contrast, a perpetual strong misfolded protein signal is required to activate the CHOP-mediated death program [89]. We have shown that *Chop* deletion improves both β–cell survival and proinsulin secretion [49]. These studies suggest that CHOP mediates apoptosis through the combined effects of 1) the induction of oxidative stress and 2) increased expression of pro-apoptotic factors, described previously. However, the relationship between signaling through the PERK/eIF2α/ATF4/CHOP pathway to production of ROS is complicated by the multiple sources from which ROS are derived. A few sources of ROS include; origination directly from the iron cluster active sites among the mitochondrial oxidative phosphorylation (OXPHOS) enzymes or other reactive centers of oxido-reductases like (PDIAs, LOXs and NOSs). Indirectly, ROS may accumulate due to calcium leak from stressed ER and/or mitochondria making both organelles less efficient at protecting from additional insults caused ROS byproducts [92-98]. Similarly, the stressed ER is expending energy through protein folding and degradation so these aspects are also variables that affect ER-Oxidative stress derived ROS. The current model proposes that ATF4-mediated induction of CHOP causes

transcriptional induction of GADD34 which encodes a regulatory subunit of protein phosphatase 1 (PP1) that negatively feeds back on the pathway by dephosphorylating eIF2α, thereby reversing the PERK mediated translational attenuation [91]. Although the most direct pathway that leads to CHOP induction is mediated through PERK-ATF4 the deletion of IRE1/XBP1 and ATF6α pathways have also exhibited increased *Chop* mRNA levels and as a binding target to XBP1[51, 53, 99]. In summary, CHOP is a rare allele because upon deletion the mice exhibit gain of protection phenotypes with regard to diabetes and ER-oxidative stress in general.

c. IRE1α and ATF6α: converging pathways for establishing the ER-secretory apparatus and increasing its capacity

Although there are alpha and beta alleles of both IRE1 and ATF6 in the mammalian genome only α isoforms are expressed in all tissues and signal the general UPR. IRE1β is selectively expressed in intestinal epithelial cells and reported to cleave the 28S rRNA while it is not known what genes are regulated by ATF6β [100-103]. IRE1α activation elicits an endoribonuclease function that induces nonconventional splicing of *Xbp1* mRNA (Figure 1-2) [14, 104, 105]. Splicing of *Xbp1* mRNA, the only known splicing substrate of IRE1, removes a 26 nucleotide long intron (Figure 1-4) that alters the translation reading frame to produce a highly active bZiP transcription factor that activates genes encoding ER protein chaperones, lipid biosynthetic enzymes, and ERAD functions [22, 58, 106]. Upon release from BiP, ATF6α trafficks to the Golgi complex where it is cleaved by the S1P and S2P processing enzymes to produce a cytosolic bZiP TF that activates transcription of genes with overlapping functions as those activated by XBP1 to restore productive ER protein folding and increase ERAD [53, 107, 108]. Indeed, cells deleted in either *Ire1α, Xbp1, or Atf6α* are defective in ERAD [22, 58, 106]; [53, 107, 108]. The transcriptional studies indicate mRNAs encoding SEC11C, SPCS2, SPCS3, SSRs 1-4, SRP54 and other pro-secretory mRNAs are regulated by both ATF6α and/or XBP1. Additional evidence was derived from *in silico* analysis of the promoters revealed ATF6a and XBP1 binding sites, some of which overlapped [51, 109].

More than 50 bZiP transcription factors have been identified in mammals, all of which possess the structurally required domains to dimerize with each other [110]. ER-stress elements within the promoters of stress-inducible genes have revealed that CHOP and ATF4 have extremely conserved binding sequence and the same has been found for XBP1 and ATF6α indentifying the lists of promoters that are specific to these 4 TFs is of interest as well because it is possible all four have promoters to which only they bind [104, 111-119]. Generally, most studies report with a few exceptions that pro-apoptotic signals generally emanate from

the ATF4/CHOP axis while increased expression of adaptive mRNAs is regulated by all three UPR pathways: IRE1α/XBP1s, ATF6α and PERK/ATF4/CHOP axis with *Hrd1*, *Grp78* and *Herpud2* being examples of ER stress-induced genes with promoters regulated by multiple UPR pathways [53, 69, 99, 114, 120-126]. IRE1α's highly conserved RNase domain (Figure 1-5) has been reported to cleave subsets of ER-localized mRNAs and several miRNAs that causes pro-apoptotic de-repression of Caspase 2 suggesting pro-apoptotic functions can be performed by IRE1α's RNase activity [127-130.] The data suggests an exquisite balance is to be maintained but it is interesting to hypothesize whether viral forced expression or inhibition of any or all four of these TFs in certain contexts might be of benefit. Examples where selective manipulation of the UPR pathways could be of benefit are, production of secreted hormones and selective pathway induction of apoptotic or survival mRNAs to kill a tumor or repair a contusion respectively.

III. Protein misfolding in the ER and oxidative stress

There is accumulating evidence to suggest that protein misfolding in the ER and production of reactive oxygen species (ROS) are linked through ion leak and ATP depletion, however, this area of ER stress is not well defined because iron containing protein sources also contribute to total cellular ROS and are numerous. A growing family of ER oxido-reductases, including PDIs (protein disulphide isomerases), catalyze these protein-folding reactions in mammalian cells [131, 132]. PDI catalyzes the formation, isomerization and reduction of disulfide bonds *in vitro*. When disulfide bond formation occurs, cysteine residues within the PDI active site [-C-X-X-C-] accept two electrons from thiol residues in the polypeptide chain substrate [131]. This electron transfer results in the oxidation of the substrate and the reduction of the PDI active site. It is now recognized that reduced PDI transfers its electrons through ERO1 to molecular oxygen as the final electron acceptor and hydrogen peroxide is formed as a byproduct from the sequential action of PDI and ERO1 in transferring electrons from thiol groups in proteins to molecular oxygen (Figure 1-3) [131]. It has been estimated that approximately 25% of the ROS generated in a cell may originate from formation of disulfide bonds in the ER during oxidative protein folding [133]. In addition, ROS may be formed as a consequence of glutathione (GSH) depletion that occurs as GSH reduces unstable and improper disulfide bonds (Figure 1-3). The consumption of GSH would return thiols involved in non-native disulfide bonds to their reduced form so they may again interact with ERO1/PDI to be reoxidized. This would generate a futile cycle of disulfide bond formation and breakage in which each cycle generates ROS and consumes GSH (Figure 1-3). As a consequence, it is expected that proteins that have multiple disulfide bonds may be

more prone to generating oxidative stress. Because, insulin has three disulfide bonds this process is of particular importance for the secretory function of the β cell. This may in part explain how antioxidants improved β cell protein folding and reduced apoptosis under conditions of ER stress [50].

IV. UPR activation in β–cells associated with type II diabetes

a. UPR activation in islets from diabetic mice and men

If ER stress and UPR signaling are important for β–cell function/survival, then 1) UPR gene induction should be detectable in the islets of diabetic mice and human patients; 2) accumulation of unfolded protein in β–cells should cause β–cell failure and diabetes; and 3) genetic deletion of critical UPR signal transduction components should cause overwhelming ER stress and diabetes. There is now evidence to support each of these predictions. Perhaps the most difficult determination of UPR association with β–cell failure is the detection of ER stress or defective ER stress signaling in islet samples from human patients. However, CHOP nuclear localization was reported in pancreata of human obese diabetic individuals but only rarely found in with nuclear localization in pancreata from control or type 1 diabetic patients [134]. Similarly, the classical UPR-induced proteins p58IPK, BiP, and CHOP were significantly elevated in islets in tissue sections from patients with type 2 diabetes patients [46]. Increased levels of eIF2α phosphorylation, increased splicing of *Xbp1* mRNA, and increased CHOP and BiP protein were detected in the islets of *db/db* mice, a common model of insulin resistance and β–cell failure [46, 135]. The detection of UPR-induced signals in these samples does not prove that ER stress was a causative event in the disease process; however, it does provide the first evidence that UPR markers are elevated specifically in the islets of diabetic men and mice. Further substantiating that excessive ER stress or defective stress signaling are pathogenic determinants of human diabetes will require more advanced knowledge of the stimuli and function of the UPR in β–cells and development of sensitive methods to detect markers of the UPR in human samples. One outstanding question is whether insulin resistance causes an increase in proinsulin synthesis that generates greater amounts of misfolded protein in β–cells. The discovery of drugs that improve ER protein folding and/or modulate ER stress signaling that can be evaluated in diabetes animal models and in human clinical trials will greatly advance our understanding of the importance ER stress has in the development and progression of diabetes.

b. β–Cell Failure: Mutant proinsulin and/or preproinsulin, both cause ER-stress derived diabetes

Studies of *Akita* and *Munich* mice reveal that mutations at cysteine residues that

interfere with proper disulfide bond formation within proinsulin induce ER stress and severe β–cell destruction [8, 136, 137, 138]. Deletion of the UPR-induced proapoptotic gene *Chop* delayed onset of hyperglycemia and β–cell failure in the *Akita* mouse [139]. Human proinsulin with the analogous *Akita C96Y* mutation was analyzed and compared with wild-type proinsulin through the development of expression constructs that fuse green fluorescence protein (GFP) with the C peptide [8]. In these studies it was possible to elucidate that processing of hPro*C96Y*CpepGFP to insulin was completely impaired in INS-1 cells and expression was "proteotoxic" in comparison to control hProCpepGFP. In humans, neonatal dominantly inherited diabetes in 16 families was associated with missense mutations in the *Ins* gene [137, 138]. The mutations are predicted to impair proinsulin disulfide bond formation and activate ER stress. The missense mutations affect residues directly involved in disulfide bond formation, crucial residues adjacent to disulfide bridges, and also introduce new cysteine residues that could interfere with correct pairing of cysteine residues as nascent proinsulin molecules undergo oxidative folding. Thus, disruption of disulfide bond pairing in proinsulin, a crucial determinant of secondary structure and protein folding, is sufficient to induce diabetes in both humans and mice. Recent reports of mutations within the signal peptide of preproinsulin have further delineated the importance of the ER process of signal peptide removal for human diabetes [140]. Those findings from human patients directly relate to our studies on the β cell-specific deletion of IRE1α that demonstrated the signal peptidase (SEC11C) mRNA expression is dependent on IRE1α-mediated *Xbp1* mRNA splicing (Chapter II) [140].

c. β–Cell failure: Deletion of the BiP Co-chaperone p58IPK

p58IPK was first described as an inhibitor of the double-stranded RNA-activated eIF2α protein kinase PKR. It was subsequently shown to inhibit activation of the eIF2α kinase PERK [141, 142]. The subcellular localization and function of this protein has been a subject of debate; however, recent evidence supports the notion that the majority of p58IPK is imported into the ER lumen [143]. p58IPK is a member of the DnaJ co-chaperone family that functions to stimulate the ATPase activity of members of the Hsp70 family. Therefore, it was proposed that p58IPK may act in the ER lumen as a co-chaperone for the Hsp70 family member BiP [143]. Mice with null mutation of *p58IPK* develop spontaneous diabetes due to destruction of the islet mass, and *p58IPK*-null mutation worsens the outcome of diabetes due to the *Akita Ins2 C96Y* mutation [144]. These intriguing findings merit further study on the role of p58IPK co-chaperone function in proinsulin folding and maturation and in diabetes. The observations suggest that there may be a number of protein-folding chaperones that play

highly significant roles in preservation of ER function in the β–cell to prevent diabetes.

d. β–cell failure: Mutations in PERK/eIF2α the first direct link between an ER stress sensor and human diabetes

Wolcott-Rallison syndrome was first reported in the early 1970s as a human disease characterized by infantile diabetes, multiple epiphyseal dysplasia, and growth retardation [145, 146]. Pancreas atrophy and endocrine and exocrine insufficiency were observed [147, 148]. Wolcott-Rallison syndrome has been associated with multiple other pathologies including osteopenia, hepatic and renal complications, cardiovascular disease, and mental retardation [147, 149, 150, 151, 152]. Remarkably, it was learned nearly 30 years later that this syndrome results from loss of protein kinase function mutations in the eIF2α kinase PERK (EIF2AK3) [30, 153]. Furthermore, polymorphisms at the *PERK* locus were linked to type 1 diabetes in South Indian populations [154]. *Perk*- deletion in the mouse recapitulates many of the defects of the human syndrome including diabetes due to degeneration of β–cell mass after birth and failure of the exocrine pancreas [155, 156] ER distention, a characteristic of ER dysfunction, was observed in pancreatic β–cells while the rate of glucose-stimulated proinsulin synthesis was enhanced, consistent with a defect in the ability to properly attenuate proinsulin mRNA translation. The findings suggested the β–cells of these mice were susceptible to ER protein overload acting as unresolved ER stress that lead to apoptosis. Conditional deletion of *Perk* at varying times in development suggested that development of β–cell mass, but not maintenance of a population of adult β–cells, is dependent upon this kinase [157]. It is possible that one or more additional eIF2α kinases, general amino acid control 2 (GCN2), heme-regulated inhibitor (HRI), or ds-RNA-activated protein kinase (PKR), are capable of supporting the minimal requirement for eIF2α phosphorylation and translational control in response to *in vivo* stimuli. However, studies on *Perk*-null mice and mice that harbor a homozygous knock-in mutation at the PERK phosphorylation site in eIF2α (*Ser51Ala*) were shown to have defects in embryonic β–cell survival, liver glycogen storage, post-natal induction of gluconeogenesis, inhibition of translation under conditions of ER stress, and transcriptional induction of UPR genes [50, 75]. The *Ser51AlaeIF2α* mutation prevents any compensatory phosphorylation due to activation of other eIF2α kinases and therefore, very effectively blocks stress-induced translation attenuation and ATF4-dependent transcriptional induction. Mice with homozygous *Ser51AlaeIF2α* mutation die from post-natal hypoglycemia [50]. This observation was the first indication that the UPR has a broader role than maintaining functional ER protein folding, but is also intimately connected with metabolic homeostasis [75]. It is now known that all UPR signaling pathways contribute to

glucose and lipid homeostasis [158, 159, 160]

Since the homozygous *Ser51AlaeIF2α* mutation was a neonatal lethal phenotype with a severe β–cell deficiency, further studies were performed by analysis of β–cell function in heterozygous *Ser51AlaeIF2α* mice [11]. The heterozygous animals did not spontaneously manifest β–cell failure due to reduced ER stress signaling. However, upon feeding a 45% high-fat diet, these mice developed elevated fasting blood glucose, glucose intolerance, and a β–cell secretion defect. It was demonstrated that the insulin secretion defect was due to a chronically increased rate of translation which overwhelmed the protein folding machinery of the ER and led to 1) distention of the ER compartment, 2) prolonged association of misfolded proinsulin with the ER chaperone BiP, and 3) reduced secretory granule content [50]. This demonstrates regulation of translational initiation through eIF2α phosphorylation is required for ER stress signaling to prevent β–cell dysfunction when insulin demand is increased due to a high-fat diet and insulin resistance. These findings demonstrated that translational control through eIF2α phosphorylation is essential to maintain the functional integrity of the ER. As ER distention and β–cell death in homozygous *Ser51AlaeIF2α* islets was apparent embryonically in the absence of any exogenous pressure to drive β–cell failure, it is likely that there are physiological stimuli that cause eIF2α phosphorylation early in development that is crucial for β–cell survival [75]. It is unlikely the β–cell requirement for eIF2α phosphorylation is mediated through increased translation of *Atf4* mRNA because *Atf4*−/− mice do not display β–cell defects [161]. However, the embryonic β–cell apoptosis observed in homozygous *Ser51AlaeIF2α* mice was at least in part, signaled through CHOP. Although disruption of the *Chop* gene did not rescue the post-natal hypoglycemia-induced lethality of *Ser51AlaeIF2α* mice, the β–cells in islets from E18.5 *Ser51AlaeIF2α*;*Chop*−/− mice were significantly increased in number and insulin content, and displayed reduced apoptosis compared to islets from *Ser51AlaeIF2α*;*Chop*+/+ mice [49]. These findings support the hypothesis that a significant portion of the β–cell apoptosis in *Ser51AlaeIF2α* mutant mice is caused by CHOP, and that CHOP induction is not solely dependent on eIF2α phosphorylation. However, importantly, these findings show that CHOP is not the only pathway leading to β–cell death in the absence of eIF2α phosphorylation. In the absence of CHOP, other death pathways involving mitochondrial- dependent and independent pathways are invoked. The sum of these findings indicate that genetic defects in the PERK/EIF2α signal transduction pathway are sufficient to deregulate mRNA translation that causes oxidative damage to ER function thereby causing reduced insulin secretion, β–cell death, and diabetes in mice and humans.

e. β–Cell failure: The IRE1-XBP1-WFS1-ATF6 pathway, a second link between diabetes and ER dysfunction

Wolfram syndrome is a rare autosomal-recessive neurodegenerative disorder that is characterized by juvenile-onset diabetes mellitus, optic atrophy, and hearing impairment and is clinically referred to as "DIDMOAD" [162]. This syndrome is caused by loss-of-function mutations in the *Wfs1* gene that encodes the protein Wolframin 1 [163]. Although WFS1 is not a direct sensor of the UPR, analysis of *Wfs1*−/− mice indicates that WFS1 function is closely linked with ER homeostasis. *Wfs1*- null mutation reduces intracellular calcium signaling upon glucose stimulation, induces UPR-regulated genes, and disrupts cell cycle control, leading to apoptosis [164-177]. A microarray study performed on neuroblastoma SH-SY5Y cells found WFS1 expression to be highly dependent on spliced XBP1, and subsequent examination determined the *Wfs1* promoter contains an (ERSE) ER Stress Element-like sequence that spliced XBP1 at least indirectly binds [178]. Recently, a physical interaction between WFS1 and the Na(+)/K(+)ATPase β1 subunit was discovered, and it was discerned that WFS1 was required for trafficking of the subunit to the cell surface [179]. Reduced levels of this ATPase subunit were detected in the plasma membrane fraction of *Wfs1* mutant fibroblasts and of *Wfs1* knockdown MIN6 β–cells. These findings suggest Wolframin 1 may provide a chaperone function to assist in the assembly of subunits of oligomeric proteins before exit from the ER [172, 178, 180]. Finally, it was reported WFS1 mediates the degradation of ATF6α thereby linking the third UPR pathway to human diabetes specifically, Wolfram Syndrome [166].

IV. The damaging role of ER derived oxidative stress in β–cell failure

To elucidate why eIF2α phosphorylation is required to preserve β–cell function, mice with conditional homozygous *Ser51AlaeIF2α* mutation in β–cells were previously studied [50]. Ubiquitous transgenic expression of wild-type *eIF2α* cDNA rescued the post-natal lethality associated with the homozygous *Ser51AlaeIF2α* mutation. The rescued mice were viable, fertile, and displayed normal glucose tolerance and homeostasis. LoxP sites flanked the wild-type *eIF2α* cDNA within the transgene so that when deleted, green fluorescence protein (GFP) was expressed. Upon breeding these mice to transgenic mice harboring the rat insulin II promoter-tamoxifen (Tam)-regulated Cre recombinase [181], the wild-type *eIF2α* cDNA was efficiently deleted in over 90% of the β–cells. Three weeks after administration of Tam, nearly all of the β–cells had deleted the wild-type *eIF2α* cDNA and while at this early stage there was no significant change in islet mass or insulin content, the mice were glucose intolerant [20]. Three weeks after Tam injection there were TUNEL-positive β–cells, prior to

detectable hyperglycemia, suggesting that β–cell failure and apoptosis was not a consequence of later occurring symptoms of lipid- or glucose-toxicity [50]. In addition, ultrastructural analysis identified significantly distended ER and swollen mitochondria in β–cells at 3 weeks after deletion of the transgene. Finally, oxidative damage was detected concurrently with the appearance of TUNEL-positive β–cells, suggesting that blockade of ER stress signaling by preventing eIF2α phosphorylation overloads the ER compartment causing accumulation of unfolded protein, oxidative stress, and subsequent irreversible commitment to cell death [50]. Next explored, was the causal relationship between ROS and disruption of glucose homeostasis in this *in vivo* mouse model of diabetes due to translation-induced overload. Diet supplemented with anti-oxidant butylated hydroxyanisole (BHA) reduced β–cell apoptosis, increase insulin content, and improve glucose homeostasis in mice with homozygous *Ser51AlaeIF2α* mutation in β–cells [50]. These findings suggest that reducing ROS in β–cells deficient in eIF2α phosphorylation could improve their function and that ROS may be a cause for the β–cell failure and apoptosis.

To determine whether CHOP contributes to the β–cell failure associated with type 2 diabetes, the effect of *Chop* deletion in three different models of murine type 2 diabetes was previously analyzed: 1) heterozygous *Ser51AlaeIF2α* mutant mice fed a high-fat diet; 2) high-fat diet and streptozotocin (STZ)-treated mice; and 3) *db*/*db* leptin receptor-null mice [49]. In all models, *Chop* deletion increased β–cell mass, improved β–cell function, reduced β–cell apoptosis, and prevented glucose intolerance [49]. Surprisingly, *Chop* deletion not only reduced apoptosis, but also preserved β–cell function as monitored by the integrity of the secretory pathway, insulin expression, and glucose-stimulated insulin secretion [49]. Analysis of gene expression suggested that *Chop* deletion may improve the capacity of the β–cell to tolerate oxidative stress [49]. Indeed, islets from *Chop*−/− mice displayed no significant difference in oxidative damage compared to wild-type mice but when incubated in the presence of tunicamycin to inhibit N-linked glycosylation and cause misfolded protein accumulation in the ER, there was a significant increase in protein oxidation and lipid peroxidation in wild-type islets that was prevented in the *Chop*−/− islets [49]. In contrast, upon treatment with the oxidant H_2O_2, similar amounts of oxidative damage were detected in islets from both strains of mice [49]. Therefore, *Chop* deletion reduced the oxidative damage that occurs in response to protein misfolding in the ER, but not in response to general oxidative stress [49]. From the data, it was concluded that *Chop* deletion not only promotes islet hyperplasia, but surprisingly also improves the function of the β–cells to maintain insulin production, possibly through reduction of oxidative stress [49].

V. The functional role of IRE1α-dependent *Xbp1* mRNA splicing during β–cell glucose-stimulation

A fundamental question regarding β-cell function and survival is what each of the UPR subpathways is required for in β-cell function and what elements of these responses are protective or detrimental to β-cell survival upon chronic, unresolved ER stress from hyperglycemia. We have recently demonstrated that β-cell-specific deletion of *Eif2α*, and *Ire1α* causes hyperglycemia due to β-cell failure (Chapters I and II). A similar diabetic phenotype manifests upon *Perk* and *Xbp1* β cell deletion therefore, signaling through the PERK/EIF2α and IRE1α/XBP1s pathways are essential for unchallenged β- cell function. In contrast, mice with homozygous deletion of *Atf6α* displayed normal glucose homeostasis on a standard chow diet and a small hyperglycemic phenotype after high fat diet may have been attributed to insulin resistance and/or β cell failure [182, 183]. Diabetes causing mutations in the *Ire1α/Xbp1* and *Atf6α* loci similar to the PERK mutations that cause Wolcott-Rallison Syndrome have yet to be discovered. Further analysis of mouse models with UPR gene deletions will help determine how the UPR sensors and their downstream bZiP TFs act in concert to orchestrate β-cell function and survival.

Conclusion

The β cell is a model secretory cell that is uniquely sensitive to glucose stimulation and oxidative stress due to its need to properly fold three disulfide bonds within the insulin molecule. In the β cell, absence of eIF2α phosphorylation, as well as excessive eIF2α dephosphorylation (through CHOP induction of GADD34), causes increased translation associated with oxidative stress [50, 81]. Coupled with the loss of transcriptional control over pro-survival mRNAs the cell tilts toward apoptosis as unfolded proteins and oxidative damage accumulate. The PERK/EIF2α undergoes increased ROS from translational overload and loss of transcriptional control over pro-survival mRNAs and seems to exhibit the most hyperglycemic phenotype followed by the β cell-specific deletion of the IRE1α/XBP1 pathways while ATF6α deletion only causes disfunction after high-fat diet. Presently, most data support the notion that CHOP is induced by the PERK/EIF2α/ATF4 pathway and some data indicate CHOP is repressed by functional IRE1α/XBP1 and/or ATF6α pathways [51, 81, 122, 157, 160, 184, 185]. CHOP increases protein translation by inducing expression of GADD34, a subunit of type 1 protein phosphatase that directs eIF2α de-phosphorylation to re-establish mRNA translation as homeostasis in the ER is restored and by inducing tRNA-synthetases (manuscript in review, Han, J) [81, 90]. CHOP is also implicated in the induction of ERO1α, a molecule that oxidizes protein disulfide isomerase (PDI) so it can function to rearrange

improperly formed disulfide bonds within unfolded proteins [81, 90]. Disulfide bond formation during oxidative protein folding in the ER generates oxidative stress as a consequence of electron transfer from cysteine residues through PDI and ERO1 to molecular oxygen to form hydrogen peroxide (Figure 1-3) [133]. Future studies should elucidate whether *Chop* deletion protects β cells from oxidative damage through the reduced expression of GADD34 and/or ERO1 or reduced protein translation.

Deletion of the IRE1α and/or the XBP1 UPR members in β cells causes a diabetic phenotype whereas the ATF6α deletion is tolerated as whole body null mice [53, 54, 182]. In these deletion contexts expression of mRNAs encoding pro-secretoy proteins was deficient and left the β cells unable to respond to glucose stimulation or repress oxidative stress and inflammation. The overlap between the ATF6α and XBP1 pathways has to some extent been reported [14, 109] and in Chapter 2 (Figure 2-14E) but future experiments performed on mice with the double deletion of *Ire1α* in the *Atf6α* null backgrounds will test whether the combined loss of these TFs causes a more severe diabetic phenotype than the loss of *Ire1α* or *Atf6α* alone. Alternatively, β cell-specific deletion of *Chop* and *Ire1α* could also be examined to see whether *Chop* deletion protects from the diabetic state loss of *Ire1α* causes. Similarly, anti-oxidant rich diet studies on any of the *Ire1α*, *Xbp1*, *Perk*, *Eif2α* mice are of interest.

Author Manuscript Chapter I and figures are adapted from our review [186]

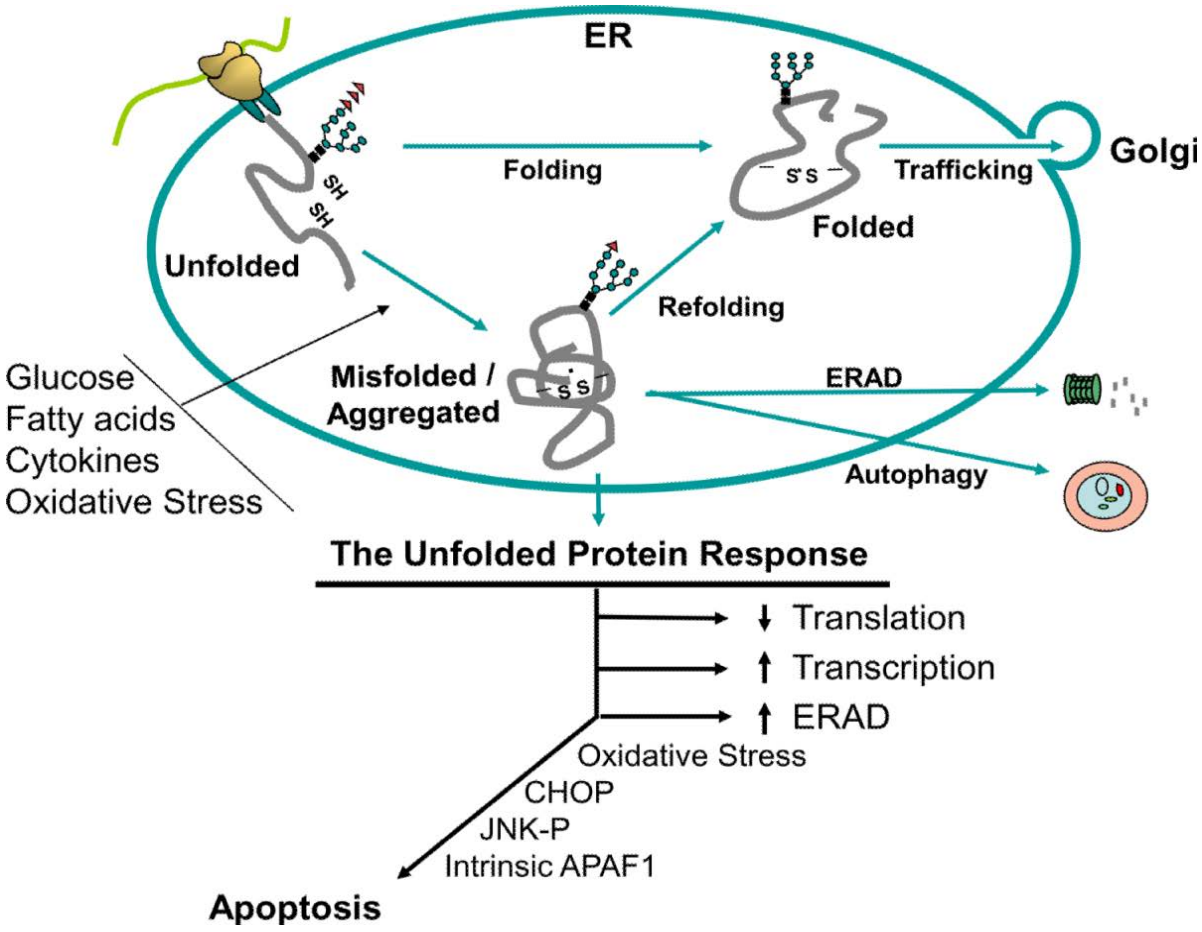

Figure 1-1. Sources of ER stress and protein misfolding
Nascent unfolded polypeptides enter the ER and interact with chaperones and catalysts of protein folding to mature into compact, thermodynamically favorable structures. Failure of this process results in persistence of misfolded polypeptide-chaperone complexes, or extraction of soluble, misfolded protein from the ER and degradation through ERAD. Formation of insoluble protein aggregates requires clearance by autophagy. ER stress stimuli impair polypeptide folding and induce adaptive increases in chaperones and catalysts within the ER lumen through UPR sensor activation. Chronic or overwhelming stimuli elicit a number of apoptotic signals including oxidative stress, JNK activation, CHOP expression, cleavage of caspase 12, and activation of the intrinsic mitochondrial-dependent cell death pathway. Physiological stimuli that can activate the UPR in the β-cell include expression of misfolded proinsulin or IAPP, oxidative stress (ROS), and increases in the extracellular concentrations of glucose, fatty acids, or cytokines.

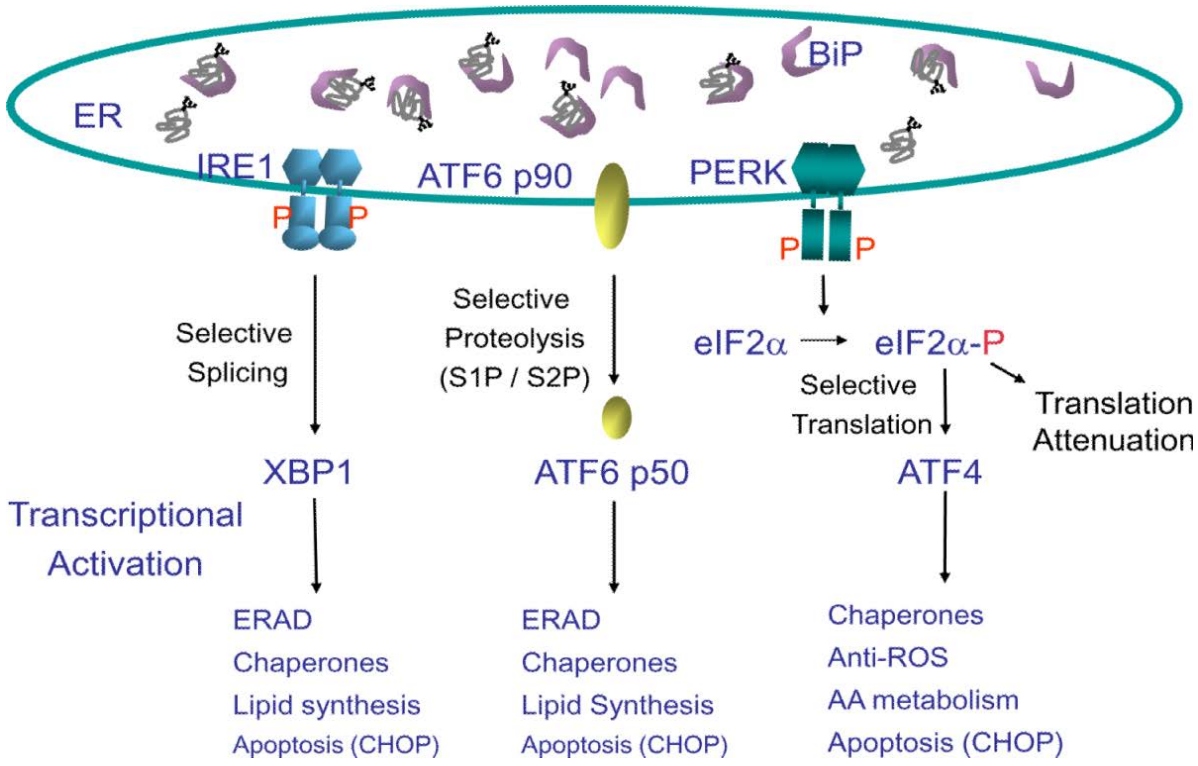

Figure 1-2. Signaling the three main pathways of the unfolded protein response.
The UPR sensors PERK, IRE1, and ATF6 control mRNA translation and transcriptional induction of UPR-regulated genes. Interaction of BiP with each UPR sensor prevents UPR signaling. Upon accumulation of unfolded protein, BiP is released from each sensor, leading to its activation. The ER protein kinase PERK is activated by homodimerization and autophosphorylation to phosphorylate eIF2α, thereby reducing the rate of mRNA translation and the biosynthetic protein-folding load on the ER. eIF2α phosphorylation paradoxically increases translation of *Atf4* mRNA to produce a transcription factor that activates expression of genes encoding protein chaperones, ERAD machinery, enzymes that reduce oxidative stress, and functions in amino acid biosynthesis and transport. Dimerization of the ER protein kinase IRE1 triggers its endoribonuclease activity to induce cleavage of *Xbp1* mRNA. *Xbp1* mRNA is then ligated by an uncharacterized RNA ligase and translated to produce XBP1s. Concurrently, ATF6 released from BiP transits to the Golgi where it is cleaved to release a transcriptionally active fragment. Cleaved ATF6 acts in concert with XBP1s to induce expression of genes encoding protein chaperones and ERAD machinery. The RNase activity of IRE1 also degrades selective cellular mRNAs to reduce the client

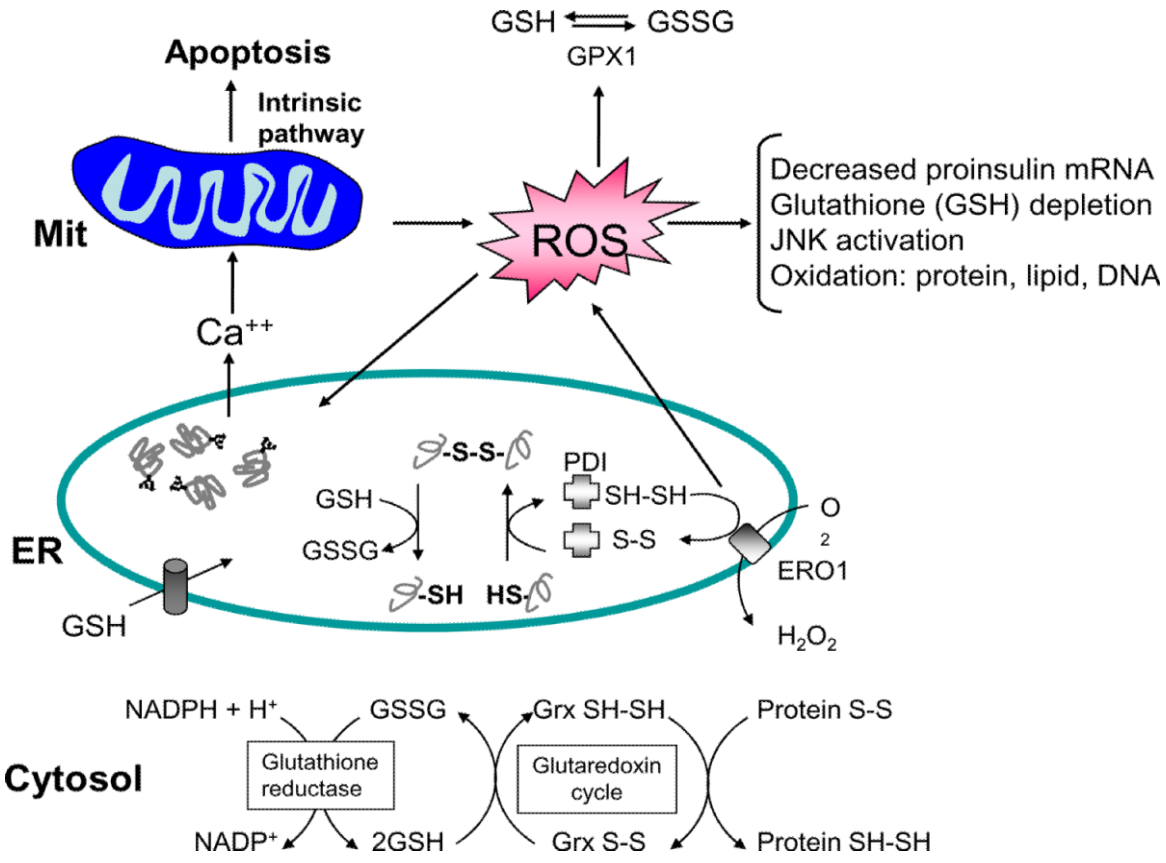

Figure 1-3. ER-mitochondrial oxidative stress.
Protein folding within the ER lumen is ushered by a family of oxidoreductases that catalyze disulfide bond formation and isomerization. ER stress causes an increase in the formation of incorrect intermolecular and/or intramolecular disulfide bonds that require breakage and reformation for proteins to attain the appropriate folded conformation. PDI catalyzes isulfide bond formation and isomerization, whereas glutathione transported into the ER reduces improperly paired disulfide bonds. Reoxidation of PDI is mediated by ERO1; however, ROS are produced in the process. Cellular ROS can deplete glutathione and increase the misfolded protein load in the ER. In turn, ROS can also cause ER stress through modification of proteins and lipids that are necessary to maintain ER homeostasis. Consumption of excessive cellular glutathione due to ER stress could inhibit glutaredoxin reduction and cause accumulation of oxidized cytosolic proteins. ER stress also causes calcium leak from the ER for accumulation in the inner mitochondrial matrix. This calcium loading in the mitochondria can generate additional ROS through disruption of electron transport and opening of the mitochondrial permeability pore. Thus, accumulation of misfolded protein in the ER increases ROS production that can further amplify ER stress, disrupt insulin production, and cause cell death.

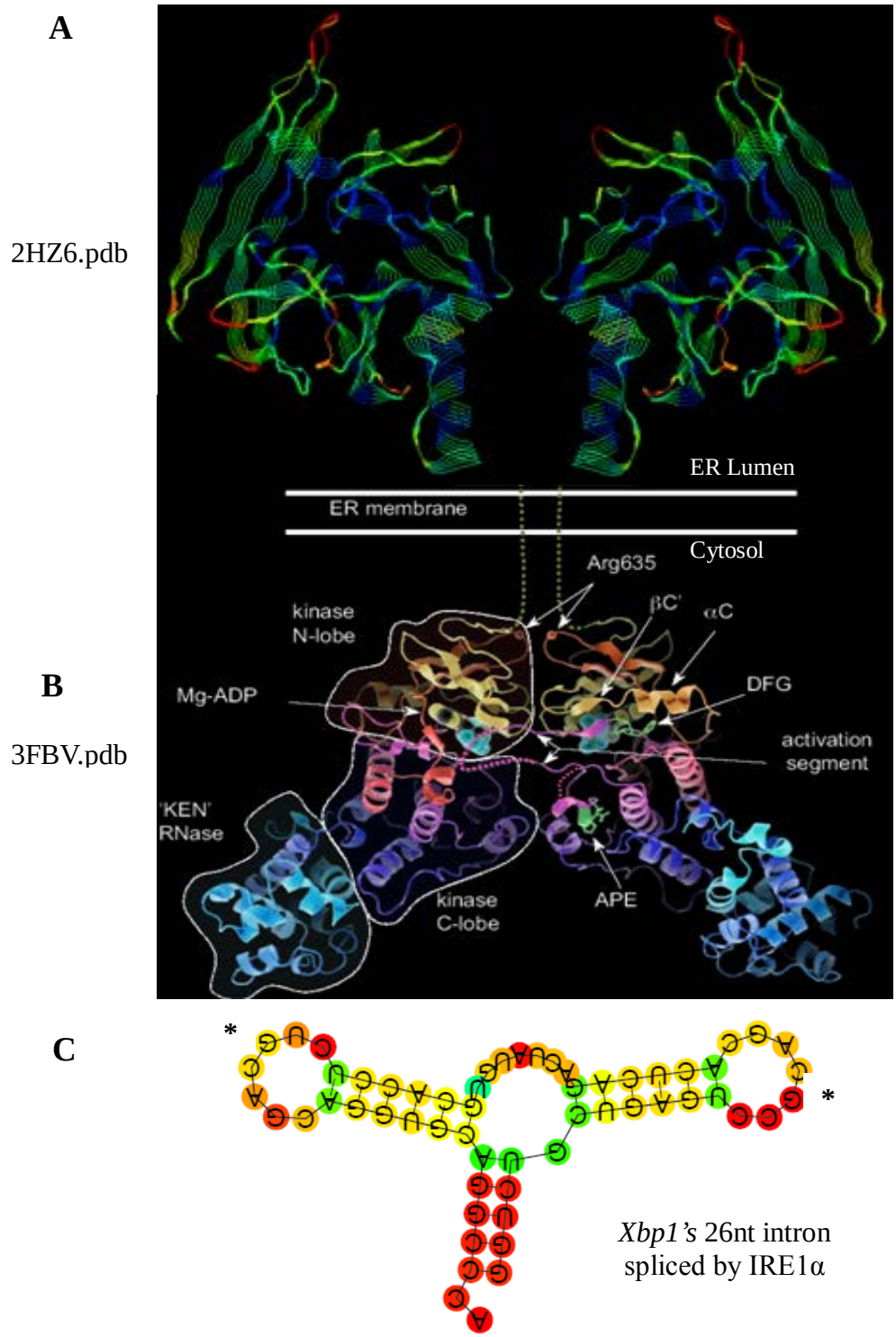

Figure 1-4. Domain structure of IRE1α and the stem loop structure it recognizes to splice 26 nucleotides from *Xbp1's* mRNA. (A) Crystal structure of hIRE1α'sER luminal domain. *Zhou J. and Kaufman RJ, 2006* (B) Crystallography of yIRE1α's cytosolic kinase and RNase domains. *Korennykh AV and Walter P, 2009* (C) RNA-FOLD energy minimization derived structure of *Xbp1's* mRNA unconventional intron spliced by IRE1α. The scale blue to red represents decreasing entropy/increasing stem base-pairing, and/or loop structural stability.

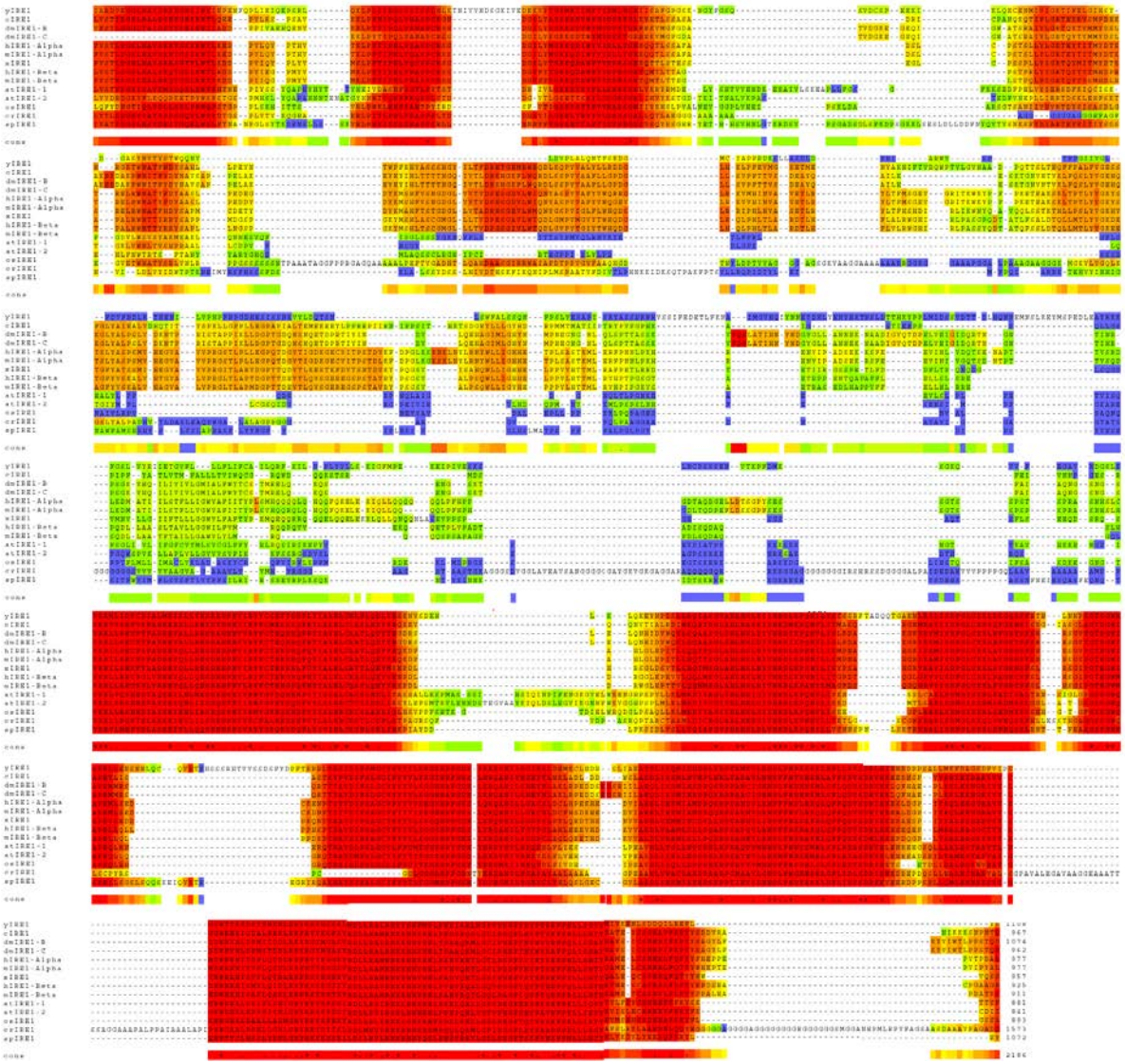

Figure 1-5. IRE1α, the most evolutionarily conserved UPR sensor
IRE1α is the most evolutionarily conserved UPR sensor. The domains with the greatest homology are the luminal; BIP-binding, cytosolic; kinase and RNase domains, while the transmembrane and linker regions are less conserved. It is noteworthy that *Saccharomyces cervisiae* is the least conserved of the group.

CHAPTER II

IRE1α/XBP1 EXPANDS THE SECRETORY CAPACITY OF THE β CELL TO ACCOMMODATE POSTPRANDIAL INCREASED DEMAND FOR INSULIN SYNTHESIS AND SECRETION.

Abstract

Pancreatic β cells have a unique ability to increase insulin synthesis and secretion in response to glucose, although the mechanism(s) is largely unknown. Here, we tested whether the unfolded protein response transducer IRE1α that initiates unconventional splicing of *Xbp1* mRNA is required for glucose-stimulated insulin secretion. β cell-specific *Ire1α* deletion in both neonatal and adult mice caused hyperglycemia due to β cell failure. Ultrastructure analysis demonstrated IRE1α is required for integrity of cellular organelles and for insulin granule biogenesis. We show IRE1α-dependent *Xbp1* mRNA splicing is required for glucose-stimulated increases in ER proteins critical for proinsulin translation, signal peptide cleavage and secretion. Inversely, *Ire1α* deletion increases mRNAs encoding extracellular matrix and plasma membrane proteins associated with oxidative stress, inflammation and fibrosis in islets. Taken together, these findings demonstrate β cells require IRE1α for glucose-stimulated expansion of the ER to support increased insulin production and prevent islet destruction.

Introduction

Type 2 diabetes (T2D) is a disease epidemic caused by a failure of pancreatic β cells due to genetic susceptibility and dietary stress prohibiting the production of sufficient insulin to maintain glucose homeostasis [187]. As a consequence of obesity, insulin resistance and hyperglycemia develop that pressure β cells to increase insulin secretion. Although β cells can compensate by increasing insulin production, approximately one-third of individuals with insulin resistance develop β cell failure and diabetes [188]. Unfortunately, the mechanisms leading to β cell failure in T2D are poorly understood, although several factors that contribute to β cell failure include hyperglycemia, hyperlipidemia and inflammatory cytokines [8, 189]. Recent studies suggest that increases in proinsulin synthesis overwhelm the capacity of the

Endoplasmic Reticulum (ER) to properly fold, process, and secrete insulin in response to glucose [10, 189, 190-192]. Under these conditions, termed ER stress, cells activate the adaptive unfolded protein response (UPR) to resolve the protein-folding defect. The UPR is a set of well-coordinated signaling events at the levels of gene expression and protein synthesis, folding and degradation [193]. As increased expression of UPR genes was observed in islets from humans with T2D [46, 134], it was proposed that the UPR is activated in β cells as part of a compensatory mechanism to increase insulin production to compensate for insulin resistance [10, 194]. However, the notion that IRE1α increases the capacity for insulin production in primary β cells is untested and recent results imply IRE1α has a role opposite of XBP1 [28].

The β cell is uniquely specialized for glucose-stimulated insulin secretion (GSIS). Immediately after glucose stimulation, insulin granules are released to maintain euglycemia. To restore secretory granule content, proinsulin transcription and translation increase up to 10-fold [195-200]. To accommodate the increased demand for proinsulin synthesis, there is an inherent requirement to expand the capacity of the secretory pathway to fold and process preproinsulin to insulin for trafficking and storage in secretory granules. However, the mechanism by which the β cell ER adapts to this acute demand to increase insulin synthesis and secretion is largely unknown.

IRE1, the most conserved transducer of the UPR, is comprised of an ER lumenal domain, a single transmembrane region, and a cytosolic domain containing both protein kinase and endoribonuclease (RNase) catalytic functions. UPR activation leads to IRE1 dimerization, *trans*-autophosphorylation, and RNase activation that initiates unconventional cytoplasmic splicing of *HAC1* mRNA in yeast and *XBP1* mRNA in metazoans causing a translational reading frame shift to produce a potent transcriptional activator [14, 104, 201-208]. HAC1 induces phospholipid synthesis and regulates ~300 genes or ~6% of the yeast genome primarily encoding functions in the ER, including protein folding, N-linked glycosylation, lipid modification, and ER-associated protein degradation (ERAD) [209 22, 210]. Similar reports have been made for metazoan spliced XBP1 (XBP1s) [51, 211-213].

In mammals, the UPR signals through two additional ER transmembrane sensors; the dsRNA-activated Protein kinase (PKR)-like ER Kinase (PERK) and the basic leucine zipper (bZiP)-containing Activating Transcription Factor 6 (ATF6). ATF6α and XBP1 have very similar DNA binding motifs and act synergistically on the ER-Stress Element II [104, 117, 214, 215]. Eukaryotes have evolved additional genes encoding tissue-specific UPR transducers as a means to increase tissue specificity and diversity in the response [100, 216-219]. The mechanism that links the UPR pathways is their common activation by the accumulation of misfolded

proteins that promotes release of the ER protein chaperone BIP from IRE1α, PERK, and ATF6 resulting in transcriptional and translational responses directed to resolve the protein folding defect. Transcription is altered by increasing the nuclear localization of the bZiP - containing transcription factors (TFs) XBP1s, ATF4, ATF6 and CHOP[79, 108, 220]. General mRNA translation is attenuated by PERK-mediated phosphorylation of eIF2α and is restored by GADD34-directed de-phosphorylation. A growing number of reports also suggest that IRE1α relieves the ER protein-folding burden by degrading ER-localized mRNAs, in addition to its well-established function in splicing of *XBP1* mRNA [127, 129, 221-225].

A physiological requirement for IRE1α in the β cell is suggested through analysis of Wolfram Syndrome, also known as DIDMOAD (Diabetes Insipidus, Diabetes Mellitus, Optic Atrophy and Deafness), that has 60% mortality by the age of 35 [226]. Wolfram Syndrome is caused by loss-of-function mutations in the *WFS1* gene that result in β cell failure characteristic of type 1 diabetes [227]. In addition, polymorphisms within the *WFS1* gene are linked to T2D [29 228-230]. *WFS1* encodes an ER-resident protein associated with protein folding, calcium homeostasis and ERAD functions [177, 172, 231, 232, 166]. WFS1 is proposed to regulate the UPR through mediating degradation of ATF6α as well as glucose-stimulated cAMP production [166, 233]. Because XBP1s binds to and activates the *WFS1* promoter [178], the IRE1α-XBP1s-WFS1 pathway represents a direct pathway between ER stress, β cell failure and diabetes.

Although studies of IRE1α function using insulinoma cell lines, primary *Ire1α* heterozygous islets and Mox-Cre RNAi mice have been reported, the mechanistic requirement for *Ire1α* in β cells *in vivo* and isolated islets is unknown [234-238]. Here, we demonstrate IRE1α is required for *Xbp1* mRNA splicing to induce glucose-stimulated genes that encode critical functions for the secretory pathway of the β cell, including ribosome recruitment to the ER, co-translational translocation, signal peptide cleavage of preproinsulin, protein folding, trafficking, ERAD and anti-oxidant protection.

Results

Developmental deletion of *Ire1α* in β cells causes hyperglycemia and hypoinsulinemia

To study the impact of the β cell-specific *Ire1α* deletion, mouse matings were performed to produce a combined genotype of one floxed *Ire1αFe* allele [99] in combination with either wild-type *Ire1α+* or *Ire1α- null* alleles [119] in the absence or presence of a transgene encoding Cre recombinase driven by the rat *Ins2* promoter (Figure 2-10A). This Cre recombinase is expressed selectively in pancreatic β cells from mid-gestation (E9-11.5) [239]. This cross yields *Ire1αFe/-; Ins-Cre+* (herein designated *Ire1α-βKO*) mice at nearly the

expected frequency (Figure 2-10B) and littermate *Ire1αFe/+;Ins-Cre+* (herein designated *Ire1α-βHet*) heterozygous animals that were used as controls. The *Ire1αFe* allele is deleted in both animals in the β cells, however, in the control group IRE1α functionality persists due to the presence of a second *Ire1α* wild-type allele. The *Ire1α* β cell-specific deletion abrogated *Xbp1* mRNA splicing in islets at 1 month of age (Figure 2-10C). Blood glucose measurements revealed that hyperglycemia appeared at 4-5 weeks in male mice and was significant at 8 weeks, while female mice did not develop hyperglycemia until 12 weeks of age (Figure 2-10D). However, glucose tolerance tests (GTTs) revealed glucose intolerance in 2-week old mice of both genders (Figures 2-1A, 2-10E). Consistent with the glucose intolerance at 2 weeks, *in vivo* insulin secretion upon short fast and re-feeding was also reduced (Figure 2-1B). Analysis of pancreatic insulin content over the first few weeks of life demonstrated a primary defect in expansion of the β cell mass in the *KO* mice (Figure 2-1C). Similarly, confocal immunofluorescence microscopy indicated that islets from *Ire1α-βKO* mice were frequently diffuse, small, disorganized and contained less insulin (Figure 2-1D). Increased β cell apoptosis was identified by the appearance of TUNEL-positive cells surrounded by insulin staining (Figures 2-1E, 2-10F). Electron microscopy revealed *KO* β cells contained fewer granules and mild ER distention, while these abnormalities were not detected in pancreas sections from control *Het* mice (Figure 2-1F). The results from the β cell-specific developmental *Ire1α* deletion demonstrate that IRE1*α* is required for neonatal expansion of β cell mass and function.

***Ire1α* deletion in adult β cells reduces proinsulin synthesis, insulin content and secretion, but not insulin mRNA levels**

Since the reduced β cell mass in newborn pups upon developmental deletion of *Ire1α* may result from decreased proliferation, differentiation and/or survival of β cells, we next determined whether adult, differentiated β cells require IRE1α. To accomplish this, *Ire1α* was deleted in an inducible manner by mating mice with the *Ire1α Fe* allele and mice transgenic for *Ins2-CreER* that encodes a Cre recombinase activated by the estrogen antagonist tamoxifen (Tam) [240]. This inducible model allows for synchronous *Ire1α* deletion in mature β cells to more precisely evaluate the requirement for IRE1α in β cell function. For this *CreER* model, unless otherwise noted, the control mice have the *Ins2-CreER* transgene in an $Ire1\alpha^{Fe/+}$ background, herein referred to as (*Het*) and the β cell-specific *Ire1α*-null mice have *Ins2-CreER* in an $Ire1\alpha^{Fe/-}$ (herein referred to as (*KO*). As the deleted $Ire1\alpha^{Fe}$ allele can produce a protein that acts as a dominant-negative, deletion of the $Ire1\alpha^{Fe}$ allele caused mild hyperglycemia in mice having a functional *Ire1α* allele and the amount of spliced *Xbp1*

mRNA was also reduced when compared to wild-type (*Ire1α*$^{Fe/+}$ in the absence of CreER) control mice (Figure 2-11B). Measurements of fasting blood glucose and GTTs performed over 42 weeks after Tam injection demonstrated hyperglycemia appears at 4 weeks in the *KO* mice (Figures 2-2A & B). Because the peak in hyperglycemia occurred at 6 weeks post-Tam injection, unless specified, further experiments were conducted at this time (Figure 2-11A). Four hours of dietary fasting followed by a 30 minute re-feeding increased serum insulin ~3-fold in *Het* mice, however, the response was significantly blunted in *KO* mice whereas proinsulin was increased, another hallmark of diabetes (Figures 2-2C & 2-11C). This secretory defect was logical considering pancreatic insulin and proinsulin contents were significantly reduced in *KO* mice to 57.1% and 80.7%, respectively (Figures 2-2D, E & 2-11D). Confocal immunofluorescence microscopy also demonstrated the Tam-induced deletion reduced pancreatic insulin and proinsulin staining (Figures 2-3A & 2-11E). Next, pulse-chase analysis demonstrated proinsulin synthesis was reduced by 47% resulting in reduced insulin in *KO* mice 6 weeks post-Tam injection (Figure 2-3B). In addition, infection of wild-type islets with adenovirus expressing a kinase-active but RNase-dead, dominant-negative IRE1α-K907A mutant (*Ad-K907*) described previously (Tirasophon W and Kaufman RJ, 2000) also reduced proinsulin synthesis to a similar extent as Tam-induced *Ire1α* deletion (Figure 2-3B). However, in isolated islets incubated for 12 hours in 12mM glucose there was no significant change in the expression of most β cell-specific mRNAs including *Ins1* and *Ins2*, despite an 88% reduction of *Ire1α* mRNA from the *Ire1α*^{Fe} allele in the *KO* group, accompanied by an 81% decrease in *Xbp1* mRNA splicing (Figures 2-3C & 2-11B, F). Significantly, these results show that functional IRE1α kinase and RNase domains are required in β cells to maintain proinsulin synthesis, yet not *Ins1* or *Ins2* mRNA expression.

***Ire1α*-null islets exhibit ER stress**

Analysis of mRNA in islets isolated from *KO* mice at 6 weeks post-Tam injection and incubated in 12mM glucose 12 hours demonstrated that *Ire1α* deletion significantly reduced expression of known XBP1s target genes *Atf6α, Pdi1, Fkbp11*, *Erdj4* and *Wfs1* [51, 58, 178, 241, 242, 243] (Figure 2-4A). However, the expression of the ER chaperones HSP5A (BIP), GRP94 and ERP72 and of the pro-apoptotic factor DDIT3 (CHOP) was increased by *Ire1α* deletion (Figure 2-4A). Results from qRT-PCR performed at 4 and 12 weeks post-Tam injection were consistent but not as significant as the 6-week deletion data (data not shown). Consistent with the increased BIP and GRP94 mRNA, immunofluorescence analysis using an antibody that reacts with the ER-retrieval signal (KDEL) to detect BIP, GRP94 and ERP57, also demonstrated increased staining in *Ire1α*-deleted β cells and increased co-localization with

the plasma membrane-resident protein GLUT2 (Figures 2-4B & 2-12A). The diffuse GLUT2 staining and increased co-localization with the ER markers is indicative of a trafficking defect from the ER to the cell surface. Western blotting also confirmed *Ire1α* deletion increased expression of BIP and GRP94 by ~2.7- and ~1.9- fold, respectively (Figure 2-4C). Electron microscopic analysis of pancreas sections 2 weeks post-Tam injection identified that *Ire1α*-null β cells contain many distended membranes and/or empty vesicles, a 43% reduction in insulin granules and multi-lamellar vesicles, suggestive of autophagy (Figures 2-4D and 2-12B-D). To more directly test whether *Ire1α* deletion causes increased misfolding of insulin an *Ire1α*-floxed insulinoma cell line was infected with Cre recombinase adenovirus or a control adenovirus then insulin was immunoprecipitated to examine the binding of KDEL-containing chaperones by western blot which indeed demonstrated that the deletion caused a dramatic loss of insulin content and binding of chaperones (Figure 2-4E). To test whether acute inhibition of IRE1α-dependent splicing of *Xbp1* mRNA disrupts the secretory pathway at the protein level, isolated wild-type islets were infected with adenoviruses expressing either β-Galactosidase or the K907A IRE1α-RNase mutant and then analyzed by mass spectrometry 72 hours post-infection (Figure 2-12E). The *Ad-K907A* infected islets demonstrated reduced levels of ER, Golgi, nucleosome and chromatin associated proteins while increased functional groups included cytoplasmic, actin-binding and rRNA processing proteins (Figure 2-12E). Groups that were enriched but common to the two groups without containing the same proteins were; mitochondrial, alternative splicing and transit peptide proteins to name a few (Figure 2-12E). Specifically decreased by IRE1α-K907A expression were the signal peptidase complex member SPCS1, the ER chaperone; CALR, trafficking proteins; ARFGAP3, TMEDs 3 and 6, and ERAD components; UFM1, UFC1. SSR1 and WFS1 fell below the level of detection when compared to control islets infected with *Ad-βGal*.

mRNA sequencing identifies *Ire1α*- and glucose- dependent mRNAs in islets

To study the effect of *Ire1α* deletion on glucose-regulated gene expression, we performed Illumina-based mRNA sequence (mSeq) analysis of mRNA isolated from islets after incubation in 6mM and 18mM glucose for 72 hours, to chronically stimulate insulin demand and since these conditions were reported to cause insulin mRNA degradation by IRE1α [234]. Treatment with 18mM glucose increased *Xbp1* mRNA splicing by 56.6% in *WT* islets compared to undetectable levels in *KO* islets when measured by conventional PCR flanking the IRE1α-dependent 26nt intron and capillary electrophoresis (Figure 2-5A). *Ire1α* deletion efficiency and *Xbp1* mRNA splicing were again confirmed by qRT-PCR (Figure 2-

13A). On average, mSeq detected over 22,000 mRNAs in the 18mM *KO* and *WT* samples that were visualized by heatmap (Figure 2-5B). Restricting the mRNAs to those with p-values $\leq$0.1 or $\leq$0.01 reduced the number of transcripts to ~4,500 and ~1,700, respectively. Expression fold changes are presented relative to the 6mM *WT* islet sample. In agreement with the qRT-PCR analysis of isolated islets incubated in 12mM glucose for 12 hours (Figure 2-4A), qRT-PCR and mSeq on 6mM and 18mM *KO* islets also indicated the expression of the XBP1s targets *Wfs1, Atf6α* and *Edem1* was reduced, whereas the expression of *Hsp5a, Grp94* and *Ddit3* was increased (Figures 2-4A & 2-13A). Similarly, under these conditions there was no significant difference in the levels of *Ins1* or *Ins2* transcripts as measured by either mSeq or qRT-PCR (Figures 2-5C & 2-13A), also consistent with the qRT-PCR results from *KO* islets isolated and incubated in 12mM glucose for 12 hours (Figure 2-3C).

In order to identify mRNAs induced and repressed in an *Ire1α*-dependent and/or glucose-dependent manner, we used 4-way Venn diagrams (Figure 2-6A). Specifically, 613 and 1338 mRNAs were decreased and increased, respectively, in *KO* islets, regardless of glucose. This analysis also identified 141 and 368 mRNAs that exhibited inverse trends during high glucose in *KO* versus *WT* islets (Figure 2-6B black versus and black and blue double brackets). These 4 gene lists were analyzed using online gene ontology (GO) programs "DAVID" and "ConceptGen" (Figure 2-6B). For mechanistic and realistic purposes those mRNAs with the lowest p-values are presented and were studied further (Figures 2-7, 2-8 & 2-9). As expected, the GO terms of the 613 genes with reduced expression regardless of glucose concentration in *KO* islets were most significantly enriched with ER, protein transport, ribosome and protein synthesis-related functions (Figure 2-6B). Analysis of the 141 genes for which expression was decreased in *Ire1α*-null islets and increased by 18mM glucose in wild-type islets generated similar GO terms (not shown). Within these 141 mRNAs dependent on both IRE1α and high glucose for expression, 24 were previously shown to bind XBP1s to their promoters [51], while 30 were shared with the 368 mRNAs increased in *Ire1α*-null islets (Figure 2-13B). Importantly, the XBP1s-dependent transcription factor MIST1/BHLHB8 was included in the *Ire1α*- and high glucose- dependent mRNAs, providing additional verification that this group of 141 mRNAs are both *Ire1α*- and XBP1s- dependent [51, 211]. Our analysis identified a new transcriptional co-activator downstream of IRE1α; ZCCHC12/SIZN1, that interacts with SMAD family members and p300/CBP and for which mutations are associated with X-linked mental retardation in males [244, 245]. Similarly, the second most significant *Ire1α*-dependent mRNA by p-value from the mSeq analysis was *Sec11C*, previously reported to be downstream of XBP1s and ATF6α [246]-

[247]. *Sec11c* was one of 11 other mRNAs involved in signal peptidase, ribosome-ER recruitment and translocon functions (*Srpr, Srprb, Srp9, Ssr(s) 1-3, Sec63, Sec61b, Sec61g, Spcs2* and *Spcs3*) (Figures 2-7A and ontology not shown) that were increased by high glucose in the wild-type islets and basally reduced in *Ire1α*-null islets, irrespective of glucose. Analysis of the promoter regions from these IRE1α-dependent mRNAs using "TFM Explorer" identified XBP1s binding sites were significantly over-represented (Figure 2-7A, 2-14A, E). Interestingly, the ATF6α binding site was the most enriched, with XBP1 ranking fifth (Figure 2-14E). In addition to known XBP1 transcriptional targets including *Erdj4*, *Wfs1* and *Mist1*, several mRNAs encoding ERAD functions normally increased by high glucose were decreased upon *Ire1α* deletion and high glucose; *Ufm1, Edems 1-3, Ube1dc1*) (not shown). Other functions of mRNAs dependent on IRE1α and high glucose for expression were associated with the extracellular matrix, protein folding and trafficking, the anti-oxidant response, and oxido-reductases (Figure 2-7).

The GO terms for the 368 mRNAs that were increased by high glucose in *Ire1α*-null islets but decreased by high glucose in wild-type islets were enriched for functions in the cell membrane, cytokines, apoptosis, oxido-reductase activities, DNA-binding, macrophage and the extracellular matrix (Figures 2-6B right panel, 2-9A). The multiple collagens identified in this latter group were reported as markers of Ehler's-Danlos syndrome [248] [249]. Taken together, these *Ire1α*-dependent mRNA expression trends suggest many intracellular processes are affected upon deletion of *Ire1α* that result in β cell ER failure and extra-cellular signaling. Next, we analyzed at a mechanistic level the consequences of these changes in gene expression that occur upon *Ire1α* deletion in the β cell.

Glucose-stimulated activation of IRE1α increases SRP-dependent ribosome recruitment and signal peptide processing.

As mentioned above, *Sec11c* was the second most significant glucose-stimulated *Ire1α*-dependent mRNA that clustered with 11 additional mRNA encoding functions in ribosome recruitment to the ER, translocon components and additional signal peptidase complex members (Figures 2-7A & 2-14A). These 12 mRNAs exhibit similar glucose-inducible IRE1α-dependent expression patterns when measured by qRT-PCR and exhibit IRE1α-dependent expression in mouse embryo fibroblasts and in murine liver (Figure 2-14B and not shown). This observation suggests there may be a defect in ribosome recruitment to the ER and/or signal peptide cleavage in the absence of IRE1α. Therefore, we first analyzed whether preproinsulin accumulates in islets after *Ire1α* deletion. Islets were isolated 12 weeks after *Ire1α* deletion and labeled to steady state with ^{35}S methionine/cysteine for 18 hours in

culture to analyze preproinsulin processing and secretion by reducing SDS-PAGE on Tris-tricine gels. The results show accumulation of both proinsulin at ~10kDa and a slower migrating ~12k Dalton species that corresponds to preproinsulin in the cell lysates and a lesser amount of synthesized, processed and secreted insulin from *Ire1α*-deleted islets (Figure 2-8B). The increased accumulation of a species corresponding to preproinsulin is attributed to reduced signal peptide cleavage. These results suggest defects in signal peptide cleavage as well as trafficking out of the cell. In this long-term isotopic labeling context, the accumulation of intracellular proinsulin in the null sample can be attributed to defective degradation and/or trafficking of proinsulin. Next, to provide additional evidence for a defect in signal peptide cleavage in the absence of IRE1α, we analyzed preproinsulin signal peptide cleavage in COS-1 cells that express the IRE1α-K907A RNase mutant delivered by adenovirus infection. *Ad-preproinsulin* infection alone or in combination with *Ad-βGal* produced a single intracellular species corresponding to proinsulin, since COS-1 cells do not process proinsulin to insulin. In contrast, co-infection of *Ad-preproinsulin* with *Ad-K907A* resulted in the accumulation of a ~2kDa slower migrating species, corresponding to preproinsulin, consistent with a defect in signal peptide cleavage in the absence of IRE1α RNase activity (Figure 2-8A). Lastly, we analyzed preproinsulin processing and glucose-stimulated ribosome recruitment to the ER immortalized β cell lines harboring two floxed *Ire1α* alleles (*Fe/Fe*) generated by breeding floxed *Ire1α* mice with transgenic mice expressing SV40 large T antigen under control of the rat insulin II promoter. Insulinomas were isolated and cultured *in vitro* to derive glucose-responsive *Ire1αFe/Fe* β cell lines. The Ad-Cre mediated deletion of this *Ire1a* floxed allele within an insulinoma cell line also resulted in preproinsulin accumulation when compared to the Ad-βGal control (Figure S5).

Next, to analyze glucose-stimulated ribosome recruitment to the ER, these *Ire1α Fe/Fe* insulinoma cells were either mock-infected or infected with *Ad-βGal* control virus and compared to *Ad-Cre* and *Ad-K907A* or both combined. At 48 hours after infection cells were shifted from 12mM glucose to 4mM or 36mM glucose for 2 hours and then cytosolic and membranous fractions were prepared for western blotting for the ribosomal small subunit protein RPS9 (Figure 2-8C) and qRT-PCR for 18S rRNA, *Ins1* and *Ins2* mRNAs (Figure 2-8D) all of which demonstrated the IRE1α-deficient contexts experienced disrupted glucose-stimulated recruitment of the ribosome, rRNA and insulin mRNAs to the membranous fraction. Similar western blotting results were obtained for another ribosomal protein RPSA (not shown). Furthermore, adenoviral expression of XBP1s alone increased secretion of insulin in the immortalized β cell line, whereas infection with *Ad-Cre* and *Ad-K907A* had the

greatest inhibitory effects on proinsulin content and insulin secretion (Figure 2-14D). These results indicate IRE1α-mediated splicing of *Xbp1* mRNA induces expression of mRNAs encoding diverse secretory functions with a significant enrichment for proteins involved in ribosome recruitment and signal peptide cleavage.

***Ire1α* deletion in β cells causes oxidative stress, inflammation and fibrosis.**

The GO analysis from mSeq of *KO* islets showed increased expression of mRNAs encoding functions related to oxidative stress, inflammation and the extra-cellular matrix many of which are plasma membrane proteins (Figures 2-6B, right panel and 2-9A). We were interested in identifying mRNAs from the mSeq data that upon exposure to high glucose, when IRE1α is activated, are increased in *Ire1α*-null islets and reduced in wild-type islets (Figure 2-9A top). The expression pattern of these mRNAs is consistent with either being: 1) degraded by IRE1α; 2) repressed by XBP1s; 3) induced by XBP1u; 4) stabilized as a consequence of defective ribosome recruitment to the ER; 4) CHOP-dependent; or 5) non-β cell derived. Venn diagram analysis of the mSeq data and previously reported RIDD target mRNAs [128, 221] identified 2 shared mRNAs with the 368 mRNAs decreased in control islets that were increased in null islets; MRC2/ENDO180 (Endocytic Collagen Receptor) and FBXW10 (F-box/WD repeat-containing protein 10). Next, we classified mRNAs where expression was increased by high glucose in wild-type islets, increased basally upon *Ire1α* deletion, and increased further by high glucose in *Ire1α*-null islets. We consider this group as *Ire1α*-independent compensatory mRNAs that include GRP94, BIP, iNOS, PDIAs 2/4 and GPX2 (Figure 2-9A middle). Lastly, we identified mRNAs that were decreased during high glucose in the control islets that were increased by *Ire1α* deletion irrespective of glucose concentration that include lysyl oxidases (LOX, LOXL1, LOXL3, LOXL4) and components of the extracellular matrix (MRC2, MMP2, VCAN, CILP, FBLN2, FMOD, COL1A2, COL3A1 and COL5A1) (Figure 2-9A bottom). Induction of these mRNAs suggests oxidative stress and/or inflammation is associated with *Ire1α* deletion that may originate from non-β cells such as α cells, macrophages, dendritic cells and/or endothelial cells, we dealt with this by also studying the floxed *Ire1α* insulinoma cell line (Figures 2-15A, 2-9D. Analysis by H2DCFDA staining of dissociated islets isolated at 14 weeks post-Tam injection detected a ~14% increase in ROS in the *Ire1α*-null β cells (Figure 2-9B). In addition, mitochondrial swelling, a hallmark of oxidative stress, was prevalent at 2 weeks post-Tam injection in *Ire1α*-deleted β cells (Figure 2-12C). Furthermore, upon acute adeno- Cre-mediated *Ire1α* deletion in *floxed (Fe/Fe)* isolated islets *in vitro,* lipid peroxides (HODE) increased ~33% compared to adeno-GFP-infected and wild-type islet control groups (Figure

2-9C). In support of the notion that the oxidative stress originated within the β cell, we observed that infection with adeno-Cre and/or the adeno-IRE1α-K907A RNase mutant in an immortalized homogenous β cell line containing the floxed *Ire1α* locus increased mitochondrial content, mitochondrial superoxide and cytosolic calcium which were reversed by co-expression of XBP1s (Figure 2-15A). According to each of our mRNA assays another potential source of ROS within the IRE1α-deficient β cell is iNOS/NOS2. Similarly, increased iNOS promoter activity was also observed in the β cell line infected with adeno-IRE1α-K907A mutant (Figure 2-9D), consistent with the increased iNOS expression measured by mSeq (Figure 2-9A) and qRT-PCR (Figure 2-16C). Although combined infection of the Fe/Fe insulinoma cells dramatically increased iNOS mRNA levels (Figure S6), we cannot rule out contribution of iNOS mRNA from macrophages, endothelial, α-cells and/or other cell types in the mRNA-Seq data on islets. For example, we detected a tendency toward increased infiltration of macrophages, measured by MAC2 staining, in the *Ire1α*-null islets, although statistical significance was not attained (Figure 2-16B). In addition, qRT-PCR did not detect increased expression of the collagens and lysyl-oxidases in upon inactivation of IRE1α in the immortalized β cell line, suggesting the increased expression of the mRNAs in *Ire1α*-null islets is derived from a cell type other than the β cell (Figure 2-16C). Similarly, Masson's trichrome stain for the collagens showed dramatic increases in intensity in the vasculature surrounding the *KO* islets, suggesting an endothelial derivation (Figure 2-9E and 2-16A) however mass spectrometry (Figure 2-12E) demonstrated increased collagens were detected in the *Adenoviral-K907A* expressing islet (not shown). These results indicate functional IRE1α within the *β* cell is required to protect from oxidative stress that otherwise contributes to β cell failure.

Discussion

An intriguing feature of eukaryotic cells is their capacity to adjust the secretory pathway according to demand. One of the most remarkable examples of this occurs during glucose stimulation of pancreatic β cells that increased proinsulin synthesis up to 10-fold. However, the mechanisms that signal this acute adaptive process are largely unknown. Our results support the notion that glucose stimulation of β cells requires IRE1α to expand the capacity of the secretory pathway to accommodate increased proinsulin synthesis, processing and trafficking. Through targeted deletion of *Ire1α* in β cells we demonstrated that IRE1α is required for two important processes early in the secretory pathway: 1) glucose-stimulated ribosome recruitment to the ER; and 2) signal peptide cleavage. In addition, protein folding, trafficking and degradation are also compromised by loss of the IRE1α pathway. Through

complementation with spliced XBP1, we show that the IRE1α endoribonuclease activity and its targeted splicing of *Xbp1* mRNA are required to activate transcription of a large set of genes that expand the β cell's secretory capacity.

Massive parallel sequencing of the transcriptomes of *Ire1α*-null and wild-type murine islets exposed to 6mM and 18mM glucose followed by Venn diagram generation has yielded many *Ire1α*- and glucose- dependent mRNAs. GO term analysis revealed that the β cell experiences hundreds of changes in its transcriptome upon *Ire1α* deletion and/or glucose stimulation. Analysis of the overlapping mRNAs that were both IRE1α- and high glucose-dependent identified they encode several of the most important functional aspects of the β cell, chiefly, pro-secretory and anti-oxidative stress response functions. Certainly, the contribution of non-β cells was observed in the mRNAs increased in *Ire1α*-null islets where β cell death, increased macrophage and endothelial cell inflammation was in part responsible. This notion was supported by findings in immortalized wild-type and *Ire1α*-null β cell lines where the expression of the lysyl-oxidases mRNAs was not altered. Surprisingly, mass spectrometry of islets infected with the K907A, RNase point mutant version of IRE1α revealed increased expression of collagens in agreement with mSeq which we originally attributed to endothelial cells due to the staining pattern obtained by microscopy and so the origin of the collagens can only be said to be islet derived at this point. Despite the confounding nature of the multiple cell types within the islet the mRNAs increased by the β cell-specific *Ire1α* deletion can now be used as markers of inflamed islets to be excluded from transplantation. Indeed, glucagon mRNA was increased significantly in both our mass spectrometry and mSeq/qRT-PCR analyses of *Ire1α*-deficient islets (Figures 2-5C and 2-13A). Our findings indicate that oxidative stress damages the *Ire1α*-deficient β cell in a cell autonomous manner, possibly through increased inducible nitric oxide synthase (iNOS) expression. In addition, islet damage is incurred by external influences, such as increased levels of lysyl-oxidases (LOXs), that are likely derived from endothelial cells and/or macrophages (Figures 2-9A, 2-9E, 2-16A and 2-16B). For mRNA-Seq analyses we did not dissociate the islets to isolate a pure β cell population because islet dissociation may introduce artefactual changes to the transcriptome. Although our study showed little overlap with reported "Regulated *Ire1α*-Dependent Decay" (RIDD) targets (MRC2 and FBXW10) (Table S4) this study did show substantial overlap with an XBP1 CHIP-Seq study that utilized immortalized β cells (MIN6) [51]. The degradation of insulin mRNAs by IRE1α was neither supported nor refuted by the expression trends we observed in *Ire1α* null islets by qRT-PCR, mSeq or in an immortalized β cell line. Instead, the interpretation from our study

is that the 12 mRNAs we focused on encoding proteins crucial for glucose-stimulated recruitment of ribosomes and their associated RNAs to the ER, translocon members and signal peptidase complex members combine to disrupt proinsulin synthesis and is the most functionally relevant explanation for the diabetic phenotype.

Surprisingly, we found *in silico* that ATF6α's binding sites like XBP1's are over-represented within the promoters of the genes we focused on in Figure 5. Future experiments where *Ire1α* is deleted in the β cells of *Atf6α*-null mice may provide an even more dramatic diabetic phenotype. Interestingly, the β cell seems to be much more sensitive to loss of *Ire1α* than fibroblasts and hepatocytes which may be due to the unique periodic increases in proinsulin synthesis coupled with basally low levels of anti-oxidant enzymes. Interestingly, while loss of *Perk* and/or *eIF2α* phosphorylation increases oxidative stress due to uncontrolled protein synthesis, the loss of *Ire1α* decreases proinsulin synthesis. Therefore the source of ROS in the *Ire1α*-deleted β cell may be different, possibly increased expression of oxidizing enzymes, reduced expression of anti-oxidant enzymes, disturbed ER-mitochondrial interactions and/or ER calcium leak. Future experiments will uncover how anti-oxidants reduce ROS derived from various sources and whether mice with *Ire1α* and *Atf6α* double-deletion are more diabetic than β-cell specific *Ire1α*-null mice.

Although it was presumed that the UPR coordinates adaptation through regulation of protein synthesis and gene expression, it is now becoming evident that each UPR sensor has evolved to fulfill specific requirements in different cell types. As far as the β cell is concerned, PERK-mediated phosphorylation of eIF2α is the most significant pathway that is essential to maintain the structural integrity of the ER, glucose responsiveness, and prevent oxidative damage. Loss of this pathway significantly compromises β cell function, as exemplified Wollcot-Rallison syndrome in humans. In contrast, ATF6α is not significantly required for beta cell function, as *Atf6α* deletion has a very modest β cell phenotype (REF). Our findings on IRE1 presented here and earlier studies on XBP1 (Lee AW and Glimcher LH, 2011) demonstrate that IRE1α-XBP1 is also required for β cell function. However, there are significant differences between the effects of deletion of PERK and IRE1α. Primarily, deletion of PERK decreases insulin gene expression, like a consequence of reduced expression of PDX1 and MAFA that accommodate oxidative stress. In contrast, *Ire1α* deletion results in a defect in glucose stimulation of proinsulin translation, without affecting insulin mRNA expression. However, both deletions cause a protein trafficking defect and oxidative stress. Taken together, both IRE1α and PERK are required to expand β cell mass through neonatal development [73, 155].

It is intriguing that deletion of *Ire1α* in some differentiated cell types, such as hepatocytes, has very little effect on cell function in the absence of an ER stress-inducing agent. In contrast, *Ire1α* deletion during embryogenesis affects multiple organs and cell types that function to secrete large amounts of protein, i.e., pancreatic acinar cells, hepatocytes, plasma cells and intestinal epithelial cells [119]. We propose that IRE1α is primarily required to expand the secretory capacity of the cells that accompanies cell differentiation, such as mature B lymphocytes into plasma cells, but is not required for the adaptive response to insults that disrupt protein folding in the ER [212, 213, 237, 250-254]. Although ATF6α has very little phenotype upon deletion in mice, cells are not capable of surviving severe acute ER stress [53]. Experiments using an inhibitor of IRE1α nuclease activity demonstrated that IRE1α is not required for the adaptive response to ER stress, but appears important in a cellular response to expand the cellular secretory capacity of a cell in response to differentiation and/ or stimuli to increase to increase protein secretion [225].

Experimental Procedures

Mouse husbandry. The generation of *Ins2-Cre* and *Ins2-CreER* mice was previously described [239]. The generation of the *Ire1α*-null [119] and "Floxed" *Ire1α Fe* [255] alleles was previously described. These alleles were back-crossed into C57Bl/6 mice for 6 generations and then bred into *Ins2-Cre* or *Ins2-CreER* transgenic C57Bl/6 mice to generate the developmental- and temporal- β cell-specific *Ire1α* deletion models, respectively. Mouse experiments were performed in triplicate and their islets were isolated at 4, 6 and 10 weeks post-Tam injection. The data presented are at 6 weeks post-Tam, except where noted. Littermate mice were used as controls. Heterozygous animals harboring the *Cre* allele were used as experimental controls to exclude Cre-dependent effects however the dominant negative nature of this group often resulted in an intermediate phenotype and so beyond figure 1 the wild-type animals are presented for clarity.

Tamoxifen injection. Tamoxifen (Sigma grade) was dissolved at 10mg/ml in corn oil overnight with agitation, and then 400ul was injected subcutaneously 6 times over a 12 day period.

Semi-quantitative real time PCR (qRT-PCR). BioRad's iScript cDNA synthesis was performed using blended oligo-dT and random primers on total RNA from islets purified using the Stratagene column based RNA purification kit. Sybr Green based detection system from BioRad was utilized and the ΔΔCt folds were calculated relative to the housekeeping genes β-Actin and 18S rRNA. Primer efficiencies were also determined to be ≥90% by cDNA dilution. General qRT-PCR primer sequences in mice were obtained from Primer

Bank; http://pga.mgh.harvard.edu/primerbank/, previously reported or available upon request if not in Supplemental Table 1.

Glucose tolerance testing. 20% glucose solution was used to inject 2g Glucose/1 Kg body weight into mice by intraperitoneal injection then blood glucose was recorded by tail snip glucometer readings over indicated times.

Pancreatic Insulin and proinsulin content and secretion measurements. CrystalChem Insulin ELISAs were used on 50mg/ml pancreas from acid ethanol extracts as previously described to determine total pancreatic content of proinsulin and insulin. Values were normalized to total protein concentration using Quant-IT fluorescence based protein detection kit. For *in vivo* secretion measurements were taken on serum.

Electron microscopy of Pancreas. Freshly dissected pancreas was fixed in Sorenson's buffer and processed by the University of Michigan Electron Microscopy Core facility. Blind scoring of MAC2 positive cells and insulin granules was performed and quantified using the tracing software Cell Profiler.

Immunofluorescent microscopy. Paraffin embedded pancreas sections were deparaffinized and rehydrated in sequential xylenes:ethanol:water 3 minute submersions then boiled for 10 minutes in citrate buffer for antigen retrieval. Antibody incubations of 1:500 anti-Insulin, 1:500 pro-insulin, 1:100 glucagon, 1:200 GLUT2, 1:500 KDEL and 1:1500 secondary conjugated fluorophores in 1% BSA, 1% FBS, TBST which was also used to block and wash with. The primary antibodies were incubated 24hrs. 4 degrees while the secondary incubation was for three hours at room temperature using 1:1000 dilutions. All images were adjusted identically as the controls for their brightness and contrast using 6 panels per mouse, 10 mice per genotype. Quantitation of signals was performed using the 'Cell Profiler' software and statistical analysis by student t-test derived p-values.

Antibodies for western blotting, immunoprecipitations and immunofluorescence. Antibodies used for proinsulin and/or insulin immunofluorescence, immunoprecipitation and western blotting were from HyTest cat. # 2PR8 (CCL-10) and Sigma cat. # K36AC10 while the insulin antibody for western blotting was from Life Technologies/Invitrogen cat. # 180067. Antibodies for KDEL and pEIF2α were from Enzo/Stressgen cat. # ADI-SPA-827 and Invitrogen/Life Technologies cat. # 44728G. Anti-pIRE1α is a homegrown rabbit antibody specific for the pS724 epitope. RPS9 goat antibody was from Santa Cruz cat. # sc162106. Rabbit anti-GLUT2 from Santa Cruz cat. # sc9117. Mouse anti-tubulin from Sigma cat. # T9026.

Adenoviral infections. 50 and 10 plaque forming units/ cell were used to infect islets and immortalized *Ire1α* Floxed β cell line; *Fe/Fe* respectively.

Glucose treatment of islets and cell lines. Islets/Insulinomas: Low glucose = 6mM/4mM (108/72mg/dL), medium glucose = 12mM/12mM (216mg/dL) and high glucose 18mM/36mM (324/648mg/dL).

Dual luciferase reporter assays. 24 hours after Fugene6 transfection of 5ug plasmid/ 1^6 cells dual luciferase activities were determined utilizing the Promega Dual Luciferase kit by normalizing to the 0.5ug co-transfected plasmid encoding Renilla luciferase. pGL2-NOS2Promoter-Luciferase was provided by Dr. Charles Lowenstein's lab by way of Addgene.

S35-Cys/Met pulse chase of islets. 50 isolated islets were picked and rinsed with 750ul cys/met free RPMI then incubated 30 minutes in 150ul Cys/Met free media supplemented with 250uCi/ml S^{35}-Cys/Met (Amersham Inc. Easy Tag Express product # NEG772002MC) before being chased by removal of hot media and addition of 500 fold excess unlabeled cys/met for 120 minutes. For gel loading, lysate immunoprecipitations were normalized by TCA precipitable counts. Samples and mock I.P.s (no Insulin Ab) underwent 16% Tris-Tricine-Urea gel electrophoresis followed by gel drying or transfer to PVDF for phosphor-imaging and quantitation using ImageQuant software.

mSeq transcriptome sequencing. The Illumina Genome Analyzer II was utilized to analyze cDNA synthesized from the mRNA purified from islets of 4 individual mice each contributing 50ng total RNA and prepared according to Illumina's mSequencing kit (Part # 1004898).

Bioinformatics analysis, gene ontology, p-value methodology and promoter analysis. IRE1α and glucose dependent mRNAs were identified by limiting the original 22k mRNAs reported on to those with ≥1.5 +/- fold changes relative to the 6mM *WT* control islets with ≤0.05 p-values in excel were loaded into the 4-way Venn diagram generator found at http://www.pangloss.com/seidel/Protocols/venn4.cgi**.** Gene ontology was determined primarily using the "DAVID Bioinformatics Database' at; http://david.abcc.ncifcrf.gov/**.** Clustering of concepts was cropped from the NCIBI web resource "ConceptGen" at /http://conceptgen.ncibi.org/core/conceptGen/index.jsp**.** "TFM-Explorer" was used for the *In silico* analysis of promoters for TF known binding site over-representation website: http://bioinfo.lifl.fr/cgi-bin/TFME/tfme.py**.**

Subcellular fractionation coupled to qRT-PCR: The Pierce kit catalog number: 78840 was used to generate cytosolic, membranous, soluble nuclear and insoluble fractions from both

islets and immortalized β cell line. Total amounts of RNA used in cDNA synthesis from each fraction were normalized to 1ug/ml and prepared according to manufacturer's protocol for the iScript-BioRad cDNA synthesis reaction. Fold changes for RN18S, INS1 and INS2 mRNA levels from the subcellular fractions are in ΔCt rather than ΔΔCt as normalizing to the RN18S (18S ribosomal RNA) would mask the ribosomal RNA recruitment defect.

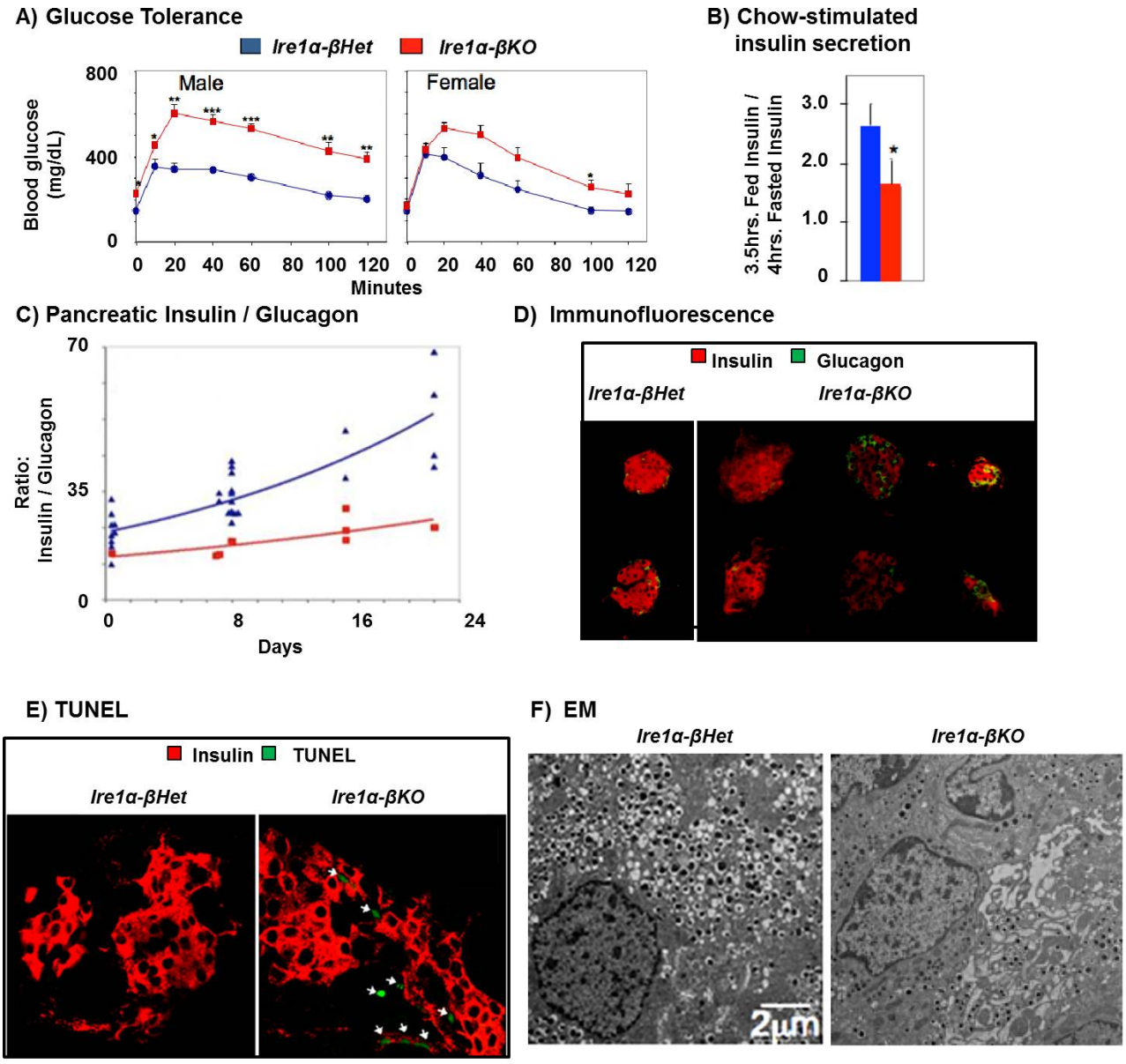

Figure 2-1. Developmental deletion of *Ire1α* in β cells causes hyperglycemia and hypoinsulinemia. (A) Glucose tolerance testing of *Ins2-Cre* 2 week old mice. (B) Chow stimulated insulin secretion *in vivo* following 4 hour fast, 2 week old mice. (C) Pancreatic insulin content normalized by glucagon. D) Immunofluorescent co-stain of insulin (red) and glucagon (green). (E) TUNEL (green)/Insulin (red) co-stain. (F) Electron microscopy of β cells show reduced insulin granule content in the null sample.

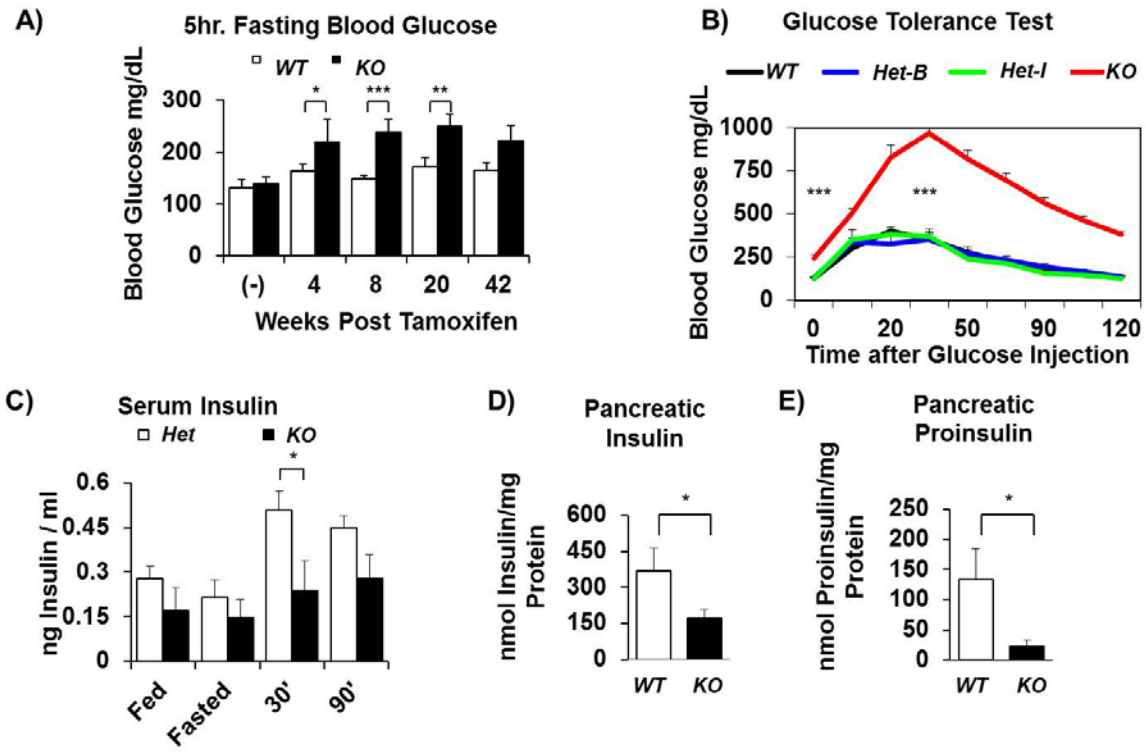

Figure 2-2. Tamoxifen-induced deletion of *Ire1α* in β cells causes a diabetic phenotype. (A) Time-course following tamoxifen administration of 5 hour fasting blood glucose levels. (B) Glucose tolerance testing on 6 weeks post-tamoxifen mice. (C) Serum insulin levels of mice 6 weeks post-tamoxifen; fed, fasted, 30 and 90 minutes after re-feeding (n=6). (D) and (E) Pancreatic insulin and proinsulin respectively from 6 weeks post-tamoxifen mice (n=5).

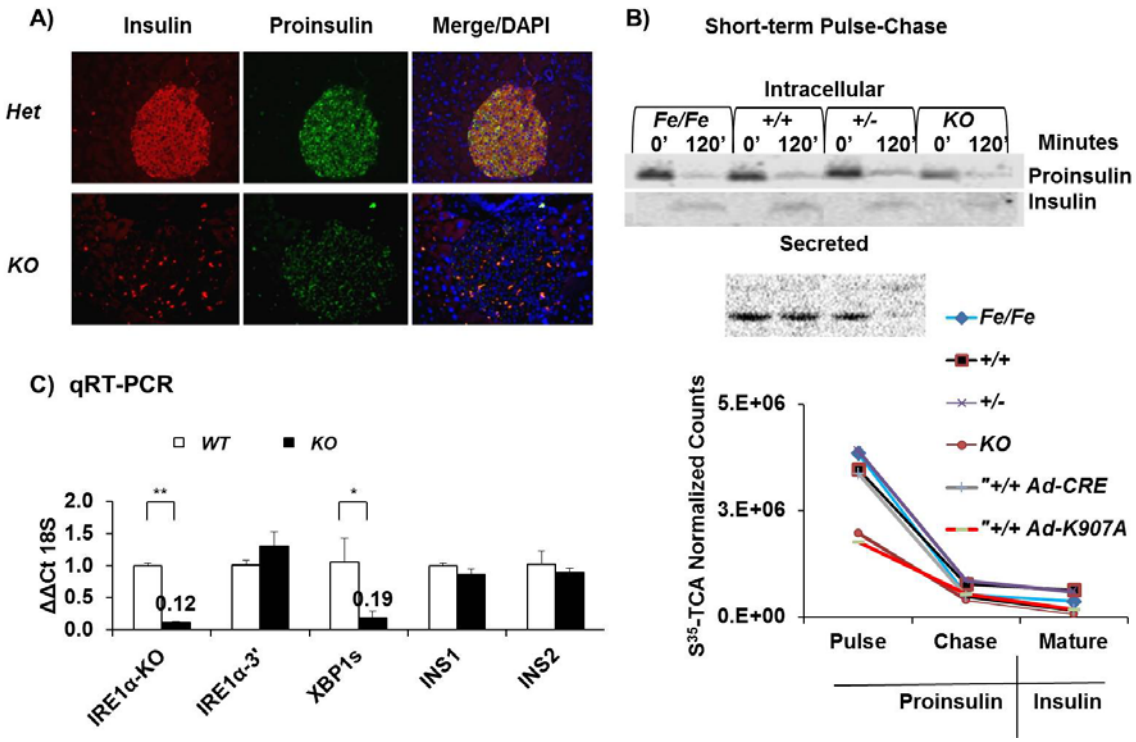

Figure 2-3. Tamoxifen induced deletion of *Ire1α* in adult β cells reduces proinsulin synthesis and insulin content but not insulin mRNA levels. (A) Immunofluorescent microscopy co-stain of Insulin (red), proinsulin (green) and DAPI (blue). (B) Short-term pulse-chase of isolated islets 6 weeks post-tamoxifen followed by total insulin Immunoprecipitations (KO; n=3). (C) Real time PCR (qRT-PCR) islets isolated 6 weeks post-tamoxifen (n=5).

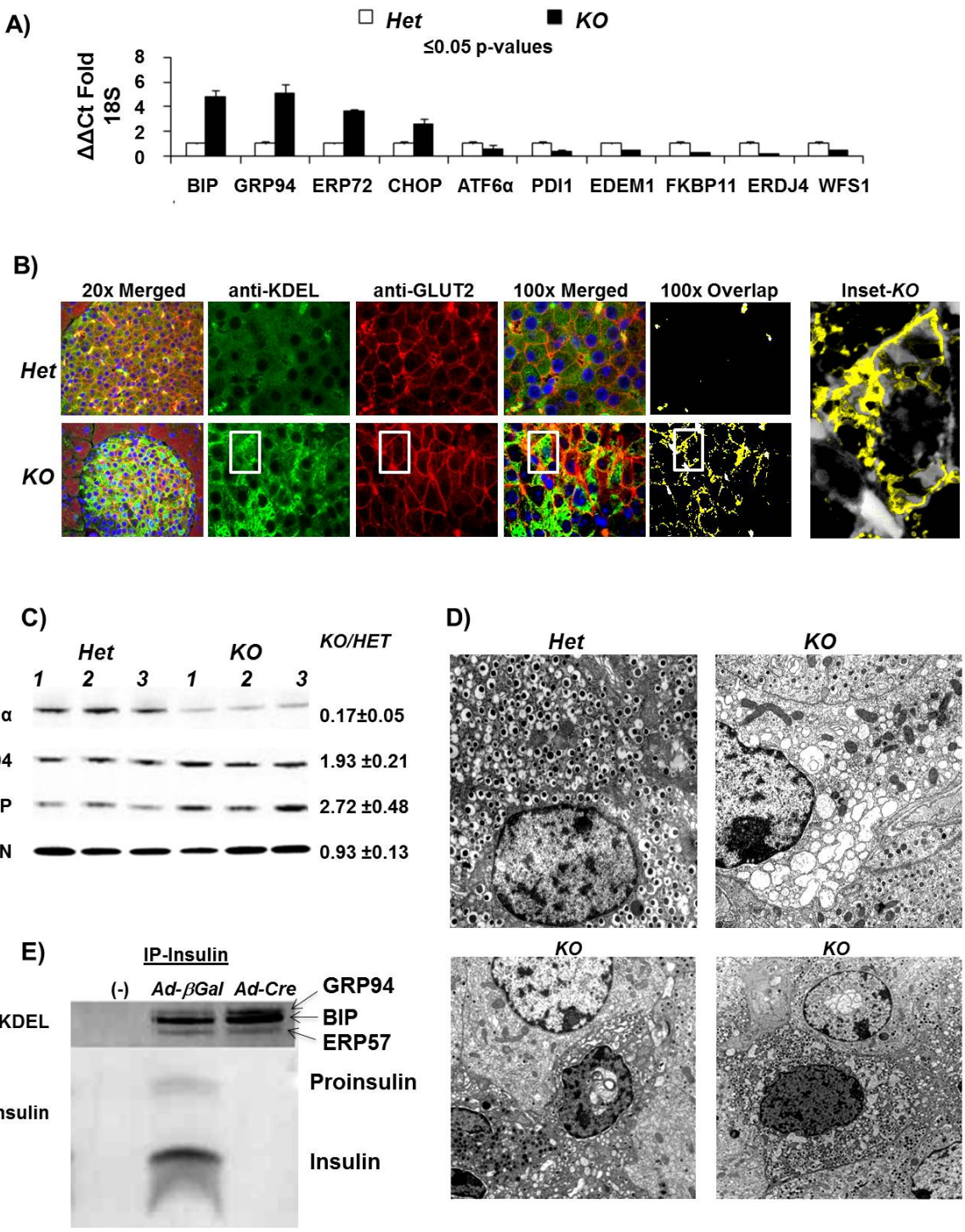

Figure 2-4. *Ire1α-KO* Islets undergo ER stress. (A) qRT-PCR on ER stress associated mRNAs found to be increased and reduced by tamoxifen increased deletion of *Ire1α* 6 weeks post-tamoxifen [(n=5)(p-values ≤0.05)]. (B) Immunofluorescent microscopy for KDEL containing BIP, GRP94 and ERP57 (green), plasma membrane protein GLUT2 (red) and DAPI (blue) with red-green overlap shown in yellow. (C) Western blotting of islets 4 weeks post-tamoxifen on IRE1α, KDEL, proinsulin and actin.(values on figure) (D) Electron microscopy of β cells from mice 4 weeks post-tamoxifen. (E) Wild-type and *Ire1α-null* insulinoma cells Immunoprecipitated with anti-insulin followed by western blotting for insulin and KDEL chaperones.

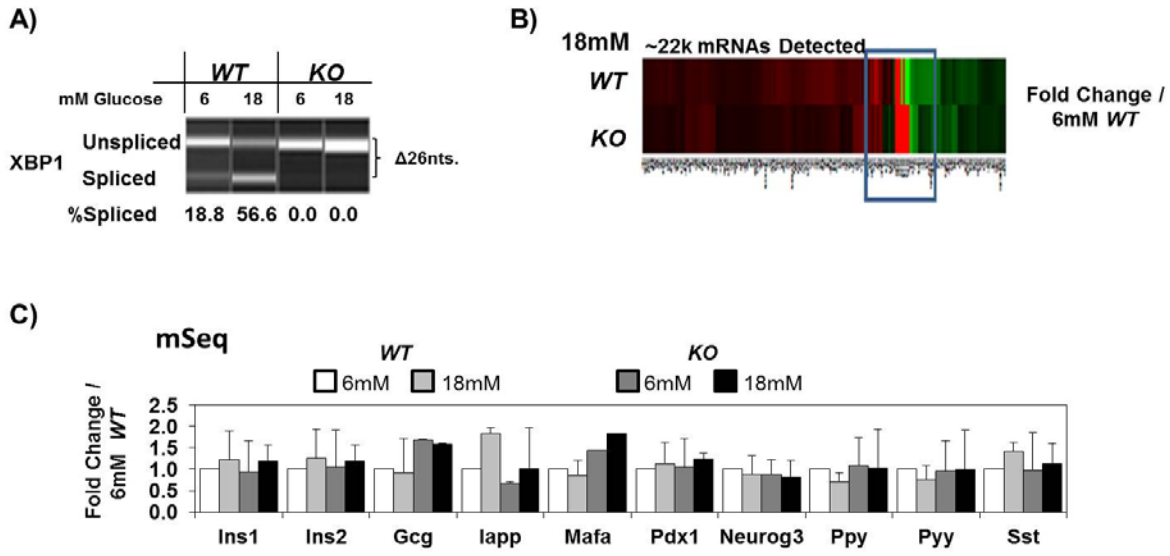

Figure 2-5. mRNA sequencing identifies *Ire1α*- and glucose- dependent mRNAs in islets. (A) PCR flanking XBP1's 26nt intron spliced out by IRE1α from the islet cDNAs used for mSeq analysis, 6mM versus 18mM glucose. (B) Global heatmap for the mRNAs detected by mSeq for 18mM *KO* & *WT* samples. (C) Select data from mSeq on β cell-specific mRNAs demonstrates no significant change to insulin transcripts.

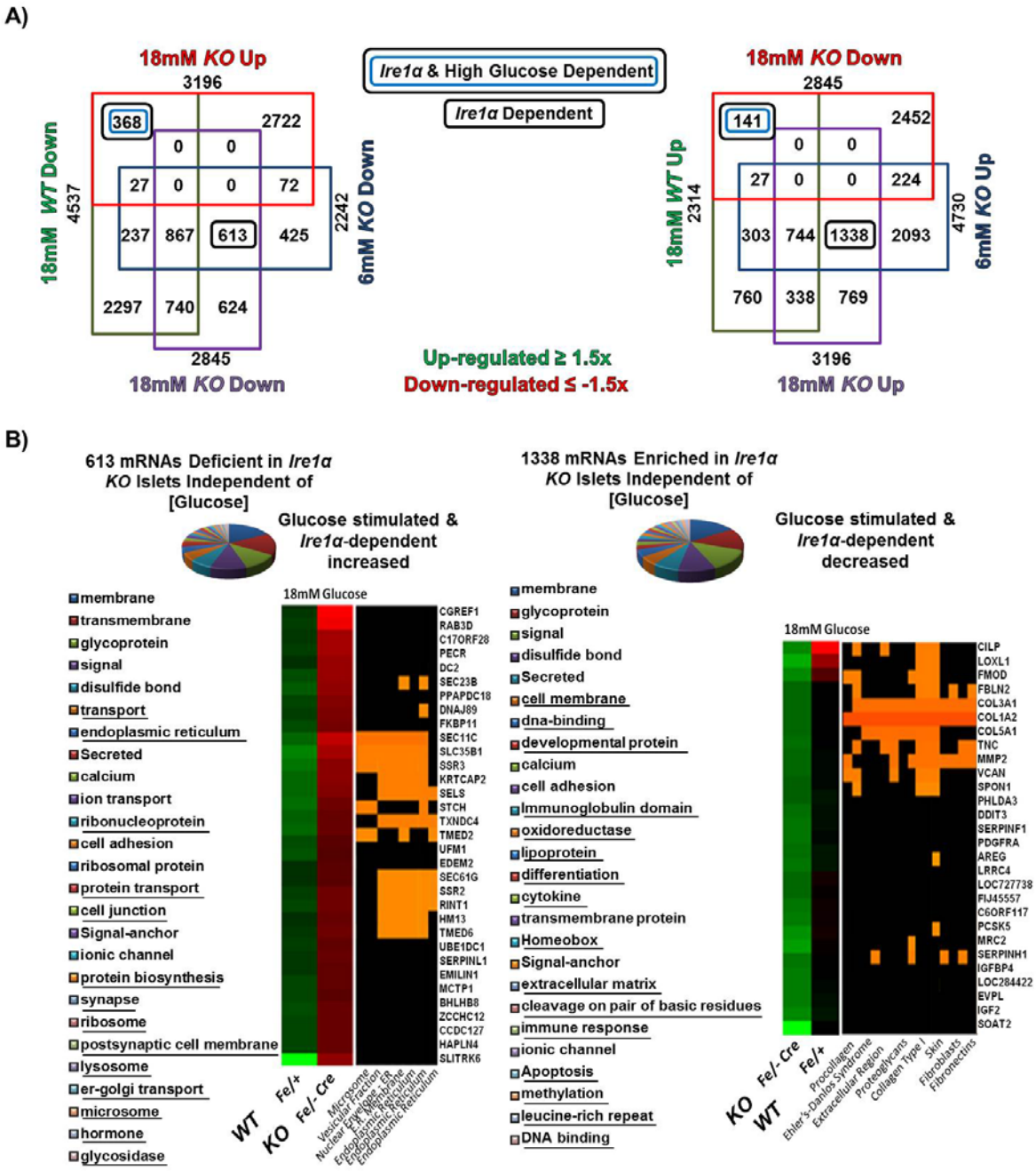

Figure 2-6. Massive parallel sequencing of the glucose stimulated *Ire1α-KO* islet. (A) 4-way Venn diagrams of *WT* versus *KO* during 6mM versus 18mM glucose exposure for 72 hours. *Ire1α-dependent* mRNAs in black bracket and additional glucose dependent mRNAs groups in black and blue double brackets. (B) Combined "DAVID" and "ConceptGen" gene ontology analysis of *Ire1α* and glucose dependent mRNAs. Underlined categories are specific to the genotype whereas the non-underlined are categories shared between KO and WT even though no single gene is shared.

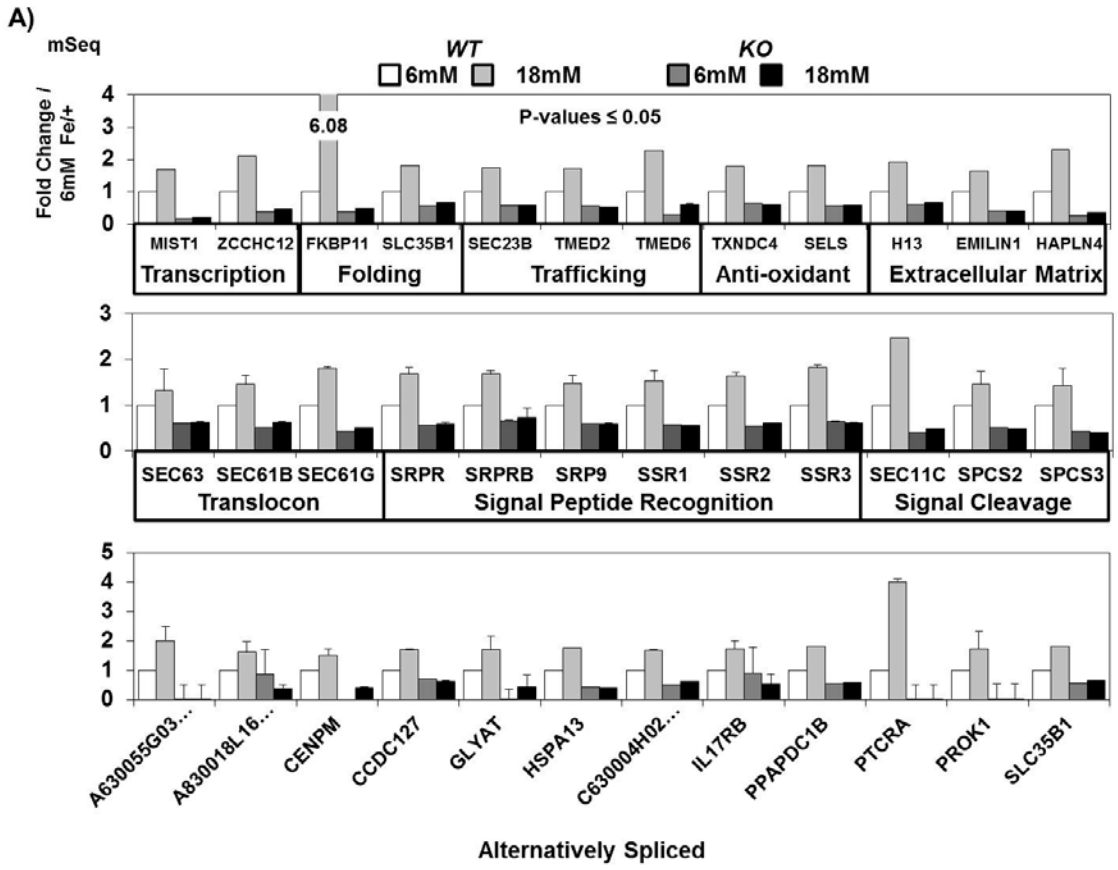

Figure 2-7. Glucose stimulated activation of IRE1α mediated *Xbp1* mRNA splicing increases pro-secretory mRNAs. (A) mSeq values for mRNAs that are both *Ire1α* and glucose dependent for their induction. (p-values ≤0.01). The bottom panel contains mRNAs singled out by "DAVID'-based gene ontology to be alternatively spliced. PTCRA (Pre-T cell Receptor alpha) is like a major determinant for repressing T-cells from infiltrating islets with function IRE1α.

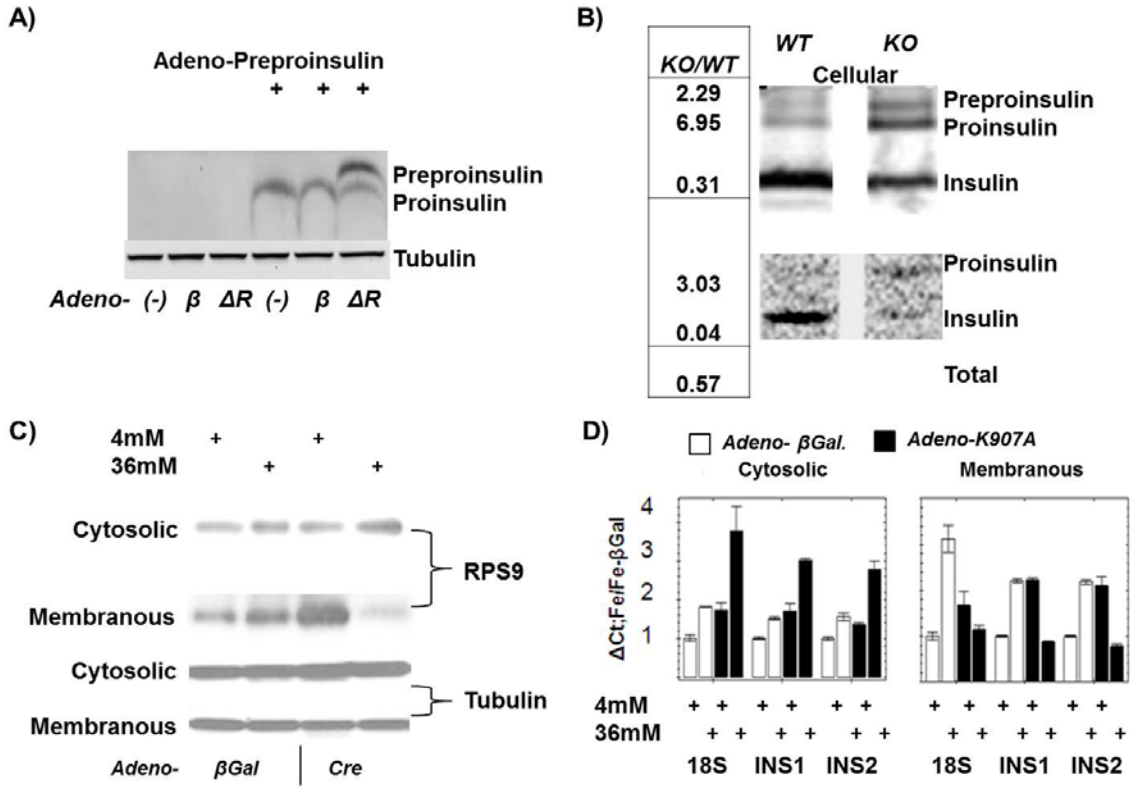

Figure 2-8. *Ire1α* is necessary for glucose stimulated signal peptide removal and ER-ribosome recruitment. (A) COS cells co-infected with adenoviruses expressing the wild-type IRE1α or the dominant negative IRE1α-K907A and preproinsulin by western blot after tricine electrophoresis. (B) 18 hour radio-labeling of isolated islets from the indicated genotypes where equal TCA precipitable counts from whole cell extracts or insulin immunoprecipitated from the media underwent tris-tricine electrophoresis and detected by phosphorimaging. (C) Subcellular fractionation of the floxed *Ire1α* β cell line after 2 hour glucose shift with and without the indicated adenoviruses were blotted for the ribosomal small subunit 9 and tubulin. (D) qRT-PCR on the fractions from (C).

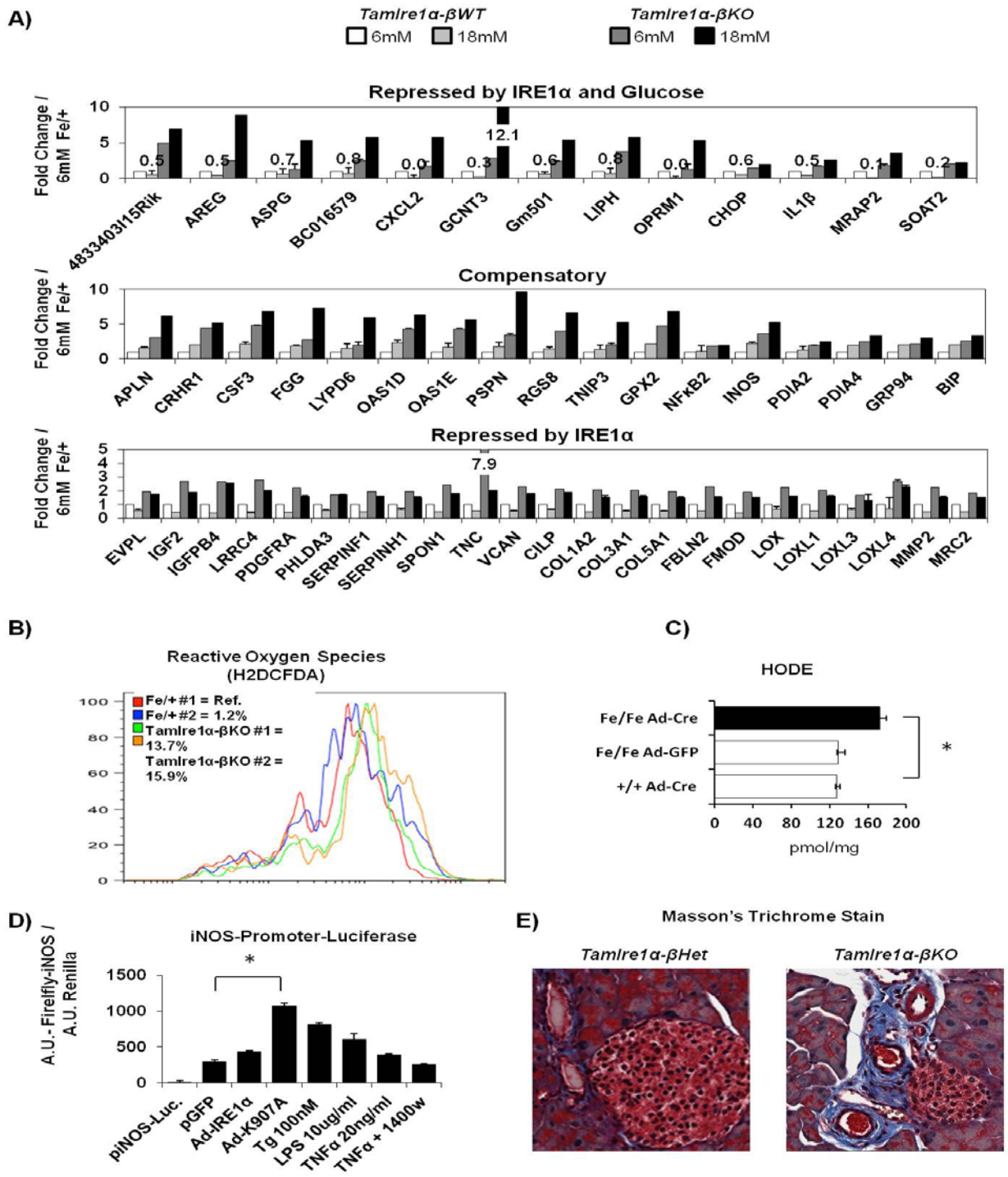

Figure 2-9. *Ire1αKO* islets accumulate oxidative stress, inflammation and fibrosis. (A) mSeq values for mRNAs found to be reduced by functional IRE1α. (B) Flow cytometry on dissociated islets for total reactive oxygen species using H2DCFDA shows an average increase of 14.8% in null islets 10 weeks post-tamoxifen (n=3, two shown). (C) Oxidized lipid (HODE) from islets of the indicated genotypes infected with Adenoviral Cre, GFP-control or no virus control. (p-value=0.0422) (D) Luciferase activity coupled to the iNOS promoter during various treatments after 4 hours or 48 hours following adenoviral infections. (p—value=0.029) (E) Masson's Trichrome stain (blue) for collagens surrounding and within *KO* islets co-stained with Haemotoxylin (red) and Eosin (black) co-stains.

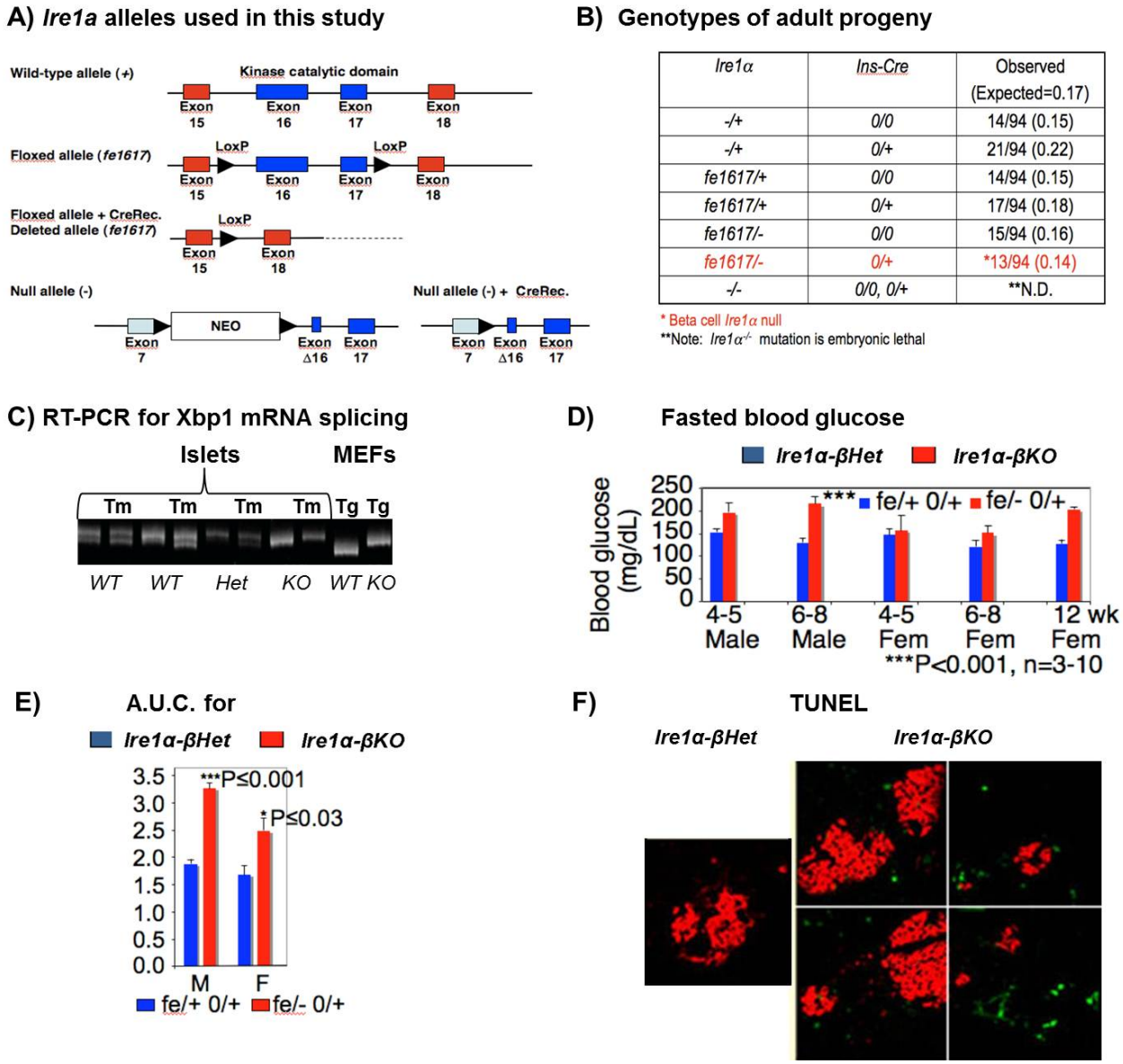

Figure 2-10. Developmental deletion of *Ire1α* in β cells, only the adaptable will survive. (A) DNA location of the alleles used to delete *Ire1α* in mice. (B) Birth outcomes for newborn mice from the *RIP-CreER* model. (B) Area under the curve for the glucose tolerance testing shown in Figure 1A. (C) Deletion of *Ire1α* abolishes *Xbp1* mRNA splicing by RT-PCR. (D) Emergence of the diabetic phenotype of hyperglycemia in newborn mice. (E) Statistical analysis of the glucose tolerance tests illustrated in figure 2-1. (F) Additional examples of *Ire1α-KO* β cell death by TUNEL stain.

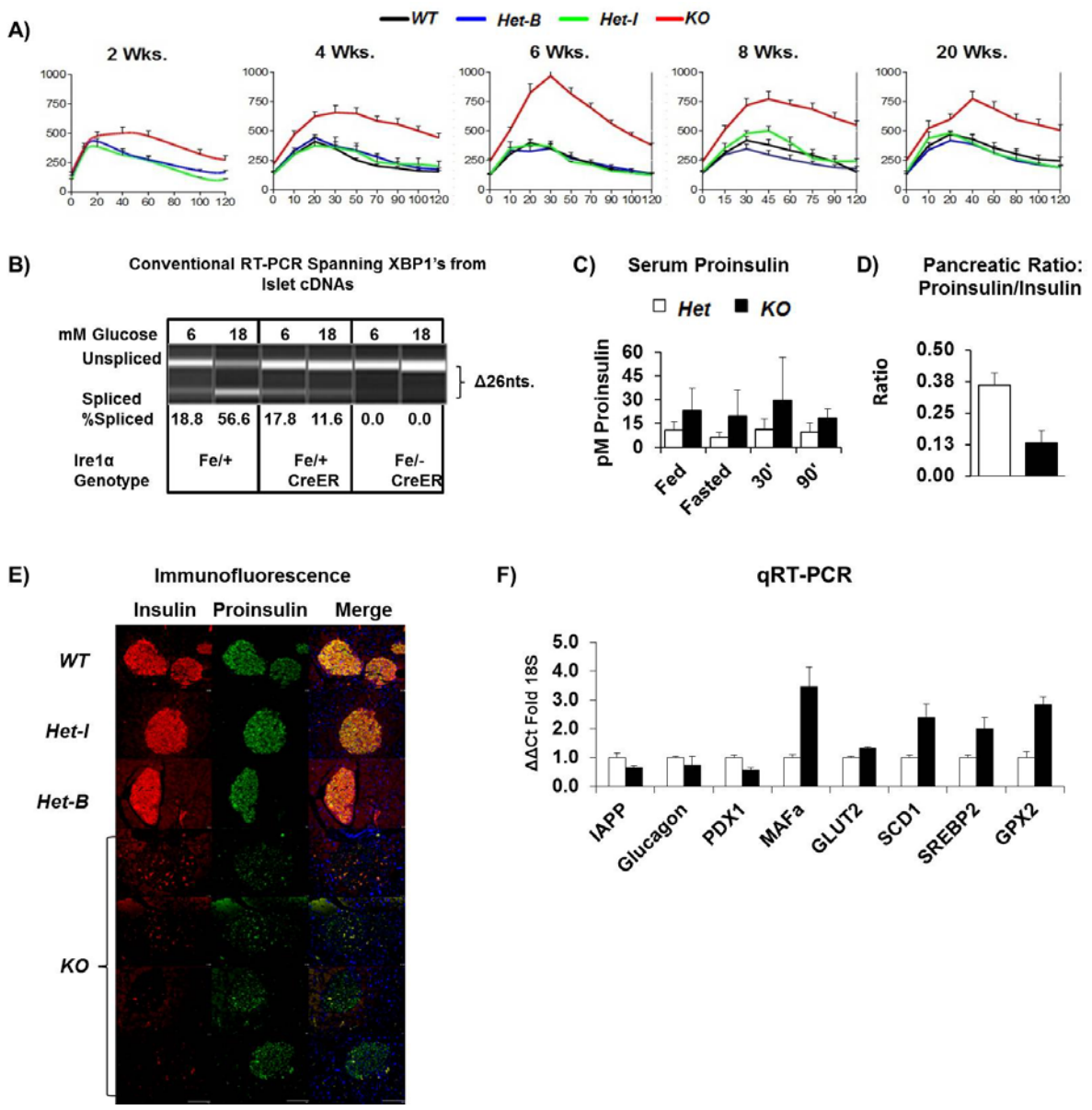

Figure 2-11. The emergence of the tamoxifen-induced *Ire1α-KO* diabetic phenotype. *(*A) Glucose tolerance testing weeks after tamoxifen injection. (B) RT-PCR demonstrating dominant negative effect of heterozygous *Ire1α* deletion on *Xbp1* mRNA splicing. (C) Serum proinsulin from mice 6 weeks post-tamoxifen. (D) Ratios of psncreatic Proinsulin/Insulin determined by ELISA. (E) Additional immunofluorescent microscopy on islets for insulin (red), proinsulin (green) and DAPI (blue). (F) Additional qRT-PCR on mRNAs reduced and increased 6 weeks post-tamoxifen in isolated islets. MAFA was found to be increased by mSeq as well.

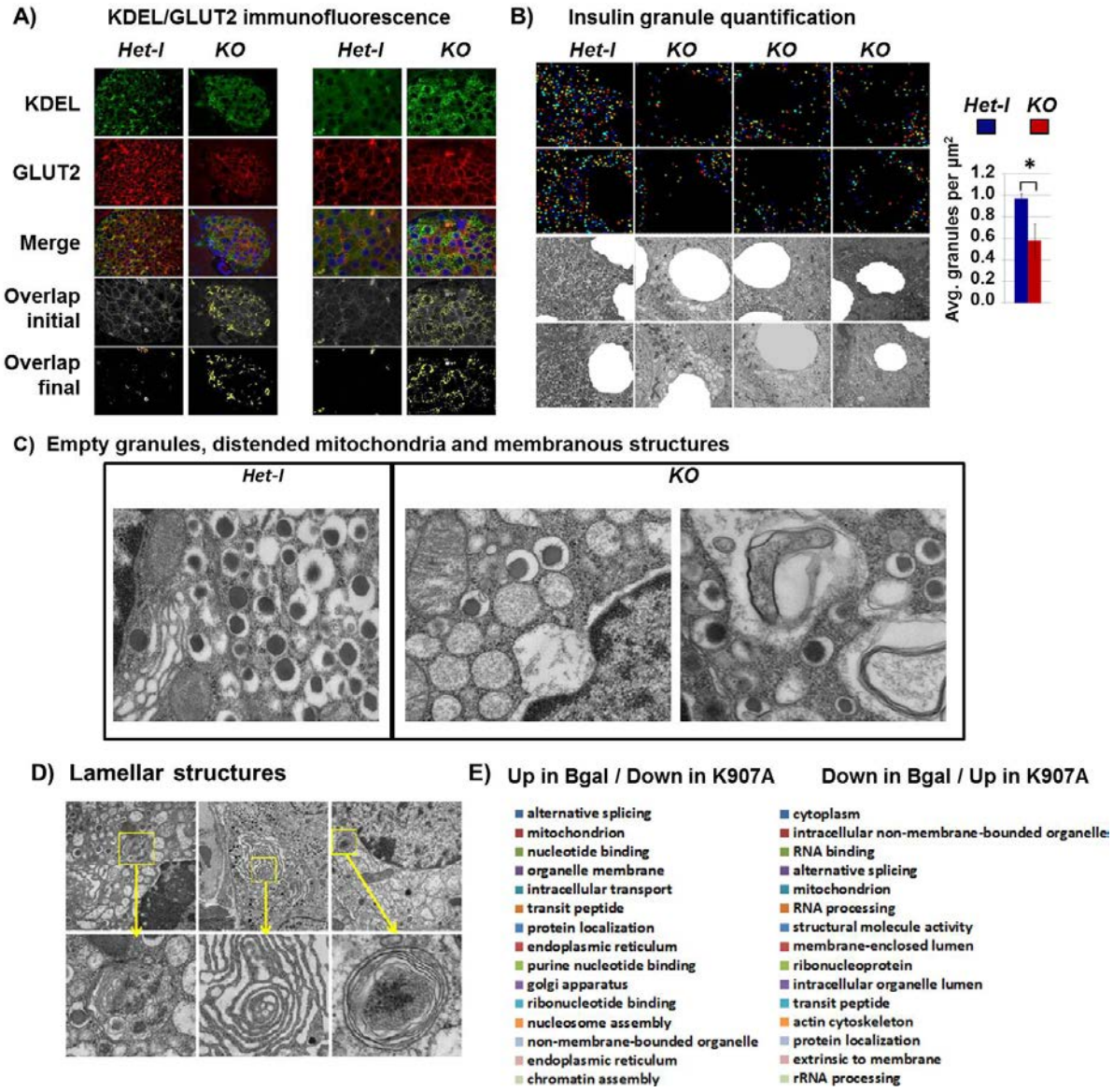

Figure 2-12. *Ire1α* deletion causes secretory pathway collapse (A) Additional immunofluorescent co-staining of KDEL and GLUT2 in islets. (B) Insulin granule quantification from electron micrographs (C) High magnification electron micrographs of defects *Ire1α* deletion causes. (D) Autophagic-like structures from electron micrographs in the *Ire1α*-knock-out β cell. (E) Mass spectrometry of *Ire1α*-dependent increased versus decreased gene ontology terms.

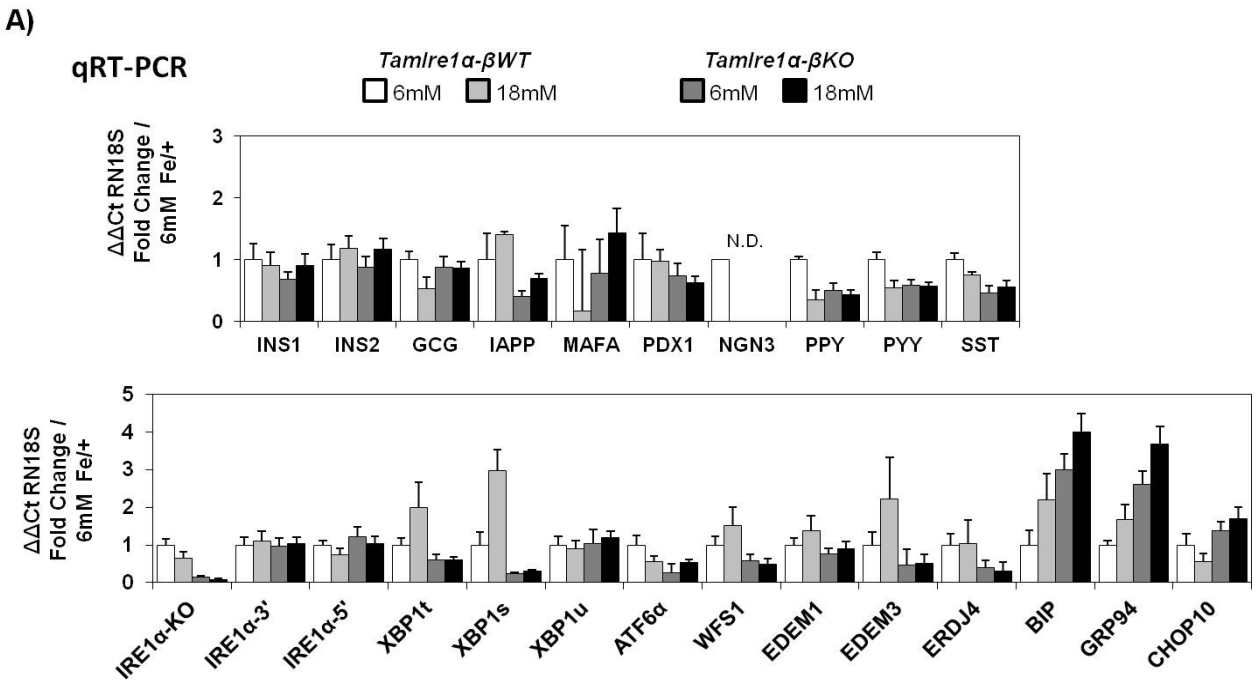

B)

A; Induced in Wt 18mM & Reduced in KO 18mM.
B; Reduced in Wt 18mM & Induced in KO 18mM.
C; ChIP study MIN6 and myotubule cells.
*; Multiple Gene Symbols altered the original totals.

D:24

DDOST
EDEM2
FEN1
Fkbp2
Gm10124
Gm6340
Gm6568
H47
LOC100044248
LOC100048726
Lman1
MYL4
Nek11
Pecr
Rpn2
SEC23B
SLC35B1
SRPR
SSR3
cks1b
dnajb9
rrm2
ssr2

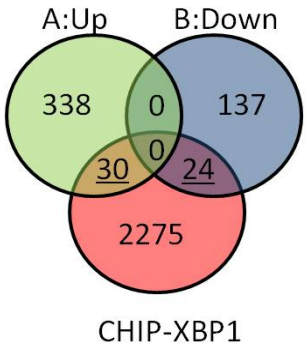

E:30

2610528J11Rik
9230105E10Rik
DDIT3
Fgf7
GABRA5
GIMAP5
Gm11275
H2-Ab1
Hist1h4a-d
Hist1h4f
Hist1h4h-k
Hist1h4m
Hist2h4
Hist4h4
ITGAL
LOC641240
LOC674678
LOC675296
LRMP
Rmcs2
SERPINH1
SLC30A3
Speer2
Zfp521

Figure 2-13. *Ire1α* deletion precludes *Xbp1* mRNA splicing (A) qRT-PCR on islet-specific and ER-stress related mRNAs to verify mSeq trends. (B) Overlapping genes from our β cell-specifc *Ire1α-KO* mSeq study and a previous CHIP-Seq study performed by Acosta-Alvear et. al. Performed on XBP1.

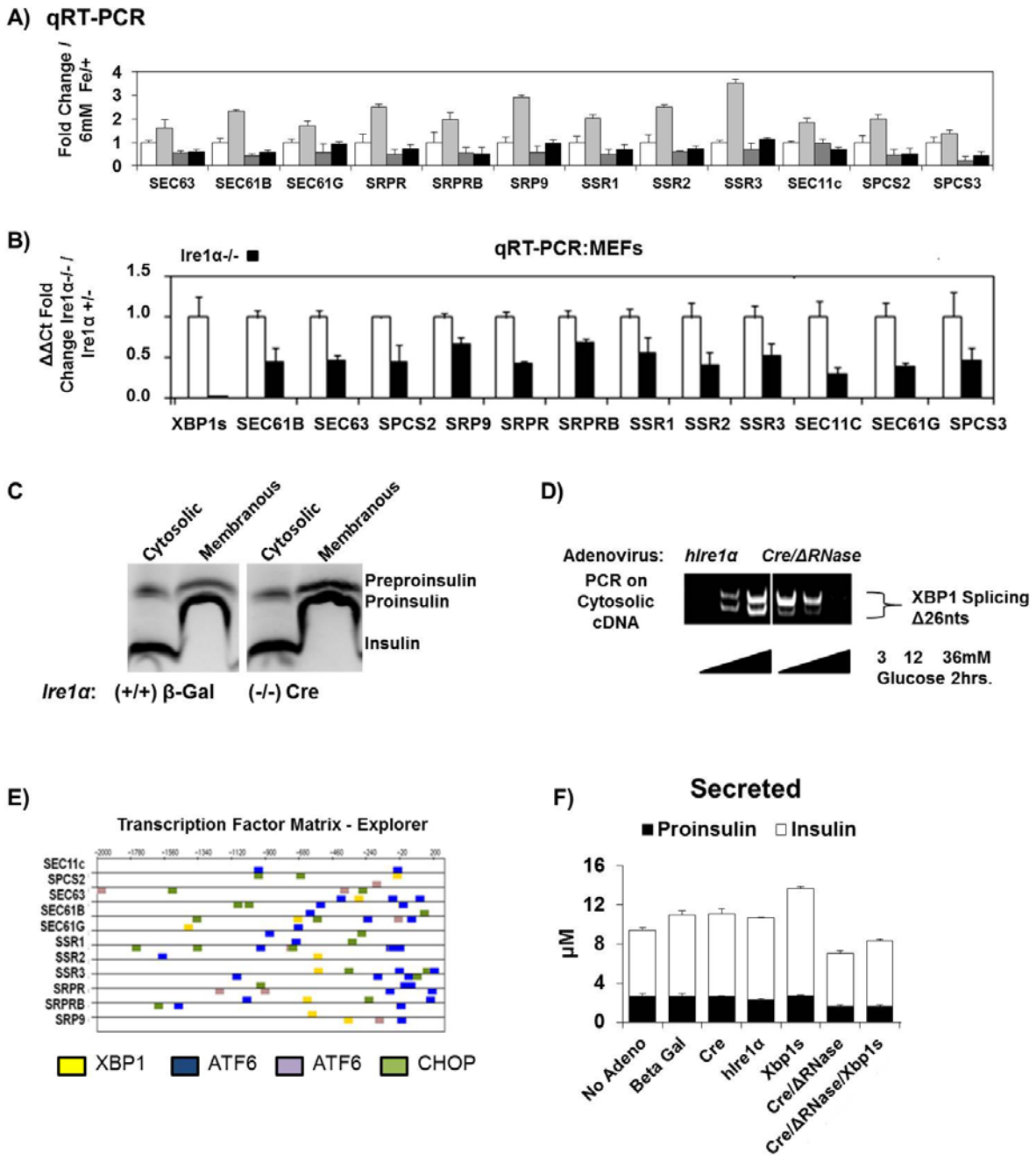

Figure 2-14. The IRE1α-XBP1s pathway increases the proximal secretory pathway. (A) qRT-PCR for the 12 mRNAs identified by mSeq shows excellent agreement between the two assays (B) qRT-PCR on *Ire1α* -/- fibroblasts for the targets from the β cell focused on previously. (C) Cytosolic and membranous subcellular fractions from the *Ire1α*-floxed immortalized β cell lines after Cre deletion were blotted for insulin and unprocessed forms. (D) The floxed insullinoma cell lines were analyzed for spliced XBP1 by conventional PCR flanking the 26nt intron targeted by IRE1α during glucose stimulation. (E) Transcription factor matrix explorer results show binding sites of XBP1 and ATF6 were significantly over-represented. (F) Insulin and proinsulin ELISAs on intracellular and secreted samples from the immortalized β cell line infected for 48 hours with the indicated adenoviruses. (performed twice).

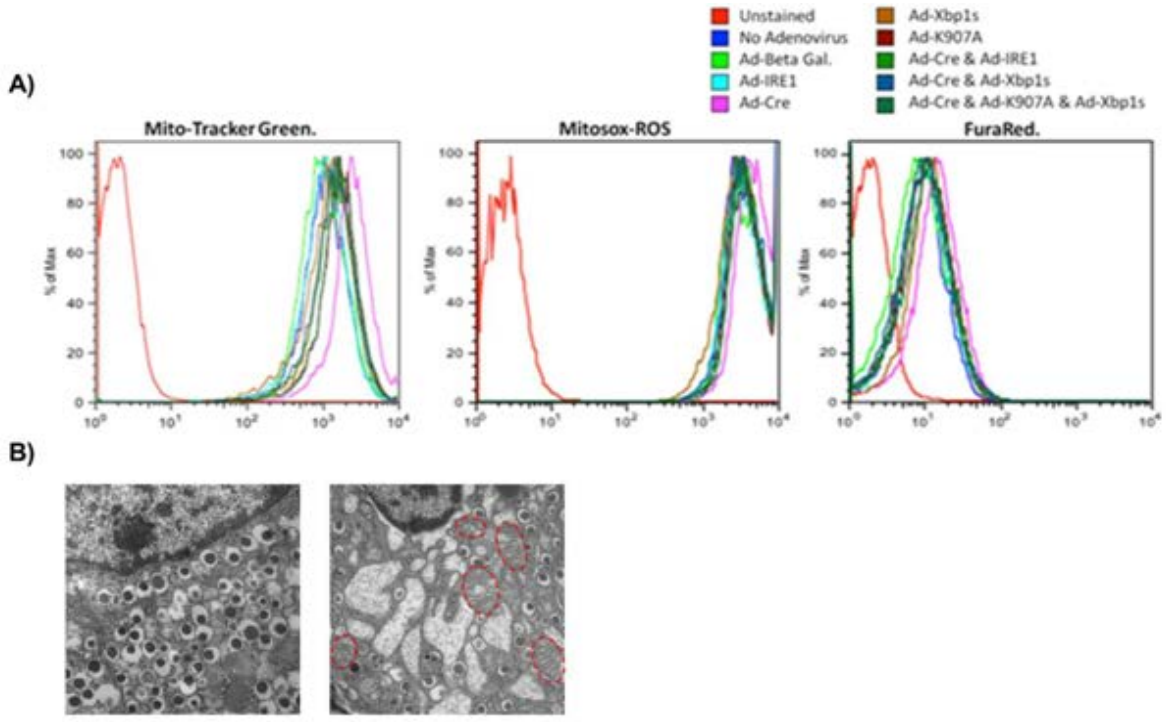

Figure 2-15. IRE1α protects the β cell from oxidative stress. (A) Flow cytometry of *Ire1α-Fe/Fe* insulinoma cells infected with various adenoviruses. Deletion of *Ire1α* caused increased mitochondrial volume, superoxide and cytosolic calcium levels (B) Electron micrographs demonstrate distended mitochondria of the *Ire1α*-null sample outlined with red dashed lines.

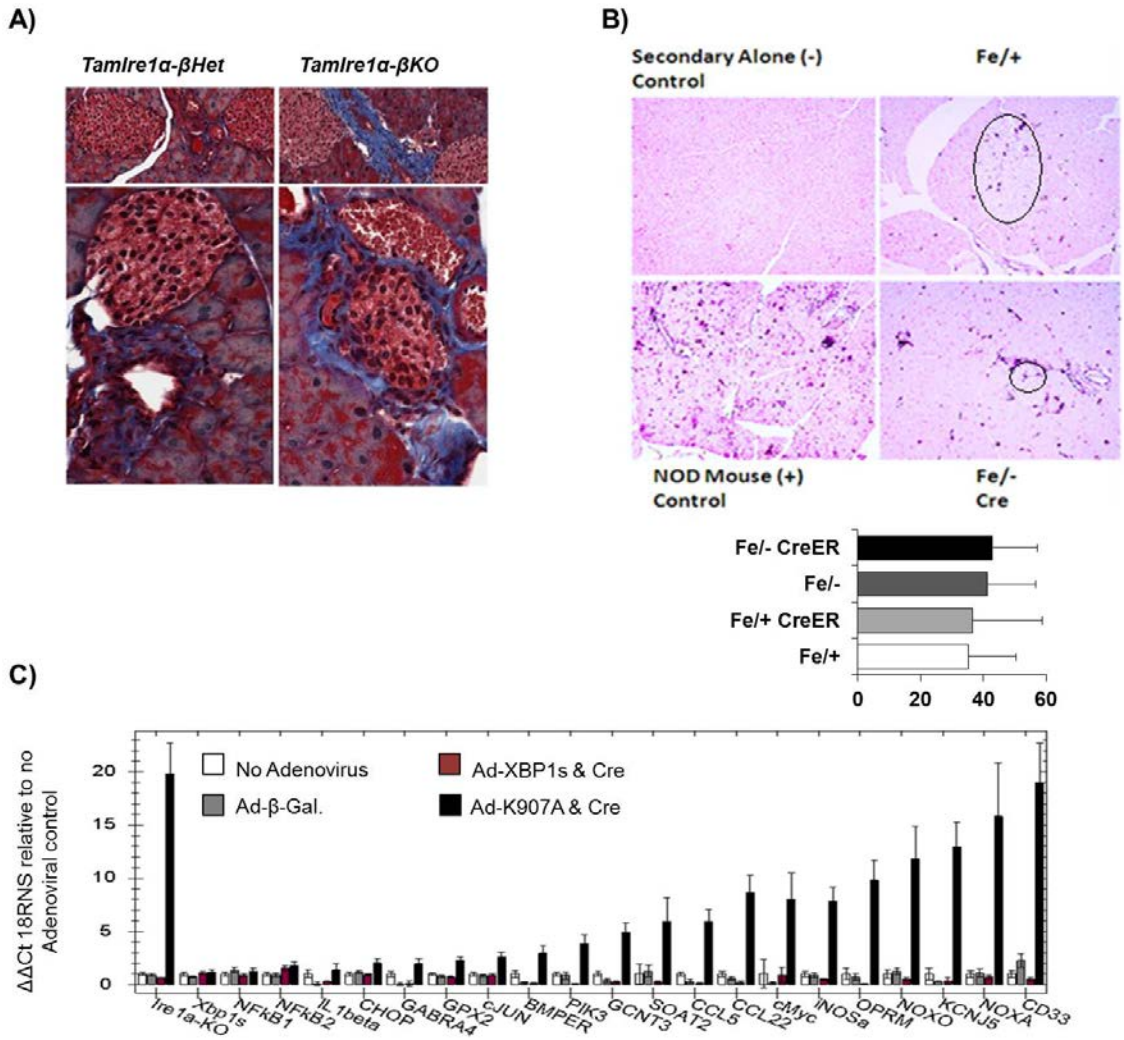

Figure 2-16. IRE1α protects the β cell from inflammation. (A) Additional Masson's trichrome stain of islets showing increased collagens surrounding the *KO* islet. (B) Mac2 immunohistochemical staining shows increased infiltration in the null and heterozygous at birth samples pancreas surrounding islets. (C) qRT-PCR on inflammation associated mRNAs isolated from *Ire1α-Fe/Fe* insulinoma cells 48 hours after being infected with the indicated adenoviruses. These mNAs were originally identified by mSeq from *KO* islets and this experiment was performed to determine whether they were of β cell origin.

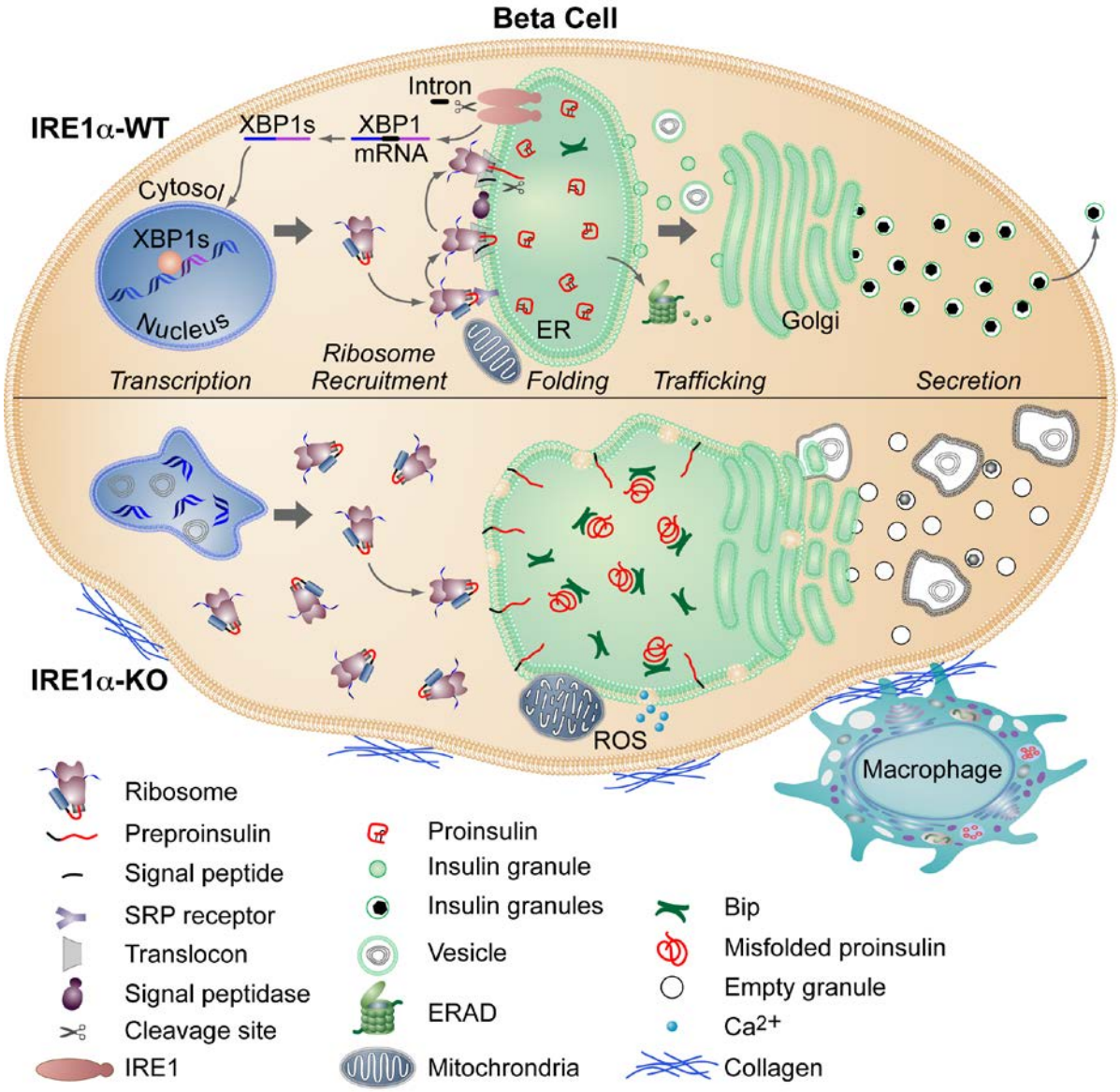

Figure 2-17. IRE1α is the gatekeeper to the secretory pathway of the β cell. An artistic rendering of the intracellular processes dependent on IRE1α within the β cell is depicted above.

CHAPTER III

THE DISCOVERY OF NOVEL, IRE1α-DEPENDENT TRANSCRIPT SPLICEOFORMS

Abstract

IRE1α is the most conserved sensor of the unfolded protein response (UPR) that is a dual enzyme with kinase and endoribonuclease (RNase) activities. Upon activation, IRE1α initiates the unconventional mRNA splicing of a 26 nucleotide long intron from *Xbp1* mRNA and was the only reported IRE1α splice target. To identify new *Ire1α*-dependent splice sites a novel algorithm to align previously unalignable sequences from massive-parallel sequencing data was utilized. As proof of principle, the chimeric reads generated by the IRE1α-dependent 26nt intron splicing of *Xbp1's* mRNA were found within this data set and therefore served as a positive control. We reasoned other novel splice targets of IRE1α could also be within this data set and knew we could use the *Ire1α-KO* cells as an excellent negative control. Putative target sites we identified possess *Xbp1*-like stem-loop regions and/or single stranded bulge regions enriched with repetitive sequences typically in the 3'-UTRs and often containing miRNA binding motifs.

Introduction

IRE1α-dependent *Xbp1* 26nt mRNA splicing is a cytosolic event that has been measured in many cellular contexts [14, 104, 105]. Previous studies reported the downstream targets of spliced XBP1, as being important for ER protein synthesis, folding and degradation [51, 211, 212, 251, 256]. A growing number of reports have shown IRE1α-dependent mRNA and most recently, miRNA cleavage events can occur [128, 129, 221, 222, 224, 234, 257]. These studies have given rise to a double edged sword where IRE1α slicing activity is proposed to nick mRNAs and miRNAs thereby leading to their degradation and in turn altering protein levels. IRE1α mediated derepression of Caspase 2 *via* miRNA cleavage is more easily attributed to being apoptotic than nicking a subset of mRNAs even if they are ER-localized yet both slicing events represent pro-apoptotic pathways emanating from IRE1α non-*Xbp1* RNase activity [128, 129, 221, 222, 224, 234, 257]. Although these numerous RNA cleavages attributed to IRE1α have been identified, to the best of our knowledge, there are no splice examples other than *Xbp1s* that

have been reported to be IRE1α-mediated. A large-scale approach in yeast indicated yIRE1p only acts upon *Hac1* mRNA [130]. To determine whether IRE1α-dependent splice sites other than the well known *Xbp1's* 26nt intron exist we derived the Read Split Walk (RSW) assay.

In order to search for additional splice targets for IRE1α, mRNA-Seq was performed on mRNA isolated from control and null mouse embryonic fibroblasts (MEFs) treated with pharmacological ER stressor to activate IRE1α. Our opportunity presented itself serendipitously, when we postulated about the data that is normally excluded from the mSeq reference genome sequence alignments, could the reads that span the spliced junction resulting from the 26nt splice event in *Xbp1's* mRNA be falling into this discarded data set? When we checked the unalignable data set for this one unique, IRE1α-dependent, unconventional spliceform within the spliced *Xbp1* mRNA, it was indeed present but never in the mRNA from the *Ire1α-KO* sample (Figure 3-4). From that point we automated the mapping of the read split-halves using one versus two nucleotide splice length minimums and applied it to the previously unalignable sequences from each sample. Finally, after subtracting the *KO* data set from the *HET* data set we derived the *Ire1α*-dependent, newly aligned, read-split half reads/chimeras, containing the XBP1 26nt splice containing reads. Examination of the splice regions within these data sets by PCR, western blot and miRNA biding site analysis is ongoing with preliminary results shown in Figures 3-8, 3-9, 3-10 and 3-11.

Results

Massive parallel sequencing of *Ire1α*-null and wild-type fibroblasts exposed to ER stressors reveals *Ire1α*-dependent mRNAs

Illumina-based "mSeq" was performed on wild-type and *Ire1α*-null primary mouse embryo fibroblasts as indicated in (Figure 3-1A). *Xbp1* mRNA splicing by IRE1α was visualized in two ways. First, RT-PCR was performed using primers flanking the 26nt intron within *Xbp1* RNA. Second, ".bed" files were loaded into the UCSC genome browser for analysis. Both methods identified the removal of the intron only within the wild-type samples (Figures 3-1B and 3-1C). Next, we filtered the mRNAs from each condition using 4-way Venn diagrams to isolate the *Ire1α*-dependent mRNAs that were shared and distinct between the different contexts (Figure 3-1D).

Gene ontology analysis of *Ire1α*- dependent mRNAs

The results from the Venn diagram analysis were analyzed using "DAVID" functional analysis (Figure 3-2). Functional categories found to be deficient in *Ire1*α-null fibroblasts

included; Polymerase II-dependent transcription, embryonic development, notably, inner-ear morphogenesis, cellular adhesion and the cell cycle (Figure 3-2). Conversely, *Ire1α*-null fibroblasts possessed increased mRNAs associate with reduction-oxidation processes, lipid and amino acid metabolism, the immune response and cellular proliferation (Figure 3-2).

Read Split Walk (RSW) of unalignable mSeq data identifies *Ire1α*-dependent splice sites

Xbp1's 26nt intron has a very symmetrical double stem-loop structure (Figure 3-3A). Intriguingly, mSeq data for this region when visualized illustrates a drop in the read coverage at this location only in *Ire1α* functional cells whereas it accumulates in the null condition (Figure 3-1A). Because conventional nucleotide read alignment programs; ERANGE, GERALD or BUSTARD rely on annotated genomes they must generate a folder containing the sequences that do not align to the genome. Once the algorithm was created a splice length minimum of 1nt was first chosen in order to capture as much data as possible with the reasoning that by subtracting the null data set from the functional data set most false-positives could be excluded. Indeed these data sets were large with 92,108 and 88,356 chimeras being aligned in the *Ire1α*+/- and *Ire1α*-/- samples respectively. After canceling out every chimera that occurred in the *Ire1α*-/- data that also occurred in the *Ire1α*+/- data, 75,851 chimeras remained in the *Ire1α*+/- sample distributed between 6,577 mRNAs of unique identity. Despite thousands of mRNAs being identified by the 1nt splice length minimum RSW only 49 mRNAs had 100 reads or more. Exclusively within this data set were the *Xbp1* mRNA chimeric reads formed by IRE1α-mediated splicing. Specifically, 201 out of 204 *Xbp1's* chimeric reads were found to represent the exact 26nts spliced by IRE1α (Figure 3-4). By sorting the data set by the two criteria of total number of chimeras (green bars) and number of chimeras within 1nt of each other, an *ad hoc* measure of specificity (black bars) we narrowed the *Ire1a*-dependent chimeras to a manageable list containing *Xbp1* and the other most enriched proposed targets (Figure 3-4). Next, because the 1nt splice minimum length was considered to be susceptible to false-positives the RSW algorithm was again applied with a 2nt splice length minimum instead (Figure 3-5). This simple change greatly reduced the size of the data set to 2,607 chimeric reads exclusive to the +/- sample with only *Xbp1* having over 100 chimeras (173) and only18 other mRNAs having greater than 10 chimeras (Figure 3-5).

Surprisingly, all the major proposed splice sites were located within the 3'-UTRs of the consensus cDNAs on record with the exception of XBP1. Since the RSWs provided exact locations in the genome we were able to retrieve the sequences and input them into RNA-FOLD, an energy minimization-based nucleotide folding program for comparison to

XBP1's 26nt intron spliced by IRE1α (Figure 3-6). These predicted structures fell into three categories: 1) those with double stem-loop structures similar to that of *Xbp1* mRNA 26nt intron and 2) single stranded-disordered or 3) a mixture of both (Figure 3-6). When the splice site sequences were aligned, almost without exception the single stranded, disordered RNA regions contained di-nucleotide repeats, usually CAs (Figure 3-7A). Because these regions were grossly over-represented within the 3-UTRs we next determined whether they contained micro-RNA target sites using the Target Scan program Perl Script for batch gene list analysis (Figure 3-7B). From this analysis we identified the repetitive sequence "ACAC", which was prevalent in the proposed splice sites, is a binding site for the micro-RNA 466 family (Figure 3-7B). Next we sought to confirm the digital results from the RSW using molecular biological techniques such as qRT-PCR. Primers that flank the regions of interest were designed and tested by PCR in order to visualize by electrophoresis whether any *Ire1α*-dependent size changes could be detected (Figure 3-8). Indeed several targets showed banding pattern differences between *Ire1α*-heterozygous and *Ire1α* null fibroblasts stressed with dithiothreitol (Figure 3-8). These bands of interest were excised and sub-cloned in order to be sequenced. RPS9, the mRNA second only to XBP1 for number of chimeric reads (80) generated the expected bands and an unexpected band of larger size in the heterozygous sample (Figures 3-8 and 3-9A). Upon sequencing several clones representing these bands the 4nt region first identified by RSW was confirmed to occur only in the heterozygous sample (Figure 3-9B).

Although, the splice sites identified by RSW were nearly all in the 3'-UTRs we tested whether these new putative targets of IRE1α were affected at the protein level. This was accomplished by western blotting of cytosolic, membranous and nuclear fractionations prepared from ER-stressed *Ire1α* heterozygous and null primary fibroblasts (Figures 3-10 and 3-11). Significant alterations to the protein levels of Osteonectin (SPARC), tissue inhibitor of metallo-proteinase 2 (TIMP2), Galectin 1 (LGALS1), Filamin B (FLNB), Vascular endothelial growth factor A (VEGFA) and Ribosomal protein small subunit 9 (RPS9) were detected between the two genotypes (Figures 3-10 and 3-11). We are currently testing many of the other targets identified by RSW by western blot. Lastly, gene ontology analysis of the top 52 mRNAs identified from both RSWs was performed. This group was enriched for phosphoproteins, acetylation, signal peptide containing, secreted, actin-binding, cytoskeleton, extracellular matrix, ribosomal proteins and methylation in descending order to name a few (Figure 3-11). Future efforts to analyze gene ontology of splice targets that are increased versus decreased are underway.

Discussion

We developed a novel algorithm that aligns previously unmapped mSeq reads to the genome. Subtraction of the data set mapped in the *Ire1α-KO* cells from that of the control cells uncovered many *Ire1α*-dependent splice events including the well-known 26nt splice event in *Xbp1* mRNA. These new splice sites are predominantly within the 3'-UTRs and often contain di-nucleotide repeats of which $(CA)_n$s that encodes the binding site for miRNA-466 family members. Molecular cloning and DNA sequencing PCR products formed using flanking primers to these *Ire1α*-dependent splice sites confirmed the presence of the splice sites occurs only in the cells with functional IRE1α for RPS9, FLNB and TIMP2. Unexpectedly, RPS9 flanking PCRs generated a larger band that maps to two genomic regions for RPS9, the second being a pseudogene many megabases away from the traditional RPS9 gene [258]. The exact origin of this PCR product is being investigated further as DNA sequencing has been inconclusive to date.

Western blotting has detected significant changes to the protein levels of TIMP2, RPS9, FLNB, LGALS1 and VEGFA in *Ire1α*-KO MEFs (Figure 3-10). These four proteins function in the ribosome, ER/Nucleus, and extra-cellular matrix (ECM) respectively, demonstrating the diverse cellular locations affected by IRE1α [238, 258-273]. SPARC was reported earlier as a "RIDD" target and found to be enriched in *Ire1α-KO* fibroblasts (Figure 3-12) and plays a role in glioma metastasis [221, 272, 274]. Gene ontology analysis suggests these mRNAs identified by RSW mostly contain signal peptides suggesting they are localized to the ER (Figure 3-12). However, the increased protein levels by western blot for the few targets we have identified (VEGFA, TIMP2 and SPARC) aren't enough to support a broad hypothesis about the physiological effects of these targets. It will be interesting to determine whether more or less of these mRNA splice targets are decreased or increased at the protein level. Their overall mRNA expression levels as measured by mSeq and qRT-PCR show slightly more targets are increased in *Ire1α-KO* fibroblasts (Figure 3-7).

Future experiments are focused on correlating the ability of *Ire1α-KO* versus control fibroblasts to survive drug exposure and if there are protective effects of anti-oxidants. Preliminary data suggest IRE1 α null cells are more sensitive ER stress so the signaling that leads to cell death in this context would be IRE1α-independent and without Caspase 2 de-repression. Lastly, comparison of western blot species present in *Ire1α-KO* and inhibited contexts to many cancer and secretory cell lines is being performed to discern if any shared isoforms are IRE1α-dependent.

Experimental procedures

Mouse embryonic fibrobasts of passage 4 were incubated with 1mM Dithiothreitol, 500nM Thapsigargin, 1ug/ml Tunicamycin or DMSO vehicle control for 4 hours before harvesting for RNA and 6 hours for rotein analysis.

Primers:

qRT-PCR primers were ordered through: http://pga.mgh.harvard.edu/primerbank/

Flanking primers for the splice sites were designed to amplify PCR products between 100 and 1000bp to amplify any genotype specific products, and then the bands were visualized, excised, eluted and subcloned into the Topo-TA PCR subcloning kit. DNA plasmid mini-preps were prepared from 10 subclones per band and sequenced using M13 forward and reverse primers. The sequences were aligned using T-COFFEE online alignment and then the Ire1a-dpependent splice sites were detected as gaps in the alignements only occurring in the control sample and not the knock-out followed by manual confirmation using BLAT alignment to the mouse genome.

The Read Split Walk (RSW) assay:

The rationale for this study doesn't concern itself with single cuts/nicking of RNAs caused by IRE1α. Instead using the intron/gap-based approach we only focused on *Ire1α*-dependent splicing events. In order to test whether IRE1α splices other mRNAs in addition to XBP1, we designed a new approach in which previously unalignable data from Illumina-based massive parallel sequencing was aligned using an algorithm that splits previously unalignable sequence reads into halves and maps the subsequent fragments separately while calculating the gap, i.e., splice length between them We reasoned that if the reads spanning the junction of the 26nt intron spliced from *Xbp1* mRNA fall into the previously unalignable reads, then the data set containing these reads/chimeras/sequences would also include any other IRE1α-dependent chimeras. In effect, the IRE1α-dependent chimeras formed from *Xbp1* mRNA served as a positive control for our approach. As a strict negative control we applied the same algorithm to *Ire1α*-null fibroblasts then subtracted that data set from the functional IRE1α data set to yield the sequences exclusively mapped in the functional IRE1α containing cells and therefore considered to be *Ire1α*-dependent.

Venn diagrams were generated at: http://www.pangloss.com/seidel/Protocols/venn4.cgi

Subcellular fractionations: Pierce kits were used for nuclear, embranous and cytosolic fraction lysate preparations.

DAVID Gene ontological reports were generated at: http://david.abcc.ncifcrf.gov/

Visualization of actual reads spanning the IRE1α-dependent 26nt intron in *Xbp1* mRNA

was performed by uploading *.bed files of the actual read data into the UCSC genome browser at: http://genome.ucsc.edu/.

RNA-FOLD was used to generate energy minnmization based structure predictions: http://rna.tbi.univie.ac.at/cgi-bin/RNAfold.cgi

RNA-Alignments were performed by uploading sequences to: http://tcoffee.crg.cat/apps/tcoffee/do:rcoffee

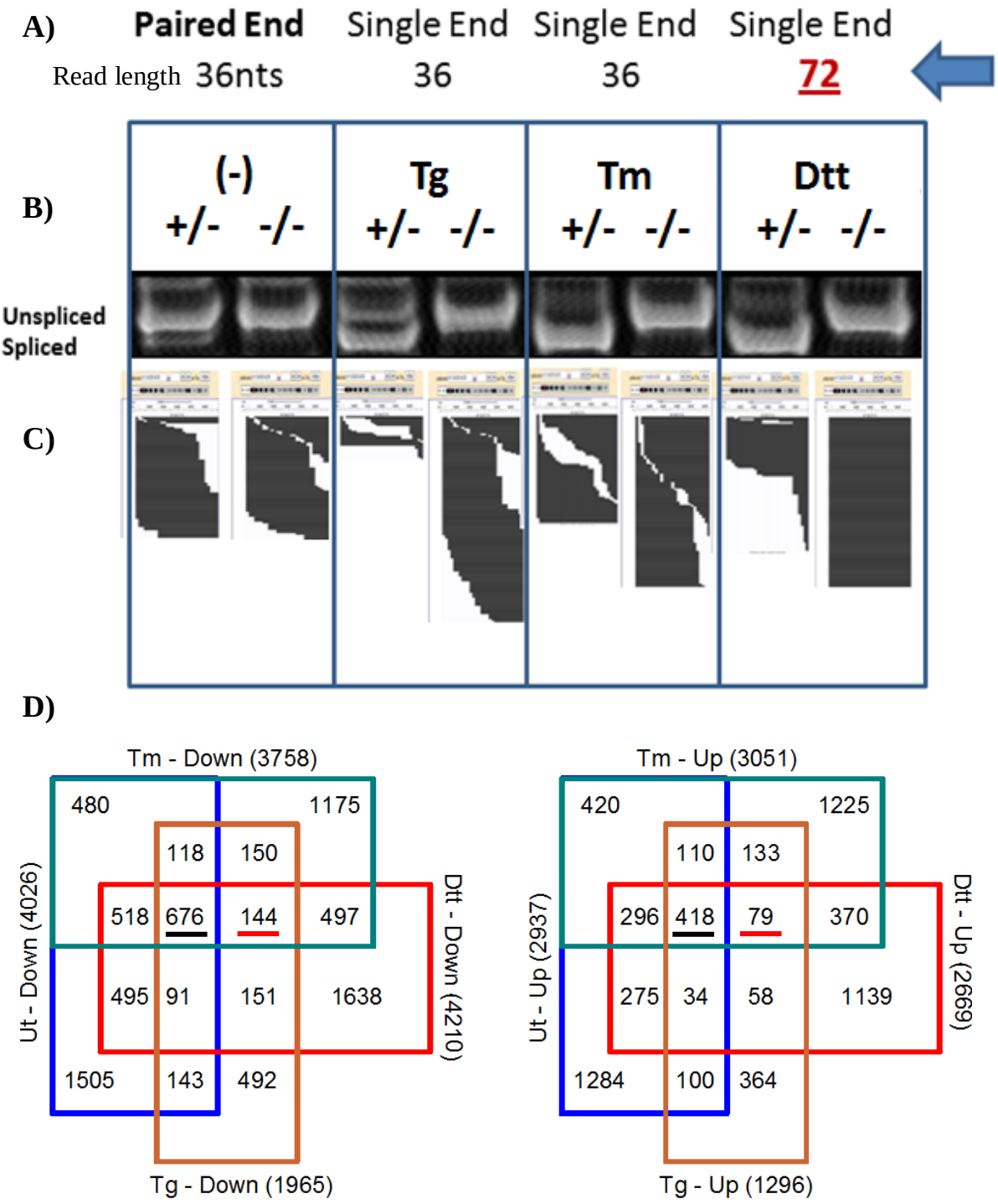

Figure 3-1. Massive parallel sequencing the transcriptomes of *Ire1α-KO* and control fibroblasts reveals *Ire1α*-dependent mRNAs. (A) ER stressors and read length used in mSeq analysis. Blue arrow indicates the samples used for Read Split Walk (RSW) assay. (B) IRE1α-dependent *Xbp1* mRNA splicing visualized by qRT-PCR. (C) IRE1α-dependent *Xbp1* mRNA splicing visualized by mSeq using the UCSC genome browser. (D) Venn diagram analysis of *Ire1α*- and ER stressor- dependent mRNAs from mSeq. Groups underlined in black represent *Ire1α*-dependent but stress independent while red underlines represent dependence on *Ire1α* and all stressors.

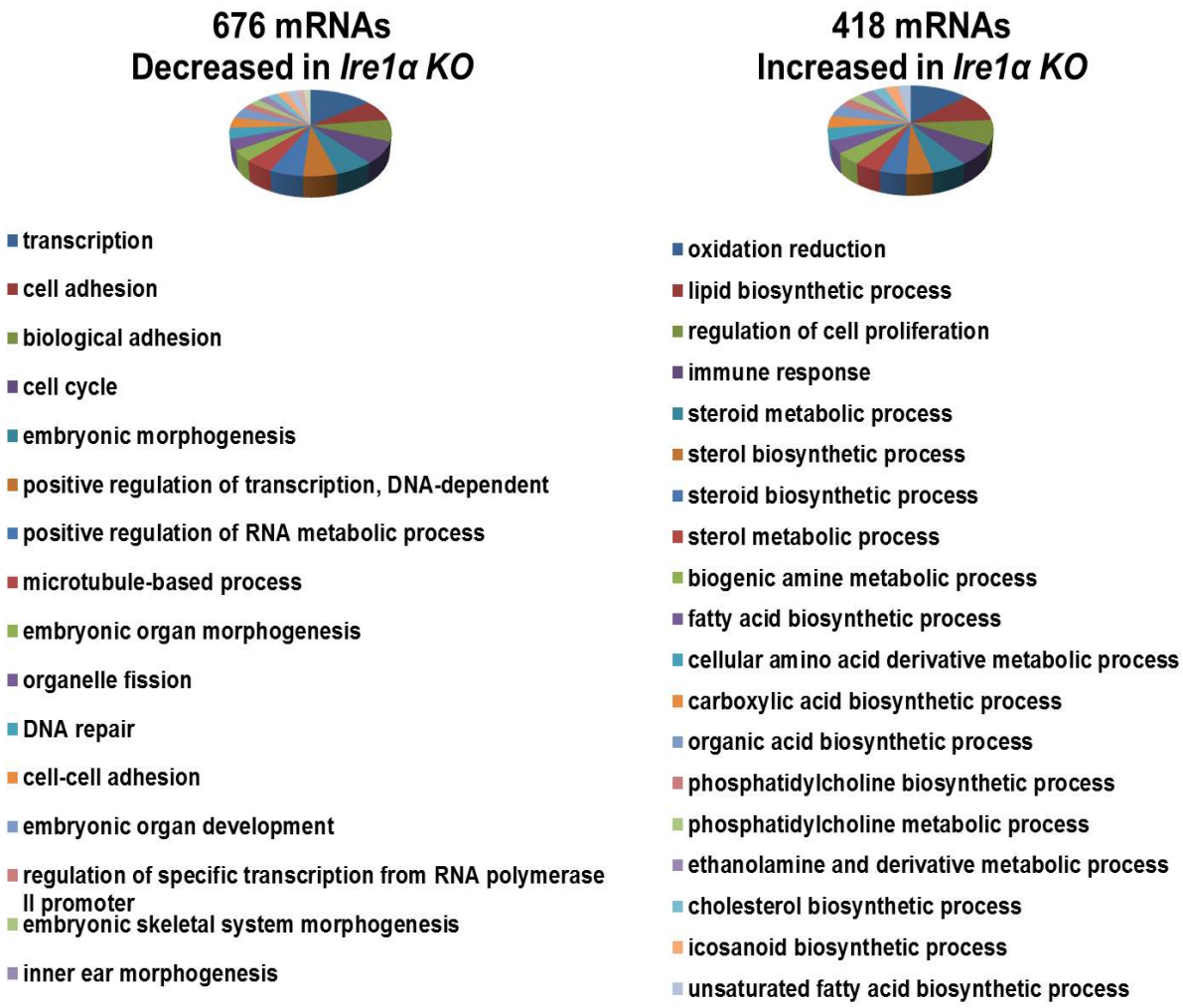

Figure 3-2. "DAVID" derived gene ontology of mRNAs decreased or increased in *Ire1α*-null MEFs identifies functions regulated by IRE1α. mRNAs from Figure 3-1 found to be *Ire1α*-dependent were analyzed for their known functions.

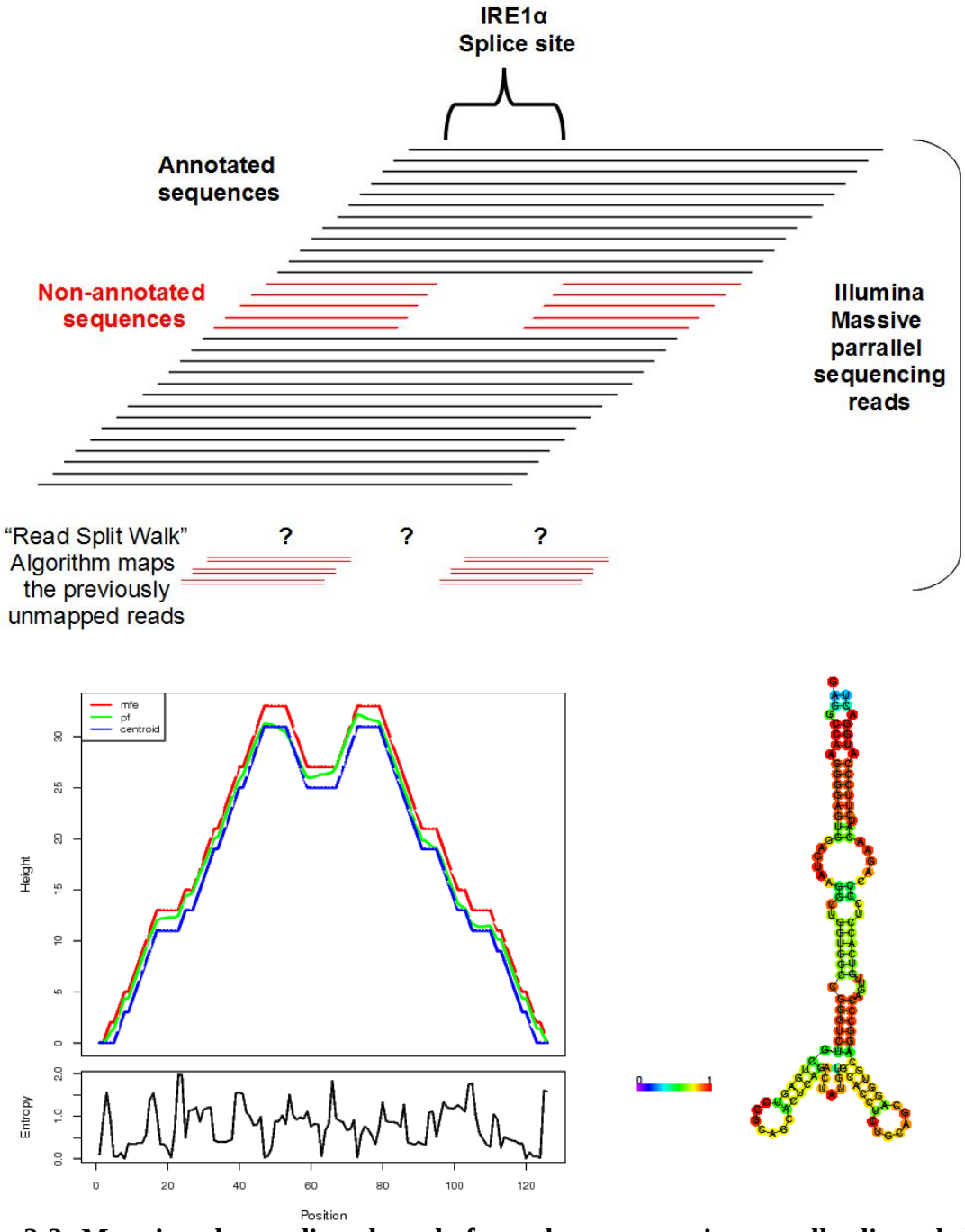

Figure 3-3. Mapping the unaligned reads from deep sequencing usually discarded by development of a novel algorithm termed "Read Split Walk" (RSW). Actual deep sequencing coverage along the *Xbp1* mRNA decreases at the *Ire1α*-dependent mRNA splice site, suggesting those reads may be falling into the unaligned data set. The, Read Split Walk (RSW) algorithm was developed to split the unaligned reads "walk" each half through the genome for alignment and simultaneously determine the intron/gap length between the halves. Black lines represent the alignable digital reads that mSeq generates. The red lines indicate the reads that do not align because a gap between exists between the two halves of the read. XBP1's 26nt IRE1α-dependent intron is presented in Figure 3-1C. (B) RNA-FOLD energy minimization "Mountain plot" and structural depiction of *Xbp1's* 26nt intron spliced by *IRE1α.*

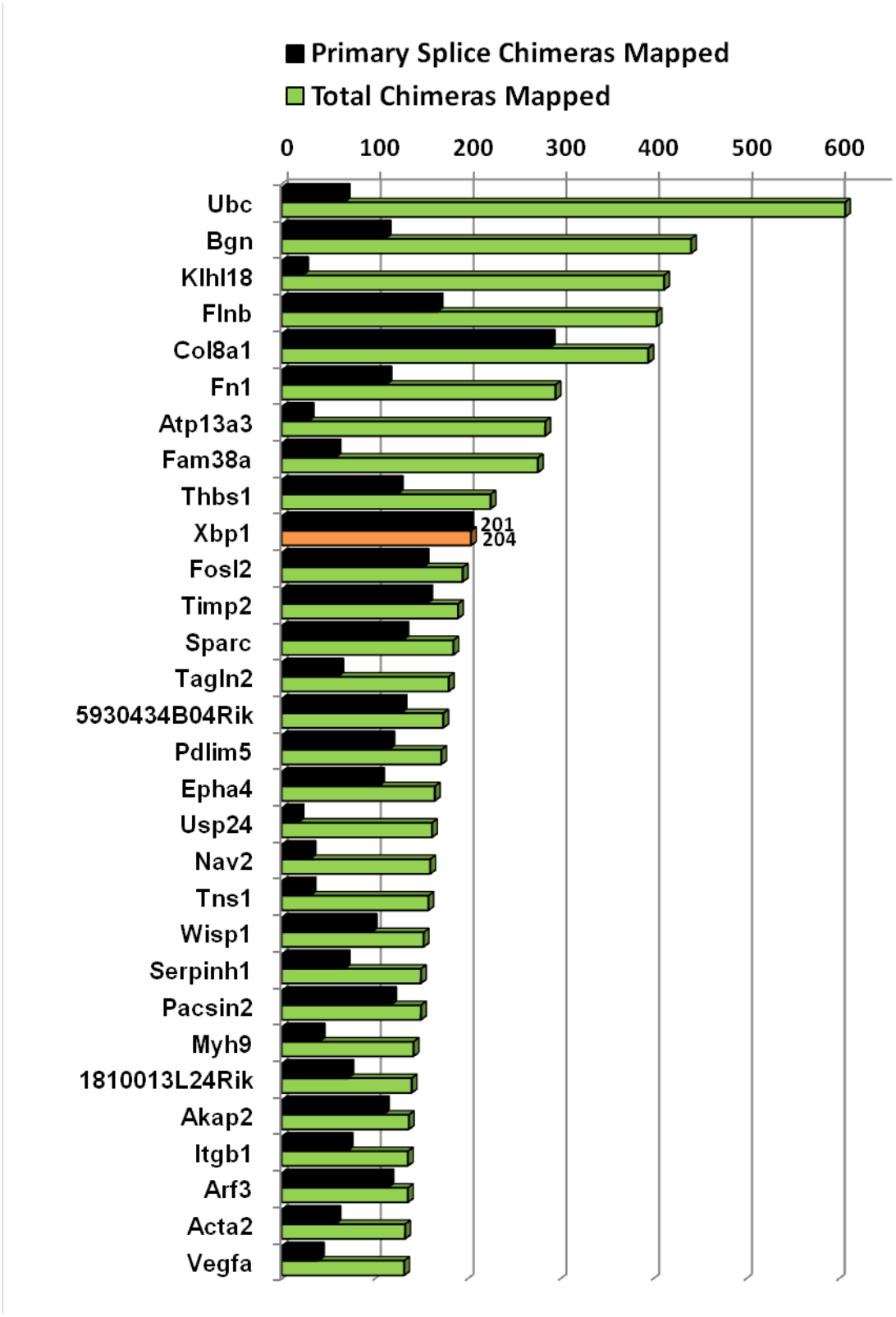

Figure 3-4. Read split walk using a 1nt minimum splice length identifies *Ire1α*-dependent splice targets. The Read split walk results for mRNA Seq data from *Ire1α* +/- and *Ire1α* -/- MEFs treated with dithiothreitol were sorted by most prevalent number of chimeric reads found in one mRNA (green) and by the number of reads at the same region (black). This analysis reveals *Xbp1* mRNA is the most specific splice target.

Het – DTT sample		2575 total splice sites mapped in 1989 mRNAs				
Gene Name	# of reads mapped	Splice_length	Chromosome	Loc-Left	Loc-Right	Location in Transcript
Xbp1	173	26	chr11	5424280	5424312	within Exon 4
Rps9	80	4	chr7	3658432	3658436	3UTR-Last Exon
1810013L24Rik	30	3	chr16	8858087	8858093	3UTR
Sparc	23	2	chr11	55208920	55208938	3UTR
Sparc	10	2	chr11	55208876	55208938	3UTR
Itpripl2	20	3	chr7	125629306	125629309	3UTR
Itpripl2	5	4	chr7	125629305	125629309	3UTR
Actb	19	2	chr5	143665405	143665443	3UTR
Actb	14	2	chr5	143665179	143665194	3UTR
Wdr89	19	3	chr12	76732031	76732038	3UTR
Poldip3	17	39	chr15	82957740	82957816	3UTR
Poldip3	5	3	chr15	82957740	82957816	3UTR
Col8a1	15	2	chr16	57624899	57624942	3UTR
Capza2	14	8	chr6	17615665	17615682	3UTR
Zfp498	12	2523	chr5	146044652	146047178	Between ex1-ex2
Maff	11	4	chr15	79189381	79189385	3UTR
Maff	2	3	chr15	79189381	79189384	3UTR
Boc	10	3	chr16	44496541	44496549	Mid Gene
Igfbp4	10	2	chr11	98913019	98913062	3UTR
Senp6	10	24694	chr9	79915377	79940073	Mid Gene
Trp53	10	398	chr11	69400475	69400873	Mid Gene spans 3 exons
Bgn	2	1292	chrX	70736769	70738061	
Bgn – Total	19		chrX	70736769	70740858	3UTR
Fn1	2	2	chr1	71632349	71632362	
Fn1 – Total	31		chr1	71632349	71687726	3UTR
Thbs1	2	2	chr2	117939144	117939152	
Thbs1 – Total	49		chr2	117939144	117952393	3UTR

Figure 3-5. Read split walk using a 2nt minimum splice length identifies fewer *Ire1α*-dependent splice targets. *Ire1α*+/- and *Ire1α*-/- primary fibroblasts treated with DTT were analyzed using the RSW algorithm and then the *Ire1α*-/- reads were subtracted from the *Ire1α*+/- data set and sorted by prevalence.

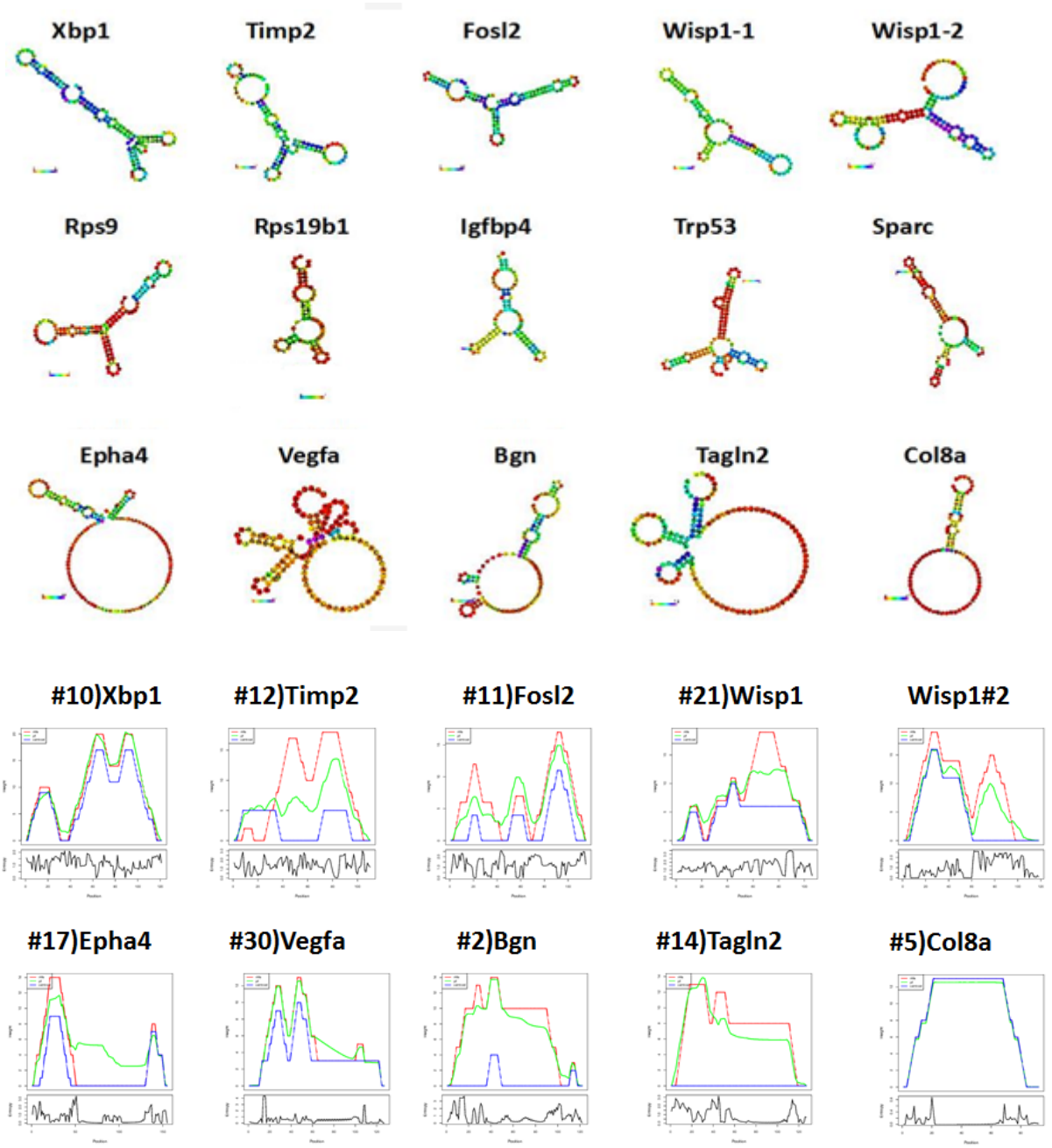

Figure 3-6. RNA-FOLD minimization shows secondary structural predictions for the *Xbp1* mRNA intron and other putative IRE1α splicing targets. (A) Secondary structure predictions are shown for the mRNA regions indicated by RSW to be targets of IRE1α. Two characteristics of these proposed splice site regions are: 1) Repetitive sequences that adopt a double stem-loop structure resembling the intron in *Xbp1* mRNA, and 2) Repetitive sequences that take on single-stranded disordered conformations. (B) "Mountain plots" of select putative splice targets compared to XBP1's. These free energy plots demonstrate a double peak in structural stability is found in many of the targets like that of XBP1's.

symbol	genename	RPKM1	RPKM2	fc	zscore	pvalue	FDR
Epha4	Eph receptor A4	32.65	15.89	-2.05	-4.6847	2.80E-06	0.00014
Fosl2	fos-like antigen 2	111.89	75.87	-1.47	-2.4244	0.01534	0.15903
Flnb	filamin, beta	152.72	110.98	-1.38	-1.7146	0.08642	0.45353
Nav2	neuron navigator 2	1.42	1.05	-1.35	-1.0591	0.28954	0.75896
Myh9	myosin, heavy polypeptide 9, non-muscle	453.89	343.14	-1.32	-1.219	0.22285	0.69448
Pdlim5	PDZ and LIM domain 5	73.49	57.81	-1.27	-1.5689	0.11668	0.52692
Fn1	fibronectin 1	1920.62	1533.21	-1.25	-0.5283	0.5973	0.83015
5930434E	RIKEN cDNA 5930434B04 gene	18.88	15.28	-1.24	-1.2983	0.19418	0.6586
Serpinh1	serine (or cysteine) peptidase inhibitor, clade H, memb	1216.25	985.08	-1.23	-0.9647	0.33471	0.7912
Usp24	ubiquitin specific peptidase 24	3.38	2.79	-1.21	-1.1538	0.24859	0.71972
Tns1	tensin 1	37.76	36.05	-1.05	-0.2991	0.76483	0.89971
Atp13a3	ATPase type 13A3	16.56	16.27	-1.02	-0.1139	0.90932	0.95837
1810013I	RIKEN cDNA 1810013L24 gene	32.84	33.78	1.03	0.18298	0.85481	0.93533
Akap2	A kinase (PRKA) anchor protein 2	27	27.99	1.04	0.23466	0.81447	0.92002
Itgb1	integrin beta 1 (fibronectin receptor beta)	552.68	574.14	1.04	0.183	0.8548	0.93533
Pacsin2	protein kinase C and casein kinase substrate in neuron	62.5	65.59	1.05	0.31713	0.75114	0.89308
Thbs1	thrombospondin 1	2324.94	2504.85	1.08	0.17631	0.86005	0.93724
Tagln2	transgelin 2	444.94	502.15	1.13	0.73612	0.46165	0.79964
Vegfa	vascular endothelial growth factor A	84.18	96.28	1.14	0.88066	0.3785	0.79964
Col8a1	collagen, type VIII, alpha 1	121.27	139.83	1.15	0.86444	0.38735	0.79964
Arf3	ADP-ribosylation factor 3	70.43	83.51	1.19	1.11639	0.26425	0.73587
Klhl18	kelch-like 18 (Drosophila)	6.59	7.91	1.20	1.08883	0.27623	0.74745
Timp2	tissue inhibitor of metalloproteinase 2	271.27	350.4	1.29	1.42285	0.15478	0.59969
Xbp1	X-box binding protein 1	180.29	234.11	1.30	1.68554	0.09188	0.46654
Acta2	actin, alpha 2, smooth muscle, aorta	4791.43	6667.89	1.39	0.90751	0.36414	0.79964
Sparc	secreted acidic cysteine rich glycoprotein	1908.91	2696.48	1.41	1.28025	0.20046	0.66704
Ubc	ubiquitin C	4962.61	7068.86	1.42	0.84334	0.39904	0.79964
Wisp1	WNT1 inducible signaling pathway protein 1	68.4	97.74	1.43	2.28523	0.0223	0.20453
Bgn	biglycan	1766.88	2725.65	1.54	1.55102	0.1209	0.5369

Figure 3-7. mSeq expression values for putative IRE1*α* splicing targets demonstrates a modest bias toward increased mRNA levels in the *Ire1α*-null genotype. Fold changes are referenced to the *Ire1α* heterozygous dithiothreitol condition. Despite being identified as targets of IRE1a's RNase activity the steady-state mRNA levels detected by mSeq demonstrate only modest fold changes in both directions. RPKM stands for reads per kilobase of a transcript per million bases of total reads. Zscore, p-value and FDR are statistical measures of significance. It is noteworthy that the previously reported cleavage target SPARC was identified by our RSW assay.

A)

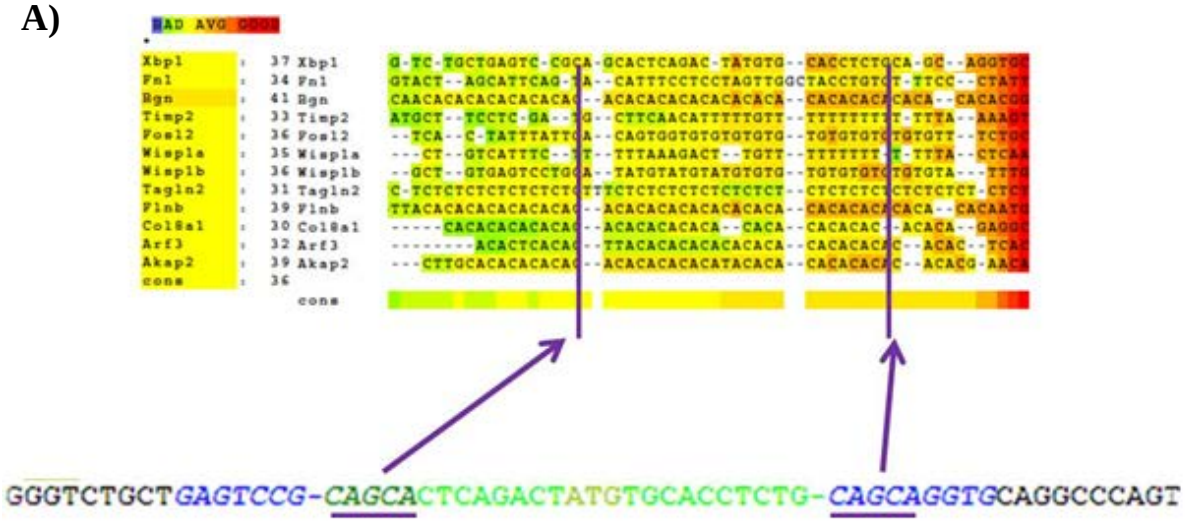

26nts

B)

Gene ID	UTR region	UTR-miRNA pairing	mature miRNA sequence	miRNA family
COL8A1	AGCAUAUGCCUGAUAACACACAC	||||||	UAUGUACAUGUACAUGUGUGUU	miR-466d/466l-5p
WISP1B	GUACAAAUACACACACACACACA	|||| |||||	AGUGUACAUGUACAUGUGUGUGU	miR-466k/466di-5p
ARF3	CACACACUCACACUUACACACAC	||||||	UAUGUACAUGUACAUGUGUGUU	miR-466d/466l-5p

Figure 3-8. Sequence alignment of the IRE1α-dependent splice sites with XBP1's 26nt intron reveals repetitive sequences containing miRNA binding sites. (A) T-COFFEE online sequence alignment was used to align the shown sequences revealing poly-AC repeats are prevalent. For this analysis, 5 additional nucleotides from the flanking sequences were added to both ends. The sequence below is the *Xbp1* intron that also possesses a repetitive sequence underlined in purple. The dashes represent the cleavages mediated by IRE1α. (B) Target-Scan was used to determine whether miRNAs are predicted to bind these sequences. The results indicate that the poly-AC repeats contain binding sites for the miRNA family members (miR-466).

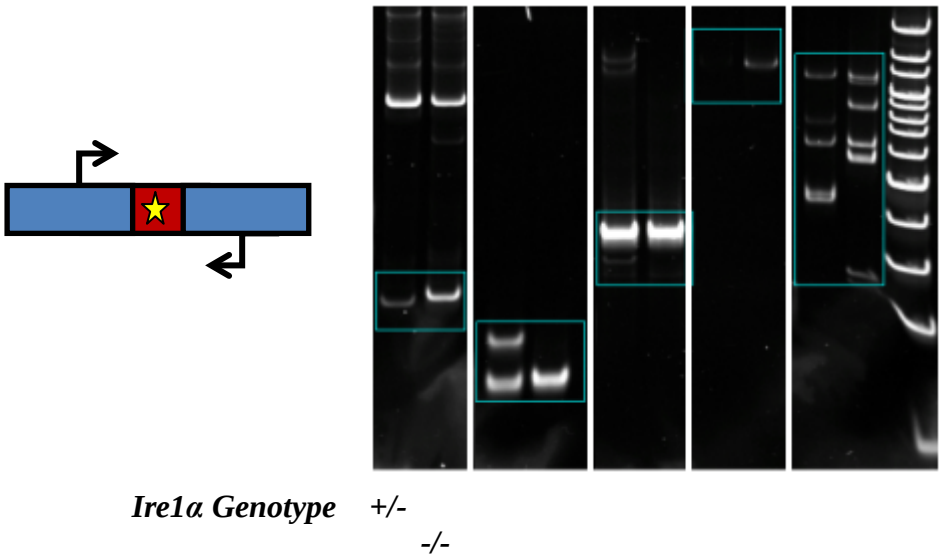

Figure 3-9. Putative IRE1α alternative splice sites that were only detected by RSW in the *Ire1α*+/- MEFs were interrogated by RT-PCR using primers flanking the spliced regions. Blue boxes represent banding patterns of interest that are different between genotypes. Subcloning the FLNB PCR products followed by DNA sequencing demonstrated that it represents a 10nt splice in the *Ire1α*+/- MEFs that was not present in the *Ire1α*-null MEFs. The sequences of bands from RPS9 align to separate regions of the genome encoding RPS9 and its pseudogene that is 45 megabases distal on the same chromosome. This implies IRE1α may be combining two separate mRNAs for RPS9. The results for RPS9, including the unexpected high molecular weight band in the *Ire1α*+/- MEFs were observed in two independent experiments.

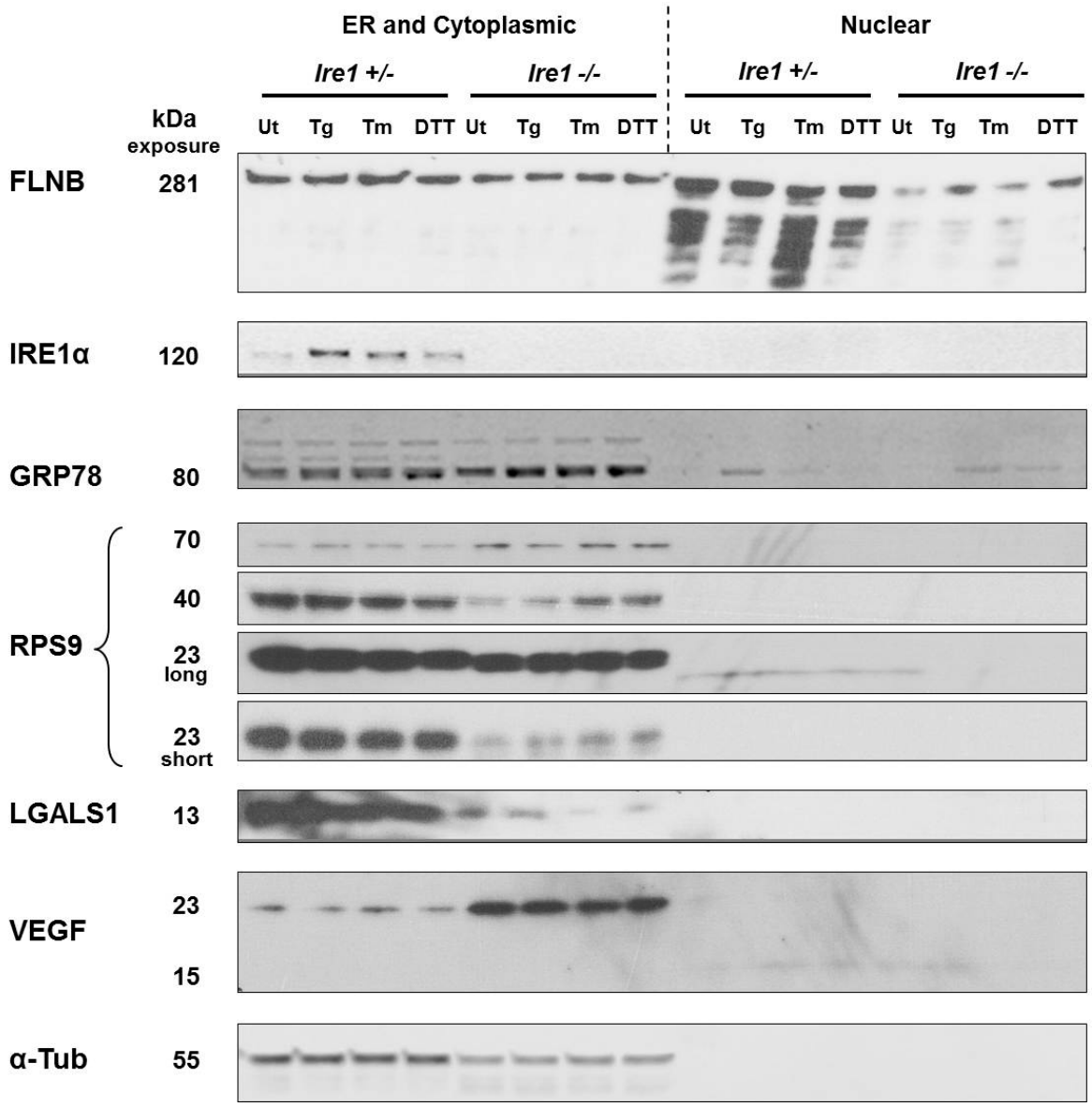

Figure 3-10. *Ire1α*-dependent splice targets exhibit differences at the protein level.
Read split walk targets were examined by western blotting of nuclear and cytoplasmic fractions of primary MEFs of the indicated genotype exposed for 6 hours with the indicated ER stressing chemical.

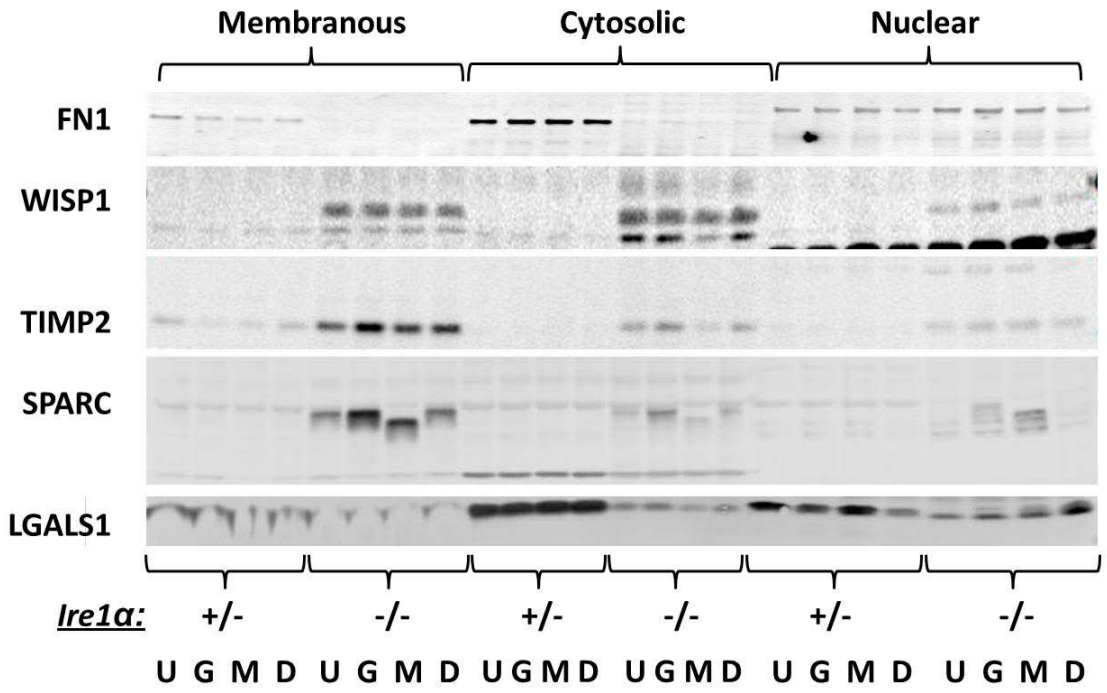

Figure 3-11. *Ire1α*-dependent splice targets exhibit differences at the protein level II.
Read split walk targets were examined by western blotting of nuclear membranous and cytoplasmic fractions of primary MEFs of the indicated genotype exposed for 6 hours to the indicated ER stressing chemical. U=Untreated/DMSO vehicle control, G=Thapsigargin 500nM, M=Tunicamycin 1ug/ml and D=Dithiothreitol 1mM. All incubations performed for 6 hours.

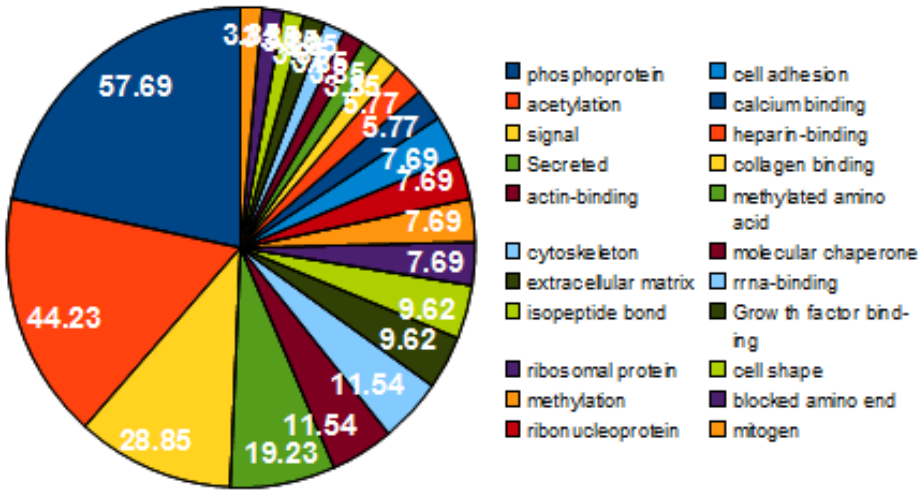

Figure 3-12. Gene ontology analyses for 52 mRNAs containing *Ire1α*-dependent splice sites. Values are in percent relative to the total 52 mRNAs. Interestingly, signal-containing and secreted proteins are enriched within this data set suggesting ER-localized mRNAs are *de facto* enriched.

CHAPTER IV

CONCLUSIONS AND FUTURE DIRECTIONS

Recently, we reported similar findings from the β cell-specific deletion of *Ire1α* and expanded on this by demonstrating defects in ribosome to ER recruitment and signal peptide cleavage at the protein level (Chapter II). There we used a combination of traditional biochemical techniques, mouse genetics and massive parallel sequencing (mSeq) to characterize the transcriptomes of *Ire1α*-null islets challenged chronically with high glucose. mSeq demonstrated with new resolution that the loss of IRE1α-mediated XBP1 splicing prohibits the glucose-induced expression of hundreds of mRNAs involved in many aspects of the secretory pathway. The mSeq analyses of islets transcriptomes detected thousands of glucose- and *Ire1α*- dependent alterations to the transcriptome. We demonstrated the physiological role of IRE1α in the β cell is to increase the glucose-stimulated ER secretory pathway though splicing *Xbp1* mRNA making it essential for maintaining control of blood glucose levels.

Future experiments where the tamoxifen-inducible, β cell-specific deletion of *Ire1α* is combined with the whole body deletion of *Atf6α* are underway. We hypothesize this double deletion event in the β cell will result in an even more diabetic phenotype than *Ire1α* deletion alone due to compensation between XBP1 and ATF6α [104, 117, 119, 275]. Because data from the EIF2α β cell-specific deletion model indicates the anti-oxidant, BHA (butylated hydroxyl anisole) infused diet prevents hyperglycemia that results from deletion, these studies are to be repeated on the *Ire1α* β cell-specific deletion mice and in the double null *Ire1α x Atf6α* β cell containing mouse [50]. Other anti-oxidants such as TUDCA and PBA may also be investigated. Similarly, assays that determine enzymatic origins of ROS are of interest especially between the nitric oxide synthases and the lysyl-oxudases since their mRNA levels were increased by *Ire1α* deletion. Despite the advantages of mSeq over microarrays, mSeq from islets did not directly identify any new splice targets of IRE1α. Gene ontology did indicate from the *Ire1α*- and high glucose- dependent mRNAs which were associated with alternate splicing historically (Figure 2-7). Although not presented here, extensive efforts were made to identify *Ire1α*-dependent spliceoforms from the islet mSeq data sets using the conventional exon-exon mapping program "Tophat" and those efforts will be continued to completion. The recent report that IRE1α de-represses Caspase 2 translation by cleaving certain miRNAs

has motivated us to analyze the islet mSeq data using TargetScan software and western blotting for Caspase 2 is planned as well. Other unanswered questions of interest regarding islet function and the UPR include detection of the misfolded proteome, including preproinuslin and/or proinsulin disulfide mispairing by immunoprecipitation using the anti-KDEL antibody followed by mass spectrometry. Ribosome profiling *Ire1α*-null insulinoma cells is also being performed. Similarly, altered cell division has been observed in *Ire1α*-null insulinoma and fibroblast cell lines and so further studies are needed to delineate the mechanistic underpinnings for this and how it might relate to cancer and cell division. One way to examine whether *Ire1α* null cells are more glycolytic is to test them using Seahorse technology which also determines the oxidative-phosphorylation. Lastly, inclusion of newly available IRE1α inhibitors into these experiments will give another IRE1α-deficient context for comparison to the genetic deletion and dominant-negative models used previously.

Here we report the development of a novel method to align sequences from deep sequencing data that is normally ignored. This Read Split Walk (RSW) study was performed three times using different splice length minimums to allow for varying stringency. We show for the first time that the positive control chimeric reads generated by IRE1α-mediated *Xbp1* mRNA splicing are in fact within this typically discarded sequencing read data set. Now that we have proof of principle for the RSW procedure we will be repeating it in a new set of primary embryonic fibroblasts. In the meantime, since the ultimate goal of the project is to identify *Ire1α*-dependent mRNA changes that result in changes to the protein levels of the targets, extensive efforts are underway to do so using western blotting and mass spectrometry. The preliminary results presented in (Figures 3-10 and 3-11) are a promising start and over time we hope to be able to draw conclusions as to whether these targets are predominantly increased or decreased at the protein level. In order to ensure the putative splice targets identified by RSW directly interact with IRE1α we are performing "PAR-CLIP" (photo-activatable ribonucleoside cross-linked immunopreciptiations) using thiouridine followed by qRT-PCR and perhaps deep sequencing. Additionally, since di-ribonucleotide repeats were found to be a characteristic of many of the RSW targets radio-labeled synthetic oligo-ribonucleotide repeats will be incubated with purified IRE1α *in vitro* to test for the presence of RNAse and/or splicing activity.

Preliminary flow cytometry results for cell-division and apoptosis not included here suggest the null fibroblasts have an increased growth rate and are susceptible to tunicamycin, ER stress-induced cell death when compared to littermate control cells. Additional experiments will address whether these trends are exhibited in response to a panel of

chemicals that cause cellular stress or serve as anti-oxidants. Inhibition of IRE1α has been reported to cause an invasive tumor phenotype however; currently no cancer type has been reported by GWAS to contain *Ire1α* loss or gain of function mutations [273]. Multiple myeloma cell have been suggested to possess hyper-activated IRE1α and determining whether some treatment benefit is through administration of IRE1α inhibitors is an area of interest [241, 250]. Similarly, IRE1α inhibitors administered to mice that are then injected with various cancer cell lines to determine whether or not the IRE1α inhibitors speed up or slow tumor growth and/or metastasis is of interest. Lastly, to interrogate the miRNA profile of *Ire1α* control and null cells the small RNA preparation procedure for mSeq could be performed.

REFERENCES

1. Ahmed, N., et al., *Frequency of metabolic syndrome in patients with type-2 diabetes.* J Ayub Med Coll Abbottabad, 2010. **22**(1): p. 139-42.
2. Kahn, B.B., *Type 2 diabetes: when insulin secretion fails to compensate for insulin resistance.* Cell, 1998. **92**(5): p. 593-6.
3. Oda, E., *Metabolic syndrome: its history, mechanisms, and limitations.* Acta Diabetol, 2012. **49**(2): p. 89-95.
4. Tang, J., et al., *[The changes of histology and biochemical parameters in retina of the patient with diabetic retinopathy].* Zhonghua Yan Ke Za Zhi, 2004. **40**(10): p. 689-91.
5. Abdessalem, R., A. Kraiem, and M. Kamoun, *[A new technic of peroperative examination of the retina before placement of an artificial lens in the diabetic patient].* Ophtalmologie, 1988. **2**(1): p. 33-5.
6. Game, F., *Choosing life or limb. Improving survival in the multi-complex diabetic foot patient.* Diabetes Metab Res Rev, 2012. **28 Suppl 1**: p. 97-100.
7. Alfred, R. and R. Wright-Pascoe, *Acute limb ischaemia in a septic patient with diabetic ketoacidosis.* West Indian Med J, 2011. **60**(2): p. 214-6.
8. Liu, M., et al., *Proinsulin maturation, misfolding, and proteotoxicity.* Proc Natl Acad Sci U S A, 2007. **104**(40): p. 15841-6.
9. Ozcan, U., et al., *Endoplasmic reticulum stress links obesity, insulin action, and type 2 diabetes.* Science, 2004. **306**(5695): p. 457-61.
10. Scheuner, D. and R.J. Kaufman, *The unfolded protein response: a pathway that links insulin demand with beta-cell failure and diabetes.* Endocr Rev, 2008. **29**(3): p. 317-33.
11. Scheuner, D., et al., *Control of mRNA translation preserves endoplasmic reticulum function in beta cells and maintains glucose homeostasis.* Nat Med, 2005. **11**(7): p. 757-64.
12. Schroder, M. and R.J. Kaufman, *The mammalian unfolded protein response.* Annual review of biochemistry, 2005. **74**: p. 739-89.
13. Oyadomari, S., et al., *Cotranslocational degradation protects the stressed endoplasmic reticulum from protein overload.* Cell, 2006. **126**(4): p. 727-39.
14. Shen, X., et al., *Complementary signaling pathways regulate the unfolded protein response and are required for C. elegans development.* Cell, 2001. **107**(7): p. 893-903.
15. Wu, J. and R.J. Kaufman, *From acute ER stress to physiological roles of the Unfolded Protein Response.* Cell Death Differ, 2006. **13**(3): p. 374-84.
16. Ma, Y., et al., *Plasma cell differentiation initiates a limited ER stress response by specifically suppressing the PERK-dependent branch of the unfolded protein response.* Cell stress & chaperones, 2010. **15**(3): p. 281-93.
17. Malhotra, J.D. and R.J. Kaufman, *ER stress and its functional link to mitochondria: role in cell survival and death.* Cold Spring Harbor perspectives in biology, 2011. **3**(9): p. a004424.
18. Rutkowski, D.T., et al., *UPR pathways combine to prevent hepatic steatosis caused by ER stress-mediated suppression of transcriptional master regulators.* Developmental cell, 2008. **15**(6): p. 829-40.
19. Wu, J., et al., *ATF6alpha optimizes long-term endoplasmic reticulum function to protect cells from chronic stress.* Developmental cell, 2007. **13**(3): p. 351-64.
20. Kaufman, R.J., et al., *The unfolded protein response is required to maintain the integrity of the endoplasmic reticulum, prevent oxidative stress and preserve differentiation in beta-cells.* Diabetes, obesity & metabolism, 2010. **12 Suppl 2**: p. 99-107.

21. Iwakoshi, N.N., A.H. Lee, and L.H. Glimcher, *The X-box binding protein-1 transcription factor is required for plasma cell differentiation and the unfolded protein response.* Immunological reviews, 2003. **194**: p. 29-38.
22. Ng, D.T., E.D. Spear, and P. Walter, *The unfolded protein response regulates multiple aspects of secretory and membrane protein biogenesis and endoplasmic reticulum quality control.* J Cell Biol, 2000. **150**(1): p. 77-88.
23. Todd, D.J., et al., *XBP1 governs late events in plasma cell differentiation and is not required for antigen-specific memory B cell development.* The Journal of experimental medicine, 2009. **206**(10): p. 2151-9.
24. Lee, A.H., et al., *XBP-1 is required for biogenesis of cellular secretory machinery of exocrine glands.* EMBO J, 2005. **24**(24): p. 4368-80.
25. Yamamoto, K., et al., *Transcriptional induction of mammalian ER quality control proteins is mediated by single or combined action of ATF6alpha and XBP1.* Developmental cell, 2007. **13**(3): p. 365-76.
26. Cavener, D.R., S. Gupta, and B.C. McGrath, *PERK in beta cell biology and insulin biogenesis.* Trends in endocrinology and metabolism: TEM, 2010. **21**(12): p. 714-21.
27. Back, S.H., et al., *Translation attenuation through eIF2alpha phosphorylation prevents oxidative stress and maintains the differentiated state in beta cells.* Cell metabolism, 2009. **10**(1): p. 13-26.
28. Lee, A.H., et al., *Dual and opposing roles of the unfolded protein response regulated by IRE1alpha and XBP1 in proinsulin processing and insulin secretion.* Proceedings of the National Academy of Sciences of the United States of America, 2011. **108**(21): p. 8885-90.
29. Barrett, T.G. and S.E. Bundey, *Wolfram (DIDMOAD) syndrome.* J Med Genet, 1997. **34**(10): p. 838-41.
30. Senee, V., et al., *Wolcott-Rallison Syndrome: clinical, genetic, and functional study of EIF2AK3 mutations and suggestion of genetic heterogeneity.* Diabetes, 2004. **53**(7): p. 1876-83.
31. Zhang, P., et al., *The PERK eukaryotic initiation factor 2 alpha kinase is required for the development of the skeletal system, postnatal growth, and the function and viability of the pancreas.* Molecular and cellular biology, 2002. **22**(11): p. 3864-74.
32. Harding, H.P., et al., *Diabetes mellitus and exocrine pancreatic dysfunction in perk-/- mice reveals a role for translational control in secretory cell survival.* Molecular cell, 2001. **7**(6): p. 1153-63.
33. Carlson, S.G., et al., *Regulation of the C/EBP-related gene gadd153 by glucose deprivation.* Molecular and cellular biology, 1993. **13**(8): p. 4736-44.
34. Luethy, J.D. and N.J. Holbrook, *The pathway regulating GADD153 induction in response to DNA damage is independent of protein kinase C and tyrosine kinases.* Cancer research, 1994. **54**(7 Suppl): p. 1902s-1906s.
35. Sylvester, S.L., et al., *Induction of GADD153, a CCAAT/enhancer-binding protein (C/EBP)-related gene, during the acute phase response in rats. Evidence for the involvement of C/EBPs in regulating its expression.* The Journal of biological chemistry, 1994. **269**(31): p. 20119-25.
36. Sylvester, S.L., et al., *Induction of GADD153, a CCAAT/enhancer-binding protein (C/EBP)-related gene, during the acute phase response in rats. Evidence for the involvement of C/EBPs in regulating its expression.* The Journal of biological chemistry, 1995. **270**(24): p. 14842.
37. Fawcett, T.W., et al., *Physical and functional association between GADD153 and CCAAT/enhancer-binding protein beta during cellular stress.* The Journal of biological chemistry, 1996. **271**(24): p. 14285-9.

38. Guyton, K.Z., Q. Xu, and N.J. Holbrook, *Induction of the mammalian stress response gene GADD153 by oxidative stress: role of AP-1 element.* The Biochemical journal, 1996. **314 (Pt 2)**: p. 547-54.
39. Wang, X.Z., et al., *Signals from the stressed endoplasmic reticulum induce C/EBP-homologous protein (CHOP/GADD153).* Molecular and cellular biology, 1996. **16**(8): p. 4273-80.
40. Fawcett, T.W., et al., *Complexes containing activating transcription factor (ATF)/cAMP-responsive-element-binding protein (CREB) interact with the CCAAT/enhancer-binding protein (C/EBP)-ATF composite site to regulate Gadd153 expression during the stress response.* The Biochemical journal, 1999. **339 (Pt 1)**: p. 135-41.
41. Harding, H.P., et al., *Regulated translation initiation controls stress-induced gene expression in mammalian cells.* Molecular cell, 2000. **6**(5): p. 1099-108.
42. Ma, Y., et al., *Two distinct stress signaling pathways converge upon the CHOP promoter during the mammalian unfolded protein response.* Journal of molecular biology, 2002. **318**(5): p. 1351-65.
43. Harding, H.P., et al., *An integrated stress response regulates amino acid metabolism and resistance to oxidative stress.* Molecular cell, 2003. **11**(3): p. 619-33.
44. Huang, C.J., et al., *Induction of endoplasmic reticulum stress-induced beta-cell apoptosis and accumulation of polyubiquitinated proteins by human islet amyloid polypeptide.* American journal of physiology. Endocrinology and metabolism, 2007. **293**(6): p. E1656-62.
45. Pirot, P., et al., *Transcriptional regulation of the endoplasmic reticulum stress gene chop in pancreatic insulin-producing cells.* Diabetes, 2007. **56**(4): p. 1069-77.
46. Laybutt, D.R., et al., *Endoplasmic reticulum stress contributes to beta cell apoptosis in type 2 diabetes.* Diabetologia, 2007. **50**(4): p. 752-63.
47. Cunha, D.A., et al., *Initiation and execution of lipotoxic ER stress in pancreatic beta-cells.* Journal of cell science, 2008. **121**(Pt 14): p. 2308-18.
48. Song, B., et al., *Chop deletion reduces oxidative stress, improves beta cell function, and promotes cell survival in multiple mouse models of diabetes.* The Journal of clinical investigation, 2008. **118**(10): p. 3378-89.
49. Song, B., et al., *Chop deletion reduces oxidative stress, improves beta cell function, and promotes cell survival in multiple mouse models of diabetes.* J Clin Invest, 2008. **118**(10): p. 3378-89.
50. Back, S.H., et al., *Translation attenuation through eIF2alpha phosphorylation prevents oxidative stress and maintains the differentiated state in beta cells.* Cell Metab, 2009. **10**(1): p. 13-26.
51. Acosta-Alvear, D., et al., *XBP1 controls diverse cell type- and condition-specific transcriptional regulatory networks.* Mol Cell, 2007. **27**(1): p. 53-66.
52. Wu, J., et al., *The unfolded protein response mediates adaptation to exercise in skeletal muscle through a PGC-1alpha/ATF6alpha complex.* Cell Metab, 2011. **13**(2): p. 160-9.
53. Wu, J., et al., *ATF6alpha optimizes long-term endoplasmic reticulum function to protect cells from chronic stress.* Dev Cell, 2007. **13**(3): p. 351-64.
54. Lee, A.H., et al., *Dual and opposing roles of the unfolded protein response regulated by IRE1alpha and XBP1 in proinsulin processing and insulin secretion.* Proc Natl Acad Sci U S A, 2011. **108**(21): p. 8885-90.
55. Bobrovnikova-Marjon, E. and J.A. Diehl, *Coping with stress: ATF6alpha takes the stage.* Developmental cell, 2007. **13**(3): p. 322-4.
56. Bommiasamy, H., et al., *ATF6alpha induces XBP1-independent expansion of the*

endoplasmic reticulum. Journal of cell science, 2009. **122**(Pt 10): p. 1626-36.
57. Usui, M., et al., *Atf6alpha-null mice are glucose intolerant due to pancreatic beta-cell failure on a high-fat diet but partially resistant to diet-induced insulin resistance.* Metabolism: clinical and experimental, 2012.
58. Lee, A.H., N.N. Iwakoshi, and L.H. Glimcher, *XBP-1 regulates a subset of endoplasmic reticulum resident chaperone genes in the unfolded protein response.* Mol Cell Biol, 2003. **23**(21): p. 7448-59.
59. Ron, D., *Translational control in the endoplasmic reticulum stress response.* J Clin Invest, 2002. **110**(10): p. 1383-8.
60. Kaufman, R.J., *Stress signaling from the lumen of the endoplasmic reticulum: coordination of gene transcriptional and translational controls.* Genes Dev, 1999. **13**(10): p. 1211-33.
61. Kaufman, R.J., *Orchestrating the unfolded protein response in health and disease.* J Clin Invest, 2002. **110**(10): p. 1389-98.
62. Schroder, M. and R.J. Kaufman, *ER stress and the unfolded protein response.* Mutat Res, 2005. **569**(1-2): p. 29-63.
63. Tsai, B., Y. Ye, and T.A. Rapoport, *Retro-translocation of proteins from the endoplasmic reticulum into the cytosol.* Nat Rev Mol Cell Biol, 2002. **3**(4): p. 246-55.
64. Ruddock, L.W. and M. Molinari, *N-glycan processing in ER quality control.* J Cell Sci, 2006. **119**(Pt 21): p. 4373-80.
65. McCracken, A.A. and J.L. Brodsky, *Recognition and delivery of ERAD substrates to the proteasome and alternative paths for cell survival.* Curr Top Microbiol Immunol, 2005. **300**: p. 17-40.
66. Aebi, M., et al., *N-glycan structures: recognition and processing in the ER.* Trends Biochem Sci, 2010. **35**(2): p. 74-82.
67. Bernales, S., F.R. Papa, and P. Walter, *Intracellular signaling by the unfolded protein response.* Annu Rev Cell Dev Biol, 2006. **22**: p. 487-508.
68. Thorp, E., et al., *A reporter for tracking the UPR in vivo reveals patterns of temporal and cellular stress during atherosclerotic progression.* J Lipid Res, 2011. **52**(5): p. 1033-8.
69. Rutkowski, D.T. and R.J. Kaufman, *A trip to the ER: coping with stress.* Trends Cell Biol, 2004. **14**(1): p. 20-8.
70. Kozutsumi, Y., et al., *The presence of malfolded proteins in the endoplasmic reticulum signals the induction of glucose-regulated proteins.* Nature, 1988. **332**(6163): p. 462-4.
71. Stoeckle, M.Y., et al., *78-kilodalton glucose-regulated protein is induced in Rous sarcoma virus-transformed cells independently of glucose deprivation.* Mol Cell Biol, 1988. **8**(7): p. 2675-80.
72. Hendershot, L.M., *The ER function BiP is a master regulator of ER function.* Mt Sinai J Med, 2004. **71**(5): p. 289-97.
73. Harding, H.P., Y. Zhang, and D. Ron, *Protein translation and folding are coupled by an endoplasmic-reticulum-resident kinase.* Nature, 1999. **397**(6716): p. 271-4.
74. Sonenberg, N. and T.E. Dever, *Eukaryotic translation initiation factors and regulators.* Curr Opin Struct Biol, 2003. **13**(1): p. 56-63.
75. Scheuner, D., et al., *Translational control is required for the unfolded protein response and in vivo glucose homeostasis.* Mol Cell, 2001. **7**(6): p. 1165-76.
76. Prostko, C.R., et al., *Phosphorylation of eukaryotic initiation factor (eIF) 2 alpha and inhibition of eIF-2B in GH3 pituitary cells by perturbants of early protein processing that induce GRP78.* J Biol Chem, 1992. **267**(24): p. 16751-4.
77. Harding, H.P., et al., *Regulated translation initiation controls stress-induced gene*

expression in mammalian cells. Mol Cell, 2000. **6**(5): p. 1099-108.
78. Lu, P.D., H.P. Harding, and D. Ron, *Translation reinitiation at alternative open reading frames regulates gene expression in an integrated stress response.* J Cell Biol, 2004. **167**(1): p. 27-33.
79. Harding, H.P., et al., *An integrated stress response regulates amino acid metabolism and resistance to oxidative stress.* Mol Cell, 2003. **11**(3): p. 619-33.
80. Jiang, H.Y., et al., *Activating transcription factor 3 is integral to the eukaryotic initiation factor 2 kinase stress response.* Mol Cell Biol, 2004. **24**(3): p. 1365-77.
81. Marciniak, S.J., et al., *CHOP induces death by promoting protein synthesis and oxidation in the stressed endoplasmic reticulum.* Genes Dev, 2004. **18**(24): p. 3066-77.
82. Silva, R.M., et al., *CHOP/GADD153 is a mediator of apoptotic death in substantia nigra dopamine neurons in an in vivo neurotoxin model of parkinsonism.* J Neurochem, 2005. **95**(4): p. 974-86.
83. Yamaguchi, H. and H.G. Wang, *CHOP is involved in endoplasmic reticulum stress-induced apoptosis by enhancing DR5 expression in human carcinoma cells.* J Biol Chem, 2004. **279**(44): p. 45495-502.
84. Oyadomari, S. and M. Mori, *Roles of CHOP/GADD153 in endoplasmic reticulum stress.* Cell Death Differ, 2004. **11**(4): p. 381-9.
85. Fornace, A.J., Jr., I. Alamo, Jr., and M.C. Hollander, *DNA damage-inducible transcripts in mammalian cells.* Proc Natl Acad Sci U S A, 1988. **85**(23): p. 8800-4.
86. Ubeda, M., et al., *Stress-induced binding of the transcriptional factor CHOP to a novel DNA control element.* Mol Cell Biol, 1996. **16**(4): p. 1479-89.
87. Wang, X.Z., et al., *Identification of novel stress-induced genes downstream of chop.* EMBO J, 1998. **17**(13): p. 3619-30.
88. McCullough, K.D., et al., *Gadd153 sensitizes cells to endoplasmic reticulum stress by down-regulating Bcl2 and perturbing the cellular redox state.* Molecular and cellular biology, 2001. **21**(4): p. 1249-59.
89. Rutkowski, D.T., et al., *Adaptation to ER stress is mediated by differential stabilities of pro-survival and pro-apoptotic mRNAs and proteins.* PLoS biology, 2006. **4**(11): p. e374.
90. Hollander, M.C., et al., *Activation of Gadd34 by diverse apoptotic signals and suppression of its growth inhibitory effects by apoptotic inhibitors.* Int J Cancer, 2001. **96**(1): p. 22-31.
91. Novoa, I., et al., *Feedback inhibition of the unfolded protein response by GADD34-mediated dephosphorylation of eIF2alpha.* J Cell Biol, 2001. **153**(5): p. 1011-22.
92. Lin, C.J., et al., *Inhibition of mitochondria- and endoplasmic reticulum stress-mediated autophagy augments temozolomide-induced apoptosis in glioma cells.* PLoS One, 2012. **7**(6): p. e38706.
93. Barateiro, A., et al., *ER Stress, Mitochondrial Dysfunction and Calpain/JNK Activation are Involved in Oligodendrocyte Precursor Cell Death by Unconjugated Bilirubin.* Neuromolecular Med, 2012.
94. Verfaillie, T., et al., *PERK is required at the ER-mitochondrial contact sites to convey apoptosis after ROS-based ER stress.* Cell Death Differ, 2012. **19**(11): p. 1880-91.
95. Ferreiro, E., et al., *Mitochondrial- and endoplasmic reticulum-associated oxidative stress in Alzheimer's disease: from pathogenesis to biomarkers.* Int J Cell Biol, 2012. **2012**: p. 735206.
96. Kim, J., et al., *Overexpressed cyclophilin B suppresses apoptosis associated with ROS and Ca2+ homeostasis after ER stress.* J Cell Sci, 2008. **121**(Pt 21): p. 3636-48.
97. Zhang, Y., et al., *Inhibition of Ca2+ influx is required for mitochondrial reactive*

oxygen species-induced endoplasmic reticulum Ca2+ depletion and cell death in leukemia cells. Mol Pharmacol, 2006. **70**(4): p. 1424-34.
98. Jacobson, J. and M.R. Duchen, *Mitochondrial oxidative stress and cell death in astrocytes--requirement for stored Ca2+ and sustained opening of the permeability transition pore.* J Cell Sci, 2002. **115**(Pt 6): p. 1175-88.
99. Zhang, K., et al., *The unfolded protein response transducer IRE1alpha prevents ER stress-induced hepatic steatosis.* EMBO J, 2011. **30**(7): p. 1357-75.
100. Wang, X.Z., et al., *Cloning of mammalian Ire1 reveals diversity in the ER stress responses.* EMBO J, 1998. **17**(19): p. 5708-17.
101. Thuerauf, D.J., et al., *Effects of the isoform-specific characteristics of ATF6 alpha and ATF6 beta on endoplasmic reticulum stress response gene expression and cell viability.* J Biol Chem, 2007. **282**(31): p. 22865-78.
102. Thuerauf, D.J., L. Morrison, and C.C. Glembotski, *Opposing roles for ATF6alpha and ATF6beta in endoplasmic reticulum stress response gene induction.* J Biol Chem, 2004. **279**(20): p. 21078-84.
103. Iwawaki, T., et al., *Translational control by the ER transmembrane kinase/ribonuclease IRE1 under ER stress.* Nat Cell Biol, 2001. **3**(2): p. 158-64.
104. Yoshida, H., et al., *XBP1 mRNA is induced by ATF6 and spliced by IRE1 in response to ER stress to produce a highly active transcription factor.* Cell, 2001. **107**(7): p. 881-91.
105. Back, S.H., et al., *Cytoplasmic IRE1alpha-mediated XBP1 mRNA splicing in the absence of nuclear processing and endoplasmic reticulum stress.* J Biol Chem, 2006. **281**(27): p. 18691-706.
106. Oda, Y., et al., *Derlin-2 and Derlin-3 are regulated by the mammalian unfolded protein response and are required for ER-associated degradation.* J Cell Biol, 2006. **172**(3): p. 383-93.
107. Lee, K., et al., *IRE1-mediated unconventional mRNA splicing and S2P-mediated ATF6 cleavage merge to regulate XBP1 in signaling the unfolded protein response.* Genes & development, 2002. **16**(4): p. 452-66.
108. Okada, T., et al., *Distinct roles of activating transcription factor 6 (ATF6) and double-stranded RNA-activated protein kinase-like endoplasmic reticulum kinase (PERK) in transcription during the mammalian unfolded protein response.* Biochem J, 2002. **366**(Pt 2): p. 585-94.
109. Bommiasamy, H., et al., *ATF6alpha induces XBP1-independent expansion of the endoplasmic reticulum.* J Cell Sci, 2009. **122**(Pt 10): p. 1626-36.
110. Tsukada, J., et al., *The CCAAT/enhancer (C/EBP) family of basic-leucine zipper (bZIP) transcription factors is a multifaceted highly-regulated system for gene regulation.* Cytokine, 2011. **54**(1): p. 6-19.
111. Ohoka, N., et al., *TRB3, a novel ER stress-inducible gene, is induced via ATF4-CHOP pathway and is involved in cell death.* EMBO J, 2005. **24**(6): p. 1243-55.
112. Ma, Y., et al., *Two distinct stress signaling pathways converge upon the CHOP promoter during the mammalian unfolded protein response.* J Mol Biol, 2002. **318**(5): p. 1351-65.
113. Gachon, F., et al., *The cAMP response element binding protein-2 (CREB-2) can interact with the C/EBP-homologous protein (CHOP).* FEBS Lett, 2001. **502**(1-2): p. 57-62.
114. Yamamoto, K., et al., *Human HRD1 promoter carries a functional unfolded protein response element to which XBP1 but not ATF6 directly binds.* J Biochem, 2008. **144**(4): p. 477-86.
115. Yamamoto, K., et al., *Transcriptional induction of mammalian ER quality control*

proteins is mediated by single or combined action of ATF6alpha and XBP1. Dev Cell, 2007. **13**(3): p. 365-76.
116. Yoshida, H., et al., *XBP1 is critical to protect cells from endoplasmic reticulum stress: evidence from Site-2 protease-deficient Chinese hamster ovary cells.* Cell Struct Funct, 2006. **31**(2): p. 117-25.
117. Yamamoto, K., et al., *Differential contributions of ATF6 and XBP1 to the activation of endoplasmic reticulum stress-responsive cis-acting elements ERSE, UPRE and ERSE-II.* J Biochem, 2004. **136**(3): p. 343-50.
118. Nozaki, J., et al., *The endoplasmic reticulum stress response is stimulated through the continuous activation of transcription factors ATF6 and XBP1 in Ins2+/Akita pancreatic beta cells.* Genes Cells, 2004. **9**(3): p. 261-70.
119. Lee, K., et al., *IRE1-mediated unconventional mRNA splicing and S2P-mediated ATF6 cleavage merge to regulate XBP1 in signaling the unfolded protein response.* Genes Dev, 2002. **16**(4): p. 452-66.
120. Ma, Y. and L.M. Hendershot, *Herp is dually regulated by both the endoplasmic reticulum stress-specific branch of the unfolded protein response and a branch that is shared with other cellular stress pathways.* J Biol Chem, 2004. **279**(14): p. 13792-9.
121. Rutkowski, D.T. and R.J. Kaufman, *That which does not kill me makes me stronger: adapting to chronic ER stress.* Trends Biochem Sci, 2007. **32**(10): p. 469-76.
122. Rutkowski, D.T., et al., *Adaptation to ER stress is mediated by differential stabilities of pro-survival and pro-apoptotic mRNAs and proteins.* PLoS Biol, 2006. **4**(11): p. e374.
123. Yoshida, H., et al., *Identification of the cis-acting endoplasmic reticulum stress response element responsible for transcriptional induction of mammalian glucose-regulated proteins. Involvement of basic leucine zipper transcription factors.* J Biol Chem, 1998. **273**(50): p. 33741-9.
124. Foti, D.M., et al., *Conservation and divergence of the yeast and mammalian unfolded protein response. Activation of specific mammalian endoplasmic reticulum stress element of the grp78/BiP promoter by yeast Hac1.* J Biol Chem, 1999. **274**(43): p. 30402-9.
125. Kokame, K., H. Kato, and T. Miyata, *Identification of ERSE-II, a new cis-acting element responsible for the ATF6-dependent mammalian unfolded protein response.* J Biol Chem, 2001. **276**(12): p. 9199-205.
126. Baumeister, P., et al., *Endoplasmic reticulum stress induction of the Grp78/BiP promoter: activating mechanisms mediated by YY1 and its interactive chromatin modifiers.* Mol Cell Biol, 2005. **25**(11): p. 4529-40.
127. Cross, B.C., et al., *The molecular basis for selective inhibition of unconventional mRNA splicing by an IRE1-binding small molecule.* Proc Natl Acad Sci U S A, 2012. **109**(15): p. E869-78.
128. Hollien, J., et al., *Regulated Ire1-dependent decay of messenger RNAs in mammalian cells.* J Cell Biol, 2009. **186**(3): p. 323-31.
129. Oikawa, D., et al., *Identification of a consensus element recognized and cleaved by IRE1 alpha.* Nucleic Acids Res, 2010. **38**(18): p. 6265-73.
130. Niwa, M., et al., *Genome-scale approaches for discovering novel nonconventional splicing substrates of the Ire1 nuclease.* Genome Biol, 2005. **6**(1): p. R3.
131. Kozlov, G., et al., *A structural overview of the PDI family of proteins.* FEBS J, 2010. **277**(19): p. 3924-36.
132. Turano, C., et al., *Proteins of the PDI family: unpredicted non-ER locations and functions.* J Cell Physiol, 2002. **193**(2): p. 154-63.
133. Tu, B.P. and J.S. Weissman, *Oxidative protein folding in eukaryotes: mechanisms and*

consequences. J Cell Biol, 2004. **164**(3): p. 341-6.
134. Huang, C.J., et al., *Induction of endoplasmic reticulum stress-induced beta-cell apoptosis and accumulation of polyubiquitinated proteins by human islet amyloid polypeptide.* Am J Physiol Endocrinol Metab, 2007. **293**(6): p. E1656-62.
135. Yusta, B., et al., *GLP-1 receptor activation improves beta cell function and survival following induction of endoplasmic reticulum stress.* Cell Metab, 2006. **4**(5): p. 391-406.
136. Herbach, N., et al., *Dominant-negative effects of a novel mutated Ins2 allele causes early-onset diabetes and severe beta-cell loss in Munich Ins2C95S mutant mice.* Diabetes, 2007. **56**(5): p. 1268-76.
137. Edghill, E.L., et al., *Insulin mutation screening in 1,044 patients with diabetes: mutations in the INS gene are a common cause of neonatal diabetes but a rare cause of diabetes diagnosed in childhood or adulthood.* Diabetes, 2008. **57**(4): p. 1034-42.
138. Stoy, J., et al., *Insulin gene mutations as a cause of permanent neonatal diabetes.* Proc Natl Acad Sci U S A, 2007. **104**(38): p. 15040-4.
139. Oyadomari, S., et al., *Targeted disruption of the Chop gene delays endoplasmic reticulum stress-mediated diabetes.* J Clin Invest, 2002. **109**(4): p. 525-32.
140. Liu, M., et al., *Impaired cleavage of preproinsulin signal peptide linked to autosomal-dominant diabetes.* Diabetes, 2012. **61**(4): p. 828-37.
141. Lee, T.G., et al., *The 58,000-dalton cellular inhibitor of the interferon-induced double-stranded RNA-activated protein kinase (PKR) is a member of the tetratricopeptide repeat family of proteins.* Mol Cell Biol, 1994. **14**(4): p. 2331-42.
142. Yan, W., et al., *Control of PERK eIF2alpha kinase activity by the endoplasmic reticulum stress-induced molecular chaperone P58IPK.* Proc Natl Acad Sci U S A, 2002. **99**(25): p. 15920-5.
143. Rutkowski, D.T., et al., *The role of p58IPK in protecting the stressed endoplasmic reticulum.* Mol Biol Cell, 2007. **18**(9): p. 3681-91.
144. Ladiges, W.C., et al., *Pancreatic beta-cell failure and diabetes in mice with a deletion mutation of the endoplasmic reticulum molecular chaperone gene P58IPK.* Diabetes, 2005. **54**(4): p. 1074-81.
145. Wolcott, C.D. and M.L. Rallison, *Infancy-onset diabetes mellitus and multiple epiphyseal dysplasia.* J Pediatr, 1972. **80**(2): p. 292-7.
146. Stoss, H., et al., *Wolcott-Rallison syndrome: diabetes mellitus and spondyloepiphyseal dysplasia.* Eur J Pediatr, 1982. **138**(2): p. 120-9.
147. Thornton, C.M., D.J. Carson, and F.J. Stewart, *Autopsy findings in the Wolcott-Rallison syndrome.* Pediatr Pathol Lab Med, 1997. **17**(3): p. 487-96.
148. Castelnau, P., et al., *Wolcott-Rallison syndrome: a case with endocrine and exocrine pancreatic deficiency and pancreatic hypotrophy.* Eur J Pediatr, 2000. **159**(8): p. 631-3.
149. Reis, A.F., et al., *Two novel mutations in the EIF2AK3 gene in children with Wolcott-Rallison syndrome.* Pediatr Diabetes, 2011. **12**(3 Pt 1): p. 187-91.
150. Ozbek, M.N., et al., *Wolcott-Rallison syndrome due to the same mutation (W522X) in EIF2AK3 in two unrelated families and review of the literature.* Pediatr Diabetes, 2010. **11**(4): p. 279-85.
151. Genevieve, D., et al., *Exclusion of the dymeclin and PAPSS2 genes in a novel form of spondyloepimetaphyseal dysplasia and mental retardation.* Eur J Hum Genet, 2005. **13**(5): p. 541-6.
152. Biason-Lauber, A., et al., *Loss of kinase activity in a patient with Wolcott-Rallison syndrome caused by a novel mutation in the EIF2AK3 gene.* Diabetes, 2002. **51**(7): p. 2301-5.

153. Delepine, M., et al., *EIF2AK3, encoding translation initiation factor 2-alpha kinase 3, is mutated in patients with Wolcott-Rallison syndrome.* Nat Genet, 2000. **25**(4): p. 406-9.
154. Allotey, R.A., et al., *The EIF2AK3 gene region and type I diabetes in subjects from South India.* Genes Immun, 2004. **5**(8): p. 648-52.
155. Harding, H.P., et al., *Diabetes mellitus and exocrine pancreatic dysfunction in perk-/- mice reveals a role for translational control in secretory cell survival.* Mol Cell, 2001. **7**(6): p. 1153-63.
156. Zhang, P., et al., *The PERK eukaryotic initiation factor 2 alpha kinase is required for the development of the skeletal system, postnatal growth, and the function and viability of the pancreas.* Mol Cell Biol, 2002. **22**(11): p. 3864-74.
157. Zhang, W., et al., *PERK EIF2AK3 control of pancreatic beta cell differentiation and proliferation is required for postnatal glucose homeostasis.* Cell Metab, 2006. **4**(6): p. 491-7.
158. Lee, A.H., et al., *Regulation of hepatic lipogenesis by the transcription factor XBP1.* Science, 2008. **320**(5882): p. 1492-6.
159. Oyadomari, S., et al., *Dephosphorylation of translation initiation factor 2alpha enhances glucose tolerance and attenuates hepatosteatosis in mice.* Cell Metab, 2008. **7**(6): p. 520-32.
160. Rutkowski, D.T., et al., *UPR pathways combine to prevent hepatic steatosis caused by ER stress-mediated suppression of transcriptional master regulators.* Dev Cell, 2008. **15**(6): p. 829-40.
161. Hettmann, T., K. Barton, and J.M. Leiden, *Microphthalmia due to p53-mediated apoptosis of anterior lens epithelial cells in mice lacking the CREB-2 transcription factor.* Dev Biol, 2000. **222**(1): p. 110-23.
162. Ganie, M.A., et al., *Presentation and clinical course of Wolfram (DIDMOAD) syndrome from North India.* Diabet Med, 2011. **28**(11): p. 1337-42.
163. Inoue, H., et al., *A gene encoding a transmembrane protein is mutated in patients with diabetes mellitus and optic atrophy (Wolfram syndrome).* Nat Genet, 1998. **20**(2): p. 143-8.
164. Hatanaka, M., et al., *Wolfram syndrome 1 gene (WFS1) product localizes to secretory granules and determines granule acidification in pancreatic beta-cells.* Hum Mol Genet, 2011. **20**(7): p. 1274-84.
165. Noormets, K., et al., *Sex differences in the development of diabetes in mice with deleted wolframin (Wfs1) gene.* Exp Clin Endocrinol Diabetes, 2011. **119**(5): p. 271-5.
166. Fonseca, S.G., et al., *Wolfram syndrome 1 gene negatively regulates ER stress signaling in rodent and human cells.* J Clin Invest, 2010. **120**(3): p. 744-55.
167. Noormets, K., et al., *Male mice with deleted Wolframin (Wfs1) gene have reduced fertility.* Reprod Biol Endocrinol, 2009. **7**: p. 82.
168. Kawano, J., et al., *Wolfram syndrome 1 (Wfs1) mRNA expression in the normal mouse brain during postnatal development.* Neurosci Res, 2009. **64**(2): p. 213-30.
169. Koks, S., et al., *Wfs1 gene deletion causes growth retardation in mice and interferes with the growth hormone pathway.* Physiol Genomics, 2009. **37**(3): p. 249-59.
170. Luuk, H., et al., *Wfs1-deficient mice display impaired behavioural adaptation in stressful environment.* Behav Brain Res, 2009. **198**(2): p. 334-45.
171. Kawano, J., Y. Tanizawa, and K. Shinoda, *Wolfram syndrome 1 (Wfs1) gene expression in the normal mouse visual system.* J Comp Neurol, 2008. **510**(1): p. 1-23.
172. Yamada, T., et al., *WFS1-deficiency increases endoplasmic reticulum stress, impairs cell cycle progression and triggers the apoptotic pathway specifically in pancreatic beta-cells.* Hum Mol Genet, 2006. **15**(10): p. 1600-9.

173. Riggs, A.C., et al., *Mice conditionally lacking the Wolfram gene in pancreatic islet beta cells exhibit diabetes as a result of enhanced endoplasmic reticulum stress and apoptosis.* Diabetologia, 2005. **48**(11): p. 2313-21.
174. Fonseca, S.G., et al., *WFS1 is a novel component of the unfolded protein response and maintains homeostasis of the endoplasmic reticulum in pancreatic beta-cells.* J Biol Chem, 2005. **280**(47): p. 39609-15.
175. Ueda, K., et al., *Endoplasmic reticulum stress induces Wfs1 gene expression in pancreatic beta-cells via transcriptional activation.* Eur J Endocrinol, 2005. **153**(1): p. 167-76.
176. Yamaguchi, S., et al., *Endoplasmic reticulum stress and N-glycosylation modulate expression of WFS1 protein.* Biochem Biophys Res Commun, 2004. **325**(1): p. 250-6.
177. Ishihara, H., et al., *Disruption of the WFS1 gene in mice causes progressive beta-cell loss and impaired stimulus-secretion coupling in insulin secretion.* Hum Mol Genet, 2004. **13**(11): p. 1159-70.
178. Kakiuchi, C., et al., *XBP1 induces WFS1 through an endoplasmic reticulum stress response element-like motif in SH-SY5Y cells.* J Neurochem, 2006. **97**(2): p. 545-55.
179. Gharanei, S., et al., *Vacuolar-type H+-ATPase V1A subunit is a molecular partner of Wolfram syndrome 1 (WFS1) protein, which regulates its expression and stability.* Hum Mol Genet, 2012.
180. Cameron, T.L., et al., *Transcriptional profiling of chondrodysplasia growth plate cartilage reveals adaptive ER-stress networks that allow survival but disrupt hypertrophy.* PLoS One, 2011. **6**(9): p. e24600.
181. Metzger, D., et al., *Conditional site-specific recombination in mammalian cells using a ligand-dependent chimeric Cre recombinase.* Proc Natl Acad Sci U S A, 1995. **92**(15): p. 6991-5.
182. Usui, M., et al., *Atf6alpha-null mice are glucose intolerant due to pancreatic beta-cell failure on a high-fat diet but partially resistant to diet-induced insulin resistance.* Metabolism, 2012. **61**(8): p. 1118-28.
183. Tang, X., et al., *Activating transcription factor 6 protects insulin receptor from ER stress-stimulated desensitization via p42/44 ERK pathway.* Acta Pharmacol Sin, 2011. **32**(9): p. 1138-47.
184. Rutkowski, D.T. and R.J. Kaufman, *All roads lead to ATF4.* Developmental cell, 2003. **4**(4): p. 442-4.
185. Rutkowski, D.T. and R.J. Kaufman, *That which does not kill me makes me stronger: adapting to chronic ER stress.* Trends in biochemical sciences, 2007. **32**(10): p. 469-76.
186. Kaufman, R.J., et al., *The unfolded protein response is required to maintain the integrity of the endoplasmic reticulum, prevent oxidative stress and preserve differentiation in beta-cells.* Diabetes Obes Metab, 2010. **12 Suppl 2**: p. 99-107.
187. Nolan, C.J., P. Damm, and M. Prentki, *Type 2 diabetes across generations: from pathophysiology to prevention and management.* Lancet, 2011. **378**(9786): p. 169-81.
188. Ashcroft, F.M. and P. Rorsman, *Diabetes mellitus and the beta cell: the last ten years.* Cell, 2012. **148**(6): p. 1160-71.
189. Back, S.H. and R.J. Kaufman, *Endoplasmic reticulum stress and type 2 diabetes.* Annu Rev Biochem, 2012. **81**: p. 767-93.
190. Eizirik, D.L., A.K. Cardozo, and M. Cnop, *The role for endoplasmic reticulum stress in diabetes mellitus.* Endocr Rev, 2008. **29**(1): p. 42-61.
191. Eizirik, D.L. and M. Cnop, *ER stress in pancreatic beta cells: the thin red line between adaptation and failure.* Sci Signal, 2010. **3**(110): p. pe7.
192. Kim, C.H., et al., *Independent impact of body mass index and metabolic syndrome on*

the risk of type 2 diabetes in koreans. Metab Syndr Relat Disord, 2012. **10**(5): p. 321-5.
193. Cao, S.S. and R.J. Kaufman, *Unfolded protein response.* Curr Biol, 2012. **22**(16): p. R622-6.
194. Eizirik, D.L., A.K. Cardozo, and M. Cnop, *The role for endoplasmic reticulum stress in diabetes mellitus.* Endocrine reviews, 2008. **29**(1): p. 42-61.
195. Rhodes, C.J., et al., *Stimulation by ATP of proinsulin to insulin conversion in isolated rat pancreatic islet secretory granules. Association with the ATP-dependent proton pump.* J Biol Chem, 1987. **262**(22): p. 10712-7.
196. Rhodes, C.J. and P.A. Halban, *Newly synthesized proinsulin/insulin and stored insulin are released from pancreatic B cells predominantly via a regulated, rather than a constitutive, pathway.* J Cell Biol, 1987. **105**(1): p. 145-53.
197. Rhodes, C.J., C.A. Lucas, and P.A. Halban, *Glucose stimulates the biosynthesis of rat I and II insulin to an equal extent in isolated pancreatic islets.* FEBS Lett, 1987. **215**(1): p. 179-82.
198. Okamoto, T., et al., *Improvement of diabetic symptoms of hereditary diabetic (KK) mice by a single injection with islet-activating protein (IAP).* J Pharmacobiodyn, 1980. **3**(9): p. 470-7.
199. Goodge, K.A. and J.C. Hutton, *Translational regulation of proinsulin biosynthesis and proinsulin conversion in the pancreatic beta-cell.* Semin Cell Dev Biol, 2000. **11**(4): p. 235-42.
200. Melloul, D., S. Marshak, and E. Cerasi, *Regulation of insulin gene transcription.* Diabetologia, 2002. **45**(3): p. 309-26.
201. Nikawa, J. and S. Yamashita, *IRE1 encodes a putative protein kinase containing a membrane-spanning domain and is required for inositol phototrophy in Saccharomyces cerevisiae.* Mol Microbiol, 1992. **6**(11): p. 1441-6.
202. Mori, K., et al., *A 22 bp cis-acting element is necessary and sufficient for the induction of the yeast KAR2 (BiP) gene by unfolded proteins.* EMBO J, 1992. **11**(7): p. 2583-93.
203. Mori, K., et al., *A transmembrane protein with a cdc2+/CDC28-related kinase activity is required for signaling from the ER to the nucleus.* Cell, 1993. **74**(4): p. 743-56.
204. Cox, J.S., C.E. Shamu, and P. Walter, *Transcriptional induction of genes encoding endoplasmic reticulum resident proteins requires a transmembrane protein kinase.* Cell, 1993. **73**(6): p. 1197-206.
205. Shamu, C.E. and P. Walter, *Oligomerization and phosphorylation of the Ire1p kinase during intracellular signaling from the endoplasmic reticulum to the nucleus.* EMBO J, 1996. **15**(12): p. 3028-39.
206. Welihinda, A.A. and R.J. Kaufman, *The unfolded protein response pathway in Saccharomyces cerevisiae. Oligomerization and trans-phosphorylation of Ire1p (Ern1p) are required for kinase activation.* J Biol Chem, 1996. **271**(30): p. 18181-7.
207. Mori, K., et al., *Signalling from endoplasmic reticulum to nucleus: transcription factor with a basic-leucine zipper motif is required for the unfolded protein-response pathway.* Genes Cells, 1996. **1**(9): p. 803-17.
208. Cox, J.S. and P. Walter, *A novel mechanism for regulating activity of a transcription factor that controls the unfolded protein response.* Cell, 1996. **87**(3): p. 391-404.
209. Cox, J.S., R.E. Chapman, and P. Walter, *The unfolded protein response coordinates the production of endoplasmic reticulum protein and endoplasmic reticulum membrane.* Mol Biol Cell, 1997. **8**(9): p. 1805-14.
210. Travers, K.J., et al., *Functional and genomic analyses reveal an essential*

coordination between the unfolded protein response and ER-associated degradation. Cell, 2000. **101**(3): p. 249-58.
211. Huh, W.J., et al., *XBP1 controls maturation of gastric zymogenic cells by induction of MIST1 and expansion of the rough endoplasmic reticulum.* Gastroenterology, 2010. **139**(6): p. 2038-49.
212. Shaffer, A.L., et al., *XBP1, downstream of Blimp-1, expands the secretory apparatus and other organelles, and increases protein synthesis in plasma cell differentiation.* Immunity, 2004. **21**(1): p. 81-93.
213. Capoccia, B.J., et al., *Transcription factor MIST1 in terminal differentiation of mouse and human plasma cells.* Physiol Genomics, 2011. **43**(3): p. 174-86.
214. Yoshida, H., et al., *Endoplasmic reticulum stress-induced formation of transcription factor complex ERSF including NF-Y (CBF) and activating transcription factors 6alpha and 6beta that activates the mammalian unfolded protein response.* Mol Cell Biol, 2001. **21**(4): p. 1239-48.
215. Kanemoto, S., et al., *XBP1 activates the transcription of its target genes via an ACGT core sequence under ER stress.* Biochem Biophys Res Commun, 2005. **331**(4): p. 1146-53.
216. DenBoer, L.M., et al., *Luman is capable of binding and activating transcription from the unfolded protein response element.* Biochem Biophys Res Commun, 2005. **331**(1): p. 113-9.
217. Kondo, S., et al., *OASIS, a CREB/ATF-family member, modulates UPR signalling in astrocytes.* Nat Cell Biol, 2005. **7**(2): p. 186-94.
218. Zhang, K. and R.J. Kaufman, *The unfolded protein response: a stress signaling pathway critical for health and disease.* Neurology, 2006. **66**(2 Suppl 1): p. S102-9.
219. Zhang, K. and R.J. Kaufman, *Protein folding in the endoplasmic reticulum and the unfolded protein response.* Handb Exp Pharmacol, 2006(172): p. 69-91.
220. Zhang, P., et al., *The GCN2 eIF2alpha kinase is required for adaptation to amino acid deprivation in mice.* Mol Cell Biol, 2002. **22**(19): p. 6681-8.
221. Hollien, J. and J.S. Weissman, *Decay of endoplasmic reticulum-localized mRNAs during the unfolded protein response.* Science, 2006. **313**(5783): p. 104-7.
222. Tirasophon, W., et al., *The endoribonuclease activity of mammalian IRE1 autoregulates its mRNA and is required for the unfolded protein response.* Genes Dev, 2000. **14**(21): p. 2725-36.
223. Han, D., et al., *IRE1alpha kinase activation modes control alternate endoribonuclease outputs to determine divergent cell fates.* Cell, 2009. **138**(3): p. 562-75.
224. Oikawa, D., M. Tokuda, and T. Iwawaki, *Site-specific cleavage of CD59 mRNA by endoplasmic reticulum-localized ribonuclease, IRE1.* Biochem Biophys Res Commun, 2007. **360**(1): p. 122-7.
225. Volkmann, K., et al., *Potent and selective inhibitors of the inositol-requiring enzyme 1 endoribonuclease.* J Biol Chem, 2011. **286**(14): p. 12743-55.
226. Kinsley, B.T., et al., *Morbidity and mortality in the Wolfram syndrome.* Diabetes Care, 1995. **18**(12): p. 1566-70.
227. Rigoli, L., F. Lombardo, and C. Di Bella, *Wolfram syndrome and WFS1 gene.* Clin Genet, 2011. **79**(2): p. 103-17.
228. Cryns, K., et al., *Mutational spectrum of the WFS1 gene in Wolfram syndrome, nonsyndromic hearing impairment, diabetes mellitus, and psychiatric disease.* Hum Mutat, 2003. **22**(4): p. 275-87.
229. Cryns, K., et al., *The WFS1 gene, responsible for low frequency sensorineural hearing loss and Wolfram syndrome, is expressed in a variety of inner ear cells.* Histochem Cell Biol, 2003. **119**(3): p. 247-56.

230. Wasson, J. and M.A. Permutt, *Candidate gene studies reveal that the WFS1 gene joins the expanding list of novel type 2 diabetes genes.* Diabetologia, 2008. **51**(3): p. 391-3.
231. Takei, D., et al., *WFS1 protein modulates the free Ca(2+) concentration in the endoplasmic reticulum.* FEBS Lett, 2006. **580**(24): p. 5635-40.
232. Zatyka, M., et al., *Sodium-potassium ATPase 1 subunit is a molecular partner of Wolframin, an endoplasmic reticulum protein involved in ER stress.* Hum Mol Genet, 2008. **17**(2): p. 190-200.
233. Fonseca, S.G., et al., *Wolfram syndrome 1 and adenylyl cyclase 8 interact at the plasma membrane to regulate insulin production and secretion.* Nat Cell Biol, 2012. **14**(10): p. 1105-12.
234. Lipson, K.L., R. Ghosh, and F. Urano, *The role of IRE1alpha in the degradation of insulin mRNA in pancreatic beta-cells.* PLoS One, 2008. **3**(2): p. e1648.
235. Fonseca, S.G., K.L. Lipson, and F. Urano, *Endoplasmic reticulum stress signaling in pancreatic beta-cells.* Antioxid Redox Signal, 2007. **9**(12): p. 2335-44.
236. Lipson, K.L., et al., *Regulation of insulin biosynthesis in pancreatic beta cells by an endoplasmic reticulum-resident protein kinase IRE1.* Cell Metab, 2006. **4**(3): p. 245-54.
237. Iwawaki, T., R. Akai, and K. Kohno, *IRE1alpha disruption causes histological abnormality of exocrine tissues, increase of blood glucose level, and decrease of serum immunoglobulin level.* PLoS One, 2010. **5**(9): p. e13052.
238. Iwawaki, T., et al., *Function of IRE1 alpha in the placenta is essential for placental development and embryonic viability.* Proc Natl Acad Sci U S A, 2009. **106**(39): p. 16657-62.
239. Gannon, M., et al., *Analysis of the Cre-mediated recombination driven by rat insulin promoter in embryonic and adult mouse pancreas.* Genesis, 2000. **26**(2): p. 139-42.
240. Lammert, E., O. Cleaver, and D. Melton, *Role of endothelial cells in early pancreas and liver development.* Mech Dev, 2003. **120**(1): p. 59-64.
241. Lee, A.H., et al., *Proteasome inhibitors disrupt the unfolded protein response in myeloma cells.* Proc Natl Acad Sci U S A, 2003. **100**(17): p. 9946-51.
242. Iwakoshi, N.N., A.H. Lee, and L.H. Glimcher, *The X-box binding protein-1 transcription factor is required for plasma cell differentiation and the unfolded protein response.* Immunol Rev, 2003. **194**: p. 29-38.
243. Iwakoshi, N.N., et al., *Plasma cell differentiation and the unfolded protein response intersect at the transcription factor XBP-1.* Nat Immunol, 2003. **4**(4): p. 321-9.
244. Cho, G., et al., *Evidence that SIZN1 is a candidate X-linked mental retardation gene.* Am J Med Genet A, 2008. **146A**(20): p. 2644-50.
245. Cho, G., et al., *Sizn1 is a novel protein that functions as a transcriptional coactivator of bone morphogenic protein signaling.* Mol Cell Biol, 2008. **28**(5): p. 1565-72.
246. Jourdan, M., et al., *An in vitro model of differentiation of memory B cells into plasmablasts and plasma cells including detailed phenotypic and molecular characterization.* Blood, 2009. **114**(25): p. 5173-81.
247. Shen, X., et al., *Genetic interactions due to constitutive and inducible gene regulation mediated by the unfolded protein response in C. elegans.* PLoS Genet, 2005. **1**(3): p. e37.
248. Borck, G., et al., *Arterial rupture in classic Ehlers-Danlos syndrome with COL5A1 mutation.* Am J Med Genet A, 2010. **152A**(8): p. 2090-3.
249. Beridze, N. and W.H. Frishman, *Vascular Ehlers-Danlos syndrome: pathophysiology, diagnosis, and prevention and treatment of its complications.* Cardiol Rev, 2012. **20**(1): p. 4-7.
250. Bagratuni, T., et al., *XBP1s levels are implicated in the biology and outcome of*

myeloma mediating different clinical outcomes to thalidomide-based treatments. Blood, 2010. **116**(2): p. 250-3.
251. Todd, D.J., et al., *XBP1 governs late events in plasma cell differentiation and is not required for antigen-specific memory B cell development.* J Exp Med, 2009. **206**(10): p. 2151-9.
252. Tate, G., et al., *A novel missense mutation of the XBP1 gene in diffuse large B-cell lymphoma.* Cancer Genet Cytogenet, 2009. **190**(2): p. 131-3.
253. Tsuchiya, M., et al., *XBP1 may determine the size of the ameloblast endoplasmic reticulum.* J Dent Res, 2008. **87**(11): p. 1058-62.
254. Brunsing, R., et al., *B- and T-cell development both involve activity of the unfolded protein response pathway.* J Biol Chem, 2008. **283**(26): p. 17954-61.
255. Zhang, K. and R.J. Kaufman, *Identification and characterization of endoplasmic reticulum stress-induced apoptosis in vivo.* Methods Enzymol, 2008. **442**: p. 395-419.
256. Romero-Ramirez, L., et al., *XBP1 is essential for survival under hypoxic conditions and is required for tumor growth.* Cancer Res, 2004. **64**(17): p. 5943-7.
257. Upton, J.P., et al., *IRE1alpha Cleaves Select microRNAs during ER Stress to Derepress Translation of Proapoptotic Caspase-2.* Science, 2012.
258. Plocik, A.M. and C. Guthrie, *Diverse forms of RPS9 splicing are part of an evolving autoregulatory circuit.* PLoS Genet, 2012. **8**(3): p. e1002620.
259. Lindstrom, M.S. and M. Nister, *Silencing of ribosomal protein S9 elicits a multitude of cellular responses inhibiting the growth of cancer cells subsequent to p53 activation.* PLoS One, 2010. **5**(3): p. e9578.
260. Pnueli, L. and Y. Arava, *Genome-wide polysomal analysis of a yeast strain with mutated ribosomal protein S9.* BMC Genomics, 2007. **8**: p. 285.
261. Kim, S.Y., et al., *Alterations in mRNA expression of ribosomal protein S9 in hydrogen peroxide-treated neurotumor cells and in rat hippocampus after transient ischemia.* Neurochem Res, 2003. **28**(6): p. 925-31.
262. Lynch, C.D., et al., *Filamin depletion blocks endoplasmic spreading and destabilizes force-bearing adhesions.* Mol Biol Cell, 2011. **22**(8): p. 1263-73.
263. Nakamura, F., T.P. Stossel, and J.H. Hartwig, *The filamins: organizers of cell structure and function.* Cell Adh Migr, 2011. **5**(2): p. 160-9.
264. Robertson, S., *FLNB-Related Disorders*, in *GeneReviews*, R.A. Pagon, et al., Editors. 1993: Seattle (WA).
265. Del Valle-Perez, B., et al., *Filamin B plays a key role in vascular endothelial growth factor-induced endothelial cell motility through its interaction with Rac-1 and Vav-2.* J Biol Chem, 2010. **285**(14): p. 10748-60.
266. Baldassarre, M., et al., *Filamins regulate cell spreading and initiation of cell migration.* PLoS One, 2009. **4**(11): p. e7830.
267. Dobbs, M.B., et al., *Case report: Congenital knee dislocation in a patient with larsen syndrome and a novel filamin B mutation.* Clin Orthop Relat Res, 2008. **466**(6): p. 1503-9.
268. Lu, J., et al., *Filamin B mutations cause chondrocyte defects in skeletal development.* Hum Mol Genet, 2007. **16**(14): p. 1661-75.
269. Zhou, X., et al., *Filamin B deficiency in mice results in skeletal malformations and impaired microvascular development.* Proc Natl Acad Sci U S A, 2007. **104**(10): p. 3919-24.
270. Bicknell, L.S., et al., *Mutations in FLNB cause boomerang dysplasia.* J Med Genet, 2005. **42**(7): p. e43.
271. Sheen, V.L., et al., *Filamin A and Filamin B are co-expressed within neurons during periods of neuronal migration and can physically interact.* Hum Mol Genet, 2002.

11(23): p. 2845-54.
272. Auf, G., et al., *Inositol-requiring enzyme 1alpha is a key regulator of angiogenesis and invasion in malignant glioma.* Proc Natl Acad Sci U S A, 2010. **107**(35): p. 15553-8.
273. Drogat, B., et al., *IRE1 signaling is essential for ischemia-induced vascular endothelial growth factor-A expression and contributes to angiogenesis and tumor growth in vivo.* Cancer Res, 2007. **67**(14): p. 6700-7.
274. Dejeans, N., et al., *Autocrine control of glioma cells adhesion/migration through Inositol Requiring enzyme 1alpha (IRE1alpha)-mediated cleavage of Secreted Protein Acidic Rich in Cysteine (SPARC) mRNA.* J Cell Sci, 2012.
275. Shang, J. and M.A. Lehrman, *Discordance of UPR signaling by ATF6 and Ire1p-XBP1 with levels of target transcripts.* Biochem Biophys Res Commun, 2004. **317**(2): p. 390-6.